1-1-1982

Morphology and mechanical properities of particulate calcium carbonate-polyethylene composites.

Varkki P. Chacko
University of Massachusetts Amherst

MORPHOLOGY AND MECHANICAL PROPERTIES OF PARTICULATE CALCIUM CARBONATE-POLYETHYLENE COMPOSITES

A Dissertation Presented

By

VARKKI P. CHACKO

Submitted to the Graduate School of the
University of Massachusetts in partial fulfillment
of the requirements for the degree of

DOCTOR OF PHILOSOPHY

May 1982

Polymer Science & Engineering Department

MORPHOLOGY AND MECHANICAL PROPERTIES OF

PARTICULATE $CaCO_3$-POLYETHYLENE COMPOSITES

A Dissertation Presented

By

VARKKI P. CHACKO

Approved as to style and content by:

Frank E. Karasz, Co-Chairperson

Richard J. Farris, Co-Chairperson

Edwin L. Thomas, Member

Richard S. Stein, Member

William J. MacKnight, Head
Polymer Science & Engineering

Dedicated to

My

Father and Mother

ACKNOWLEDGEMENTS

I am grateful to my coadvisors, Professors Frank Karasz and Richard Farris, for their advice and support during graduate school. I owe a great deal to Professor Edwin Thomas, who played an important role in the shaping of the microscopy work in this dissertation. The association with him was both challenging and enjoyable. I would like to thank Professor Richard Stein for serving on my committee and offering thoughtful advice and criticism.

Financial support for this work cam from AMP Inc., U.S. Air Force and the MRL, and is gratefully acknowledged.Dr. E.G. Howard of the duPont Co. was kind enough to provide sample of a novel composite which sparked initial interest in the study. I would also like to acknowledge the gift of polyethylene resins from Hercules Powder Co. and Phillips Petroleum Co. $CaCO_3$ filler was kindly supplied to us by Thompson, Weinman & Co. I wish to thank Mrs. Judith Allardice for the superb job of typing and for keeping a pleasant disposition through this all.

It is with much pleasure that I acknowledge the role of my many friends in making my stay at Amherst enjoyable. In particular, I would like to thank Vivek Soni, Ameeta Narula, Katarina Djordjevic, Miomir Djordjevic, Andrei Filippov, Sung Soo Chang and Arun Wadhawan for help and friendship. In addition, Arun did all the figures quite cherefully. I thank my brother, sister, Madhura and all my family for love, affection and encouragement through the last few years.

MORPHOLOGY AND MECHANICAL PROPERTIES OF PARTICULATE CALCIUM CARBONATE-POLYETHYLENE COMPOSITES

(May 1982)

Varkki P. Chacko, B.E.(Honors), M. Sc. (Honors)
Birla Institute of Technology and Science
M.S., Ph.D., University of Massachusetts

Co-Advisors: Professors Frank E. Karasz
Richard J. Farris

Abstract

The microstructure, small and large strain mechanical properties and modes of microstructural failure in one novel and a range of conventional particulate $CaCO_3$ polyethylene (PE) composites were investigated by electron microscopy, Instron testing, dilatometry and differential scanning calorimetry.

The novel PE-$CaCO_3$ composite (63.5 weight % $CaCO_3$; $\overline{M}_w$ of PE = 1.5×10^6) used was prepared elsewhere by polymerizing ethylene on catalyst coated filler surface. The conventional PE-$CaCO_3$ composites were prepared with a range of PEs ($\overline{M}_w$ = 59,000, 200,000 and 2×10^6) and filler content (0, 2, 4, 8 and 19 volume %). Particulate $CaCO_3$ ($\overline{D}_w$ = 2.5 μm) both with and without titanate coupling agent were utilized. Electron microscopy showed that long range organization of polymer microstructure is not present at levels of filler studied. Radially oriented lamellar growth up to 500 - 1000 nm away is observed

at the interface.

Dynamic mechanical spectra of unfilled and filled PEs obtained at 11 Hz over the temperature spectrum 100K to 400K revealed that the storage modulus expectedly increases upon introduction of filler. Filler presence decreased tanδ in the vicinity of the γ-transition of PE while increasing it at higher temperatures. Complex moduli of model viscoelastic composites were determined using the correspondence principle to explain these observations.

Tensile tests showed that yield stress and elongation at break both decreased in presence of filler. Volume dilatation studies revealed that beyond the yield point the presence of filler increased dilatation. Titanate treatment of filler suppressed the dilatation observed.

Scanning electron microscopy studies of specimens undergoing deformation revealed formation of void-fibril microfailure zones which resemble crazes.

Another area of investigation was the diffraction contrast imaging of thin PE films in the electron microscope. Image contrast is shown to arise from differential diffraction efficiency of differently oriented lamellae. Development of new scanning transmission electron microscopy imaging techniques permitted observation of multiple bend contours arising from curvature of lamellae and consequently estimation of lamellar dimensions.

LIST OF TABLES

LIST OF FIGURES

LIST OF FIGURES (cont'd.)

LIST OF FIGURES (concluded)

TABLE OF CONTENTS

TABLE OF CONTENTS (cont'd.)

TABLE OF CONTENTS (cont'd.)

TABLE OF CONTENTS (Concluded)

FORWARD

Thesis Problem

This study of particulate $CaCO_3$-polyethylene composites has the objective of investigating their microstructure, their mechanical behavior at small and large strains and the nature of microstructural failure in them. Material parameters include polymer molecular weight, volume content of $CaCO_3$ in the composite and polymer-filler interface. The $CaCO_3$ filled polyethtylene composites are compared with the unfilled polyethylene so as to study the role of filler presence in modifying polymer matrix morphology and mechanical behavior.

This study was initiated as an attempt to understand the rather remarkable properties of a novel composite prepared in a unique fashion. The behavior of this novel composite is also compared with conventionally prepared PE-$CaCO_3$ composites.

This study has a multifaceted character. In addition to various electron microscopy techniques (transmission, scanning and scanning transmission electron microscopy, deformation microscopy), other techniques used include dynamic testing, Instron testing, dilatometric studies and calorimetric studies. It is believed that such a concerted study would be most suited to shedding light on the structure and mechanical properties of semicrystalline polymer-filler composites.

Thesis Outline

In Chapter I, novel techniques to prepare improved particulate

filled polymer composites are discussed. The preparation and analysis of the novel ultrahigh molecular weight polyethylene-$CaCO_3$ composite of particular interest to this study is studied in some detail. The properties of the polyethylenes and $CaCO_3$ filler used in this study are listed.

In Chapter II we digress from polymer composites and consider the diffraction contrast imaging of polyethylene thin films in the electron microscope. Diffraction contrast mechanism is considered and its implications in evaluating features found in images of polyethylene thin films are investigated. Improved imaging techniques for damage prone polymer thin films are discussed.

In Chapter III the role of volume filling crystalline fillers on the morphology of polyethylene is investigated by optical and electron microscopy. The morphology of the polymer-filler interface is also studied.

In Chapter IV the dynamic mechanical behavior of unfilled and filled polyethylenes is investigated. The behavior of real materials is evaluated in the light of the behavior of models of viscoelastic composites as predicted by the use of the elastic-viscoelastic correspondence principle.

In Chapter V the stress-strain-dilatational behavior of unfilled and filled polyethylene is investigated. Their behavior is compared to existing models of material behavior at and beyond the yield point.

In Chapter VI the microfailure modes in unfilled and filled polyethylene is investigated by scanning electron microscopy and these

results are evaluated in the light of the dilatational and tensile properties determined in Chapter V.

In the concluding chapter, an attempt is made to highlight the findings of this study and to draw together the various conclusions of the earlier chapters. In addition unexplored areas are briefly discussed.

CHAPTER I

INTRODUCTION

1.1 Background

Polymer composites have attained great prominence in the last decade and show signs of exponential growth in the near future. In such multicomponent, multiphase materials the intent is to use additive and synergistic processes between phases to design a material with optimum properties for the end use considered. Particulate filled polymers are one class of this kind of material, other examples being glass fiber reinforced plastics and rubber modified plastics. Inorganic minerals are a common form of particulate filler which offer a substantial cost advantage when compounded with increasingly more expensive resins. The benefits of incorporating such fillers include increased heat stability, improved molding and greater stiffness and hardness. Such advantages are usually accompanied by deterioration in ultimate properties such as impact strength, elongation at break and tensile strength. This is especially true when the matrix polymer is a semicrystalline thermoplastic.

Optimization of composite properties would involve careful selection of components and improved techniques in their preparation. One way of "compatibilizing" inorganic and usually hydrophilic minerals with the commonly used hydrophobic synthetic organic polymers is by altering the surface of the filler. This is achieved either by

coating their surface with organic moieties like stearates or by the use of oligomeric and polymeric interfacial agents like organo-silanes or organo-titanates.

Such interfacial coupling agents are commonly tailored for specific polymer-filler combinations. They reduce agglomeration which arises due to electrostatic attraction between particles, improve wetting and cause increases in impact strength.

Other approaches to this problem have also been pursued. Five of these approaches will be discussed below in some detail. The first two techniques and the latter three techniques have a certain commonality in approach.

1.2 Novel Particulate Filled Composites

1.2.1 Ceraplasts. Recognizing that deleterious stress concentrations are always present at the interface of polymer and filler, Fallick and coworkers [1,2] conceived of introducing a graded interphase (see Fig. 1.1) by encapsulating the high modulus filler with a highly crosslinked polymer of tensile modulus in between that of filler and polymer. This encapsulating layer, which may even be formed during the compounding step, is covalently bonded to the polymer matrix and ionically bonded to the mineral. Hence, for the case of kaolin-polyethylene composites, the reactants which comprise the encapsulant may typically contain (1) a compound with polymerizable unsaturation also possessing amino groups which bind to the filler surface (2) a compound with two or more unsaturations to form a tightly crosslinked shroud and (3)

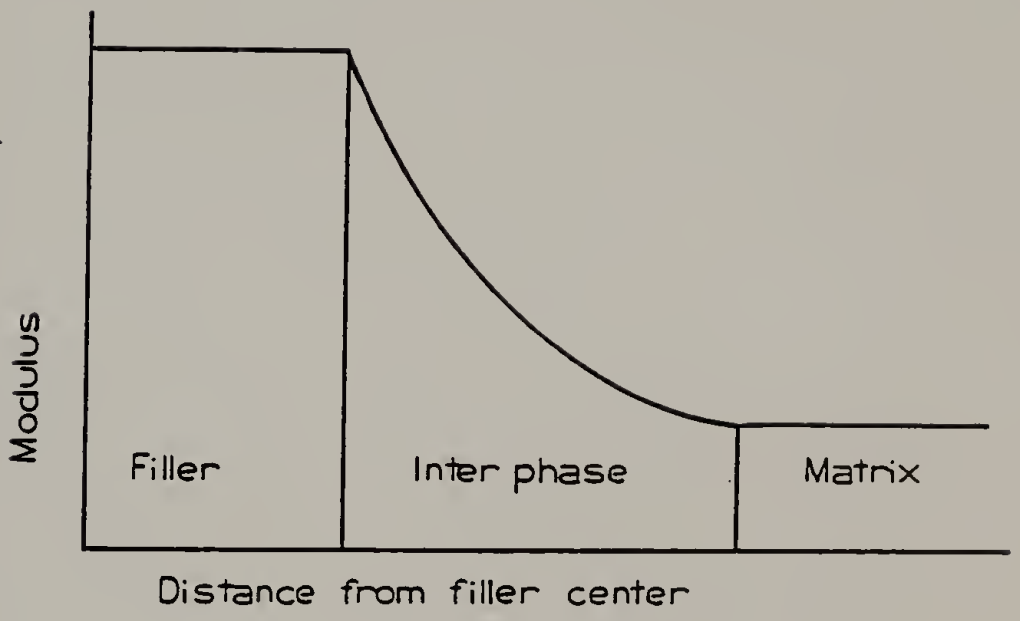

Figure 1.1 Schematic of Modulus Distance Relationship for a Polymer-Filler Composite with a Graded Interphase.

a thermally activated free radical initiator both to polymerize the unsaturated compounds and to graft the matrix polyethylene (PE) to the encapsulating layer. The thickness of this layer was estimated to be about 120 Å thick and is believed therefore to be thicker than that of conventional surface treatment procedures which are 5 - 20 Å thick. As an example of the improvement in mechanical properties, elongation at break for 40 wt% kaolin ceraplast filled PE is 60% vs 5% for untreated kaolin. Very importantly, impact strength and tensile strength improve substantially (8.5 ft-lb/in and 29.4 MPa for the Ceraplast versus 0.3 ft-lb/in and 25.5 MPa for the untreated Kaolin, respectively).

1.2.2. Maleic Anhydride Grafted PE/Clay Composites. Based on a similar approach Gaylord and coworkers [3,4] introduced maleic anhydride (MAH) along with a free radical initiator t-butyl perbenzoate to polyethylene during the process of compounding with kaolin clay and observed improved properties in the composite. This improvement was attributed to the grafting of MAH onto PE followed by covalent bond formation between the MAH moieties and hydroxyl groups on the clay forming linkages such as -Si-O-CO or Al-O-CO.

A substantial advantage was noted when the compounding step was broken up into two steps. In the first step, the process outlined above was followed using a high melt index PE. In a subsequent step this was compounded with a low melt index PE. This two-step procedure resulted in remarkable improvements over the earlier process. For

example the elongation at break for a 30 wt% kaolin-PE composite using the two step process was 25% versus 4% for the one-step process. Both impact strength and tensile strength improved very significantly (3.1 ft-lb/in vs 0.6 ft-lb/in and 33.6 MPa vs 30.1 MPa, respectively).

It is pertinent to note the connection between melt index and molecular wieght in the context of one material parameter of this study. In general the lower the melt index the higher the molecular weight of the polymer.

1.2.3. Ionic Polymerization on Filler Surfaces. D.H. Solomon and coworkers [5,6] have done quite extensive work in the field of mineral catalyzed reactions and improvements in polymer filler adhesion. Two techniques developed by them are of particular relevance; one is coating of minerals by oxyaluminum acrylates (e.g. diisopropoxyaluminum methacrylate) a procedure similar to the use of organotitanates mentioned previously. The second procedure involves rendering the surface of the mineral acidic and using the acidic surface to intitiate the cationic polymerization of vinyl and divinyl monomers resulting in an encapsulated reinforecment. These are then compounded with the polymer in a separate step. An advantage to using divinyl monomers is that the encapsulating polymer layer can be fabricated with residual unsaturation capable of yielding adsorbed peroxide species by aerial oxidation. During compounding these peroxides decompose to free radicals which graft the adsorbed coating to the matrix polymer. Such encapsulation results in higher tensile strengths in composites, e.g., a tensile strength of 29.4 MPa for 4% piperiylene coated kaolin (20

wt % filler in PE) as compared to 27.6 MPa for the untreated case. However the elongation and impact strength are not significantly improved. The oxyaluminum methacrylate coated polymers have reported tensile strengths of 29.0 MPa. However their elongation at break (430%) and impact strength are reported to compare favorably with even the unfilled polymer itself.

1.2.4. Free Radical Polymerization on Filler Surfaces. A patent assigned to Union Carbide [7] claims to improve the mechanical properties of filled compositions by pretreating the filler with a free radical polymerization initiator which adheres to the surface of the filler and then polymerizing an ethylenically unsaturated monomer onto the filler. The polymerization may be carried out to the extent that the entire matrix is polymerized in situ; on the other hand, the filler may be initially coated with a layer of polymer and then this blended with more polymer. The choice of succinic acid peroxide as free radical initiator is recommended because of good adhesion to the inorganic surface. Hence improvements in flexural strength (92.3 vs 64.8 MPa) and flexural modulus (5.7 vs 3.9 GPa) are reported for 30 wt% of 0.5 wt% polyacrylonitrile-coated glass in styrene acrylonitrile copolymer as compared to the untreated glass in SAN. However elongation at break is not significantly affected by the use of such a technique.

1.2.5. Coordination Polymerization of Ultrahigh Molecular Weight PE on Filler Surface - duPont Homogeneous Composite (DPCC). The

last approach to improved reinforced composites which shall be reviewed is the one of greatest interest to us since the product has been examined in some detail in this study. A series of patents assigned to duPont Co. [8,9,10], describe the preparation of novel composites based on ultrahigh molecular weight PE and a wide variety of inorganic fillers such as clay, talc, calcium carbonate, asbestos and the like. The essential step in the preparation involves the polymerization of ethylene onto the catalytically activated surface of minerals. The product is essentially homogeneous i.e. each particle has polymer chains associated with it and each polymer chain is uniquely associated with a filler particle. The resulting advantage of homogeneous dispersion and optimum wetting of a high volume content of filler by polymer combined with the very high molecular weight of PE matrix results in stiff, hard and tough composite materials. In addition this is perhaps the only route of dispersing reinforcing particles uniformly in ultrahigh molecular weight PE which has oustanding impact strength but an equally high melt viscosity rendering melt mixing a difficult task. The discussion that follows is from the work of Howard and coworkers [9,11,12].

Calcined kaolin clay is inherently active as an ethylene polymerization catalyst. This is undoubtedly due to the presence of trace amounts of titanium dioxide which are, as it were, catalyst sites locked into the mineral surface. However, it is found the polymerization of ethylene onto this calcined kaolinite, results in a grossly non-uniform material with low impact strength. This is because

calcined kaolinite is extensively aggregated both when dry and in a slurry. Deaggregation of calcined kaolinite can be achieved by treating the mineral surface with an organophilic reagent such as an alunimum alkyl (see Fig. 1.1).

While calcined clays are intrinsic catalysts, other mineral surfaces have to be made active by the attachment of coordination-catalysts to their surface. This can be achieved by one of two methods: (1) attaching a common coordination catalyst irreversibly to the surface and (2) by using catalysts which are essentially surface active.

Titanium oxide can be incorporated into the surfaces of many minerals by reaction with $TiCl_4$ followed by hydrolysis and heat treatment. This step must be followed by the removal of unreacted reagent since unattached polymer will form otherwise. Upon subsequent addition of an aluminum alkyl, the titanium modified mineral forms an active coordination catalyst for ethylene polymerization. Transition metals other than titanium, e.g. chromium chelates can also be used similarly; in fact, they complement the titania systems as they are more active on minerals containing silica.

The category of even greater interest is that of surface active catalysts since their use would eliminate the need for the chemical treatment and drying step necessary in the earlier procedure. Howard et al. found that tetra alkyl zirconium catalysts used alone or in conjunction with an aluminum alkyl can be used to catalyze ethylene polymerization on a variety of mineral surfaces.

Some minerals such as calcium carbonate cannot be used directly since they are either basic or have alkali metal ions absorbed in the surface. This problem can be circumvented by surface coating the mineral with acidic alumina or silica prior to the incorporation of catalyst.

The procedure for the preparation of the PE/$CaCO_3$ composites can be outlined as follows:

1. Surface treatment of $CaCO_3$ with alumina so as to render the surface acidic. The resultant particles have 1 - 2% of alumina on the surface.

2. The absorption at the surface of the particle of the tetralkyl zirconium with or without the presence of alkyl alumnimum in an inert hydrocarbon solvent such as cyclohexane.

3. Introduction of ethylene at around 100 psi at 50°C to a vigorously stirred suspension of active particles in an autoclave until completion of reaction.

4. Isolation of a product by filtering and drying. The resulting homogeneous composite is a free flowing powder a few hundred microns in diameter.

In Table 1.1 are compared properties of composites prepared by all the techniques discussed compared with those of melt blended mixtures of polymer and untreated filler.

1.3 Introduction to Thesis Problem

Very simply stated, the initial objective of this study was to

Some minerals such as calcium carbonate cannot be used directly since they are either basic or have alkali metal ions absorbed in the surface. This problem can be circumvented by surface coating the mineral with acidic alumina or silica prior to the incorporation of catalyst.

The procedure for the preparation of the PE/$CaCO_3$ composites can be outlined as follows:

1. Surface treatment of $CaCO_3$ with alumina so as to render the surface acidic. The resultant particles have 1 - 2% of alumina on the surface.

2. The absorption at the surface of the particle of the tetralkyl zirconium with or without the presence of alkyl alumnimum in an inert hydrocarbon solvent such as cyclohexane.

3. Introduction of ethylene at around 100 psi at 50°C to a vigorously stirred suspension of active particles in an autoclave until completion of reaction.

4. Isolation of a product by filtering and drying. The resulting homogeneous composite is a free flowing powder a few hundred microns in diameter.

In Table 1.1 are compared properties of composites prepared by all the techniques discussed compared with those of melt blended mixtures of polymer and untreated filler.

1.3 Introduction to Thesis Problem

Very simply stated, the initial objective of this study was to

understand why the novel composites, in particular the duPont composite (DPCC), were superior to composites prepared by conventional techniques. Three possible causes were guessed at: homogeneity of dispersion, polymer molecular weight and polymer-filler interface.

Since what made the DPCC composite unique is the polymerization of ethylene onto the surface of filler, the initial guess was to understand the role of the polymer-filler interface. However, the scope of the problem was broadened with time to include understanding of the role of polymer molecular weight, nature of $CaCO_3$ surface and filler loading upon the properties of the composite. This broadening was in some part due to the difficulty of incorporating $CaCO_3$ into ultrahigh molecular weight PE and thus preparing a fairly representative PE/$CaCO_3$ composite which differed from the duPont process only in that the polymerization was not carried out on the surface of the $CaCO_3$.

1.4 Analysis of the duPont PE/$CaCO_3$ Composite (DPCC)

The initial step in constructing a matrix of materials for further study was the analysis of the physical characteristics of the PE and $CaCO_3$ in DPCC.

1.4.1. Recovery of PE from DPCC. This was done by refluxing a 0.2% solution of DPCC in previously dried xylene for 6 hours under a nitrogen blanket. This refluxing step results in detachment of polymer from filler.

The refluxed solution was transferred to an Erlhenmeyer flask

which was maintained at around 105°C. Drops of HCl were added to the solution over a period of 10 minutes dissolving the $CaCO_3$ particles.

The polymer was then precipitated, collected on a filler and cleaned by repeated washing with dilute HCl, xylene and acetone.

The above steps were repeated until the infrared spectra of the precipitated polymer and chemical microanalysis confirmed the absence of $CaCO_3$ in the polymer.

Molecular weight characterization of the PE was performed by intrinsic viscosity and GPC. The procedure used for GPC was ASTM D1606-61. Reasonable test flow rates were attained by reducing the concentration of polymer solution to 1/10 of that recommended in the procedure. An average intrinsic viscosity of 17.9 was obtained. The selection of grade of Hifax 1900, an ultra high molecular weight PE was based on this estimate of molecular weight. A grade with intrinsic viscosity of 19 was obtained. High temperature GPC of these two PE's was performed. The molecular weights reported (Table 1.2) are from the GPC results and is based on column calibration with a NBS standard linear PE sample.

1.4.2. Particle Size Estimate. Separation of $CaCO_3$ particles from the polyethylene was performed quite simply by burning the PE away in a flame.

Particle size analysis was performed on a scanning electron microscope using the procedure of approximating particle diameter by the length of a horizontal line which bisects the projected area of

the particle. The weight average diameter was estimated by the formula

$$\overline{Dw} = \frac{\Sigma\ D_i^4}{\Sigma\ d_i^3}$$

where the summation is over the number of particles counted. A weight average diameter of 2.3 μ with maximum particle size of 15 μm was determined. Based on this measurement, a choice of $CaCO_3$ was made from commercially available grades.

1.4.3. Description of System of PE and $CaCO_3$ Studied. So as to investigate the role of polymer molecular weight, filler loading and polymer-filler interface, three different linear polyethylenes, and two types of $CaCO_3$,one untreated and the other treated (see below), were investigated.

The three linear PE's are Alathon® 7050 ($\overline{M}w$ = 59,000, $\overline{M}w/\overline{M}n$ = 3), Marlex® 6003 ($\overline{M}w$ = 200,000, $\overline{M}w/\overline{M}n$ = 7-13) and Hifax® 1900 ($\overline{M}w$ = $2x10^6$, $\overline{M}w/\overline{M}n$ = 4.6). Together they cover a large spectrum of molecular weight of polymer.

Atomite, a grade of $CaCO_3$ (Dw = 2.5 μm, D_{max} = 40 μm) sold by Thompson, Weinman & Co., was selected from available grades of $CaCO_3$ as being the closest to the $CaCO_3$ in DPCC. Quite fortunately Atomite was also available treated with 2% KR-TTS®, a coupling agent, from the same supplier (Atomite Code A).

KR-TTS® (Isopropyl triisostearyl titanate), available from Kenrich Petrochemicals Inc., is a coupling agent of the type described earlier in this chapter. The isopropyl group reacts with hydroxyl groups of

the $CaCO_3$ surface whereas the isostearyl chains are organophilic. This fact is claimed to improve polymer filler wetting.

A description of the materials described above is given in Table 1.2.

1.5 References

1. R.W. Hausslien and G.J. Fallick, Appl. Polymer Symposia, 11, 119, 1969.
2. H. J. Bixler and G.J. Fallick, U.S. Patent 3,471,439 (October 1969).
3. N.G. Gaylord and A. Takahashi, ACS Preprints, Organic Coatings and Plastics, Chemistry Div., 46, 95, 1982.
4. N.G. Gaylord, U.S. Patent 4,071,494 (January 1978).
5. D.G. Hawthorne, J.H. Hodgkin, B.C. Loft and D.H. Solomon, J. Macromol. Sci., A8(3), 649, 1974.
6. D.G. Hawthorne and D.H. Solomon, J. Macromol. Sci., A8(3), 659, 1974.
7. A.C. Frechtling, N.W. Johnston, R.G. Shaw, U.S. Patent 3,971,753 (July 1976).
8. R.D. Lipscomb, U.S. Patent 3,950,303 (April 1976).
9. E.G. Howard Jr., U.S. Patent 4,097,447 (June 1978).
10. R.L. Adelman and E.G. Howard, U.S. Patent 4,151,126 (April 1979).
11. E.G. Howard, R.D. Lipscomb, R.N. McDonald, B.L. Glazar, C.W. Tullock and J.W. Collette, Ind. Engr. Chem., Prod. Res. Dev., 20, 421 (1981).
12. E.G. Howard, B.L. Glazar and J.W. Collette, Ind. Engr. Chem. Prod. Res. Dev., 20, 429 (1981).

TABLE 1.2

CHARACTERISTICS OF POLYETHYLENES AND $CaCO_3$ USED IN THIS STUDY

A. Polyethylenes	$\bar{M}w$	$\bar{M}w/\bar{M}n$
Alathon 7050 (E.I. duPont de Nemours & Co.)	57,000	3
Marlex 6003 (Phillips Petroleum Co.)	200,000	7-13
Hifax 1900[a] (Hercules Powder Co.)	2×10^6	7.6
duPont PE/$CaCO_3$ Composite[a]	1.5×10^6	3.6

B. $CaCO_3$	$\bar{D}w(\mu m)$	D_{max} (μm)
Atomite (Thompson, Weinman & Co.)	2.5	45
Atomite Code A (2% TTS) (Thompson, Weinman & Co.)	2.5	45
duPont PE/$CaCO_3$ Composite	2.3	15

C. Coupling Agent

Isopropyl Trisostearyl titanate (KR-TTS) (Kenrich Petrochemicals Inc.)

[a]GPC analysis of these samples by Springborn Laboratories, Enfield, CT.

CHAPTER II

IMAGING OF POLYETHYLENE BY DIFFRACTION CONTRAST

2.1 Introduction

In this chapter the reasons for image contrast in electron microscopy (EM) images of thin films of polyethylene are examined. Of particular interest are diffraction contrast features which arise due to the crystallinity of the film and require that electron flux through the film be controlled so as to avoid radiation damage of the very susceptible polymer film. Scanning transmission electron microscopy is particularly suited for such work in polymers.

While this work grew out of an interest in the morphology of PE/$CaCO_3$ composite thin films, the results which are presented have rather more general ramifications. Electron microscopy studies of undamaged polyethylene thin films are still rare in the literature and the development of techniques such as those presented here will most certainly contribute to a clearer perspective of the morphology of semicrystalline polymeric materials. In particular the imaging of crystal defects and the study of crystal deformation will need the development of diffraction contrast techniques.

One imaging condition which was developed, 110/200 annular STEM Dark Field, is of particular interest, since it distinguishes polyethylene lamellae lying edge-on to the electron beam. This allows the determination of lamellar orientation at interfaces, something of use in resolving details of the PE-$CaCO_3$ interface.

2.2 Background

There is presently a sizeable effort to study microstructural organization in melt crystallized polyethylene. Such inquiries, typically using scattering methods (small angle x-ray scattering, small angle neutron scattering) and microscopy have the objective of determining the ways macromolecules organize themselves into lamellar crystals and these lamellae into higher order structures such as spherulites.

Electron microscopy studies of polyethylene usually involve either replication techniques or staining techniques. These methods are employed because it is difficult to prepare thin sections of polyethylene and the polymer is rapidly damaged by the electron beam at the current densities usually employed in conventional transmission electron microscopy (CTEM)[1]. This deterioration has two aspects: (1) loss of crystallinity and (2) sample distortion resulting from thinning of lamellae in the chain axis direction and expansion in the other directions. Therefore, electron damaged specimens do not convey an accurate image of the micromorphology [2]. Staining, especially that involving chlorosulphonation [3] can prevent much of the distortion of the thin film during exposure and consequently detailed examination of the local morphology primarily by use of mass thickness contrast and selected area diffraction (SAD) is possible. Staining techniques along with replication and small angle scattering have been used to understand the effects of crystallization temperature, molecular weight, pressure and other intrinsic and extrinsic parameters on

the micromorphology of polyethylene [4,5,6]. Chlorosulphonation, however, does result in apparent lamellar thinning [4]. The study of untreated crystalline thin films or sections has advantages not realizable with treated or replicated specimens. Most importantly the sample crystallinity permits the use of a variety of microscopic imaging modes, Bright Field imaging (BF), Dark Field imaging (DF) and Micro Beam Diffraction (MBD), to obtain complementary images as well as crystallographic orientation of local regions in the film [7].

For radiation sensitive polymers, Scanning Transmission Electron Microscopy (STEM) techniques facilitate consecutive imaging of a region of a polymer crystalline thin film. This makes it possible to vary the diffraction conditions and therefore study crystalline contrast mechanisms in polymeric thin films, a procedure which is quite difficult with CTEM. The advantages of STEM techniques on polyethylene have been demonstrated by Vesely et al. [8] as well as in papers from this laboratory [9,10].

The objective of this paper is to examine crystalline contrast in thin films of polyethylene and to note deductions that can be made about the lamellar structure.

2.3 Experimental

Thin films of Hifax® 1900, an ultra high molecular weight linear polyethylene ($\overline{M}w = 2.0 \times 10^6$, MWD = 4.6) were prepared for microscopy by the following method: a dilute solution of the polyethylene (0.2%) was prepared in previously filtered, dried xylene and drops of the hot

solution placed onto the surface of glycerol kept at 140°C. After all the xylene had evaporated, the glycerol and polyethylene film were transferred to a Mettler FP-2 hot stage. The film was then remelted at 160°C for fifteen minutes and then rapidly (1°C/sec) cooled to 120°C. The crystallized thin films were then transferred onto distilled water, washed and then picked up on grids. At all stages of preparation, care was taken to avoid oxidation by using a nitrogen blanket.

BF and DF CTEM and STEM of the thin polyethylene films were performed using a JEOL 100 CX 'TEMSCAN'. For CTEM, micrographs of specimen areas with minimum electron damage were obtained by focusing on an area, translating to an adjacent area and recording the image on Kodak SO163 plates using approximately 60% of the crystal lifetime dose. DF imaging was obtained by tilting the incident beam so that the objective aperture selected a portion of the reflection of choice.

STEM BF and DF imaging was utilized quite extensively in this study. So as to limit incident beam divergence, a 20 μm diameter second condenser aperture was used. Details of the optics are given in the section on STEM imaging. Polaroid type 55 P/N film was employed.

2.4 CTEM Imaging: Diffraction Contrast

Figure 2.1a is a CTEM BF image of a part of a polyethylene spherulite. The spherulite is of the banding type with alternate bands of lamallae oriented flat and edge-on with respect to the

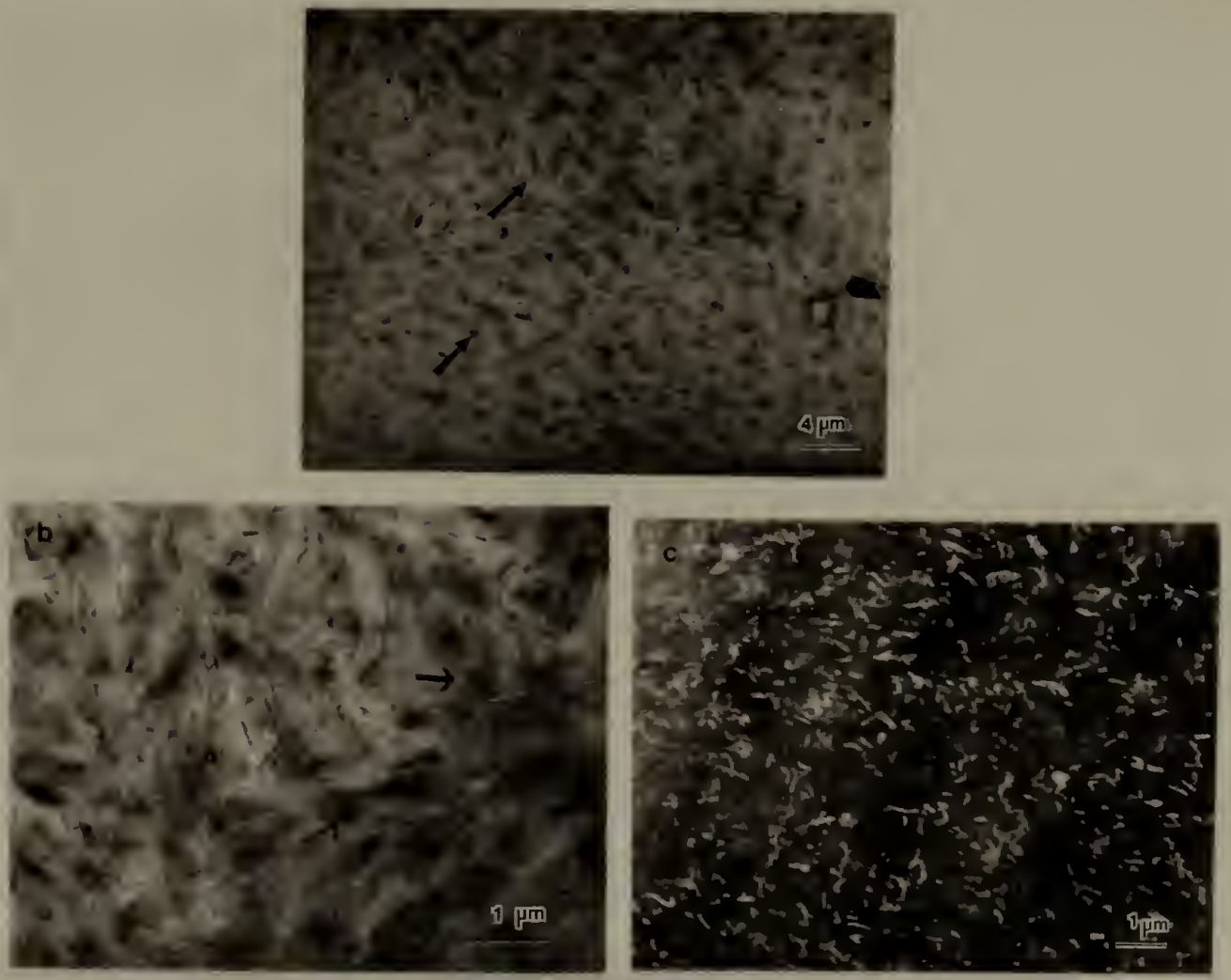

Figure 2.1 (a) Bright Field CTEM image of Hifax Thin Film. Arrows indicate banding. (b) BF CTEM image of Hifax Thin Film. At Region A, lamellae are clearly resolved. Arrows indicate bend contours. (c) 110/200 DF CTEM image of Hifax thin film.

electron beam. An important feature of this micrograph is the good definition of lamellae (see region A) whenever the orientation of the crystal is (100) i.e. the electron beam is perpendicular to the $\underset{\sim}{b}$ and $\underset{\sim}{c}$ axes which are in the plane of the film. The observation of lamellae must be remarked upon because until now the resolution of nearly undamaged lamellae in unstained, spherulitic films is not noted in the literature. It is believed that this kind of resolution is achieved with Hifax because of its high, amorphous content (approximately 40%) which lies predominantly between the lamellae. The contrast varies depending upon the orientation of the lamellae, i.e., it is light for lamellae viewed edge-on (100) and dark for lamellae viewed flat (001). Figure 2.1b is a higher magnification micrograph of an adjacent region. Many of the (001) oriented regions have two or three lines intersecting at a common point giving the impression of a cross or a star. One objective of this study is to discuss the cause for this type of contrast. It will be shown that the apparent "crosses" are band contours which arise due to the curvature of lamellae.

The diffraction or Bragg condition can be expressed as a vector equation

$$(\underset{\sim}{k} - \underset{\sim}{k}_0 = \underset{\sim}{g})$$

where $\underset{\sim}{k}_0$ and $\underset{\sim}{k}$ are unit vectors of the incident and scattered beams and $\underset{\sim}{g}$ the reciprocal lattice vector for the reflection considered. For crystals of finite thickness, scattering occurs for small deviations ($\underset{\sim}{s} > 0$) from the Bragg condition. Fig. 2.2a shows schematically the relation between $\underset{\sim}{k}_0$, $\underset{\sim}{k}$, $\underset{\sim}{g}$ and $\underset{\sim}{s}$. In Figure 2.2b is shown

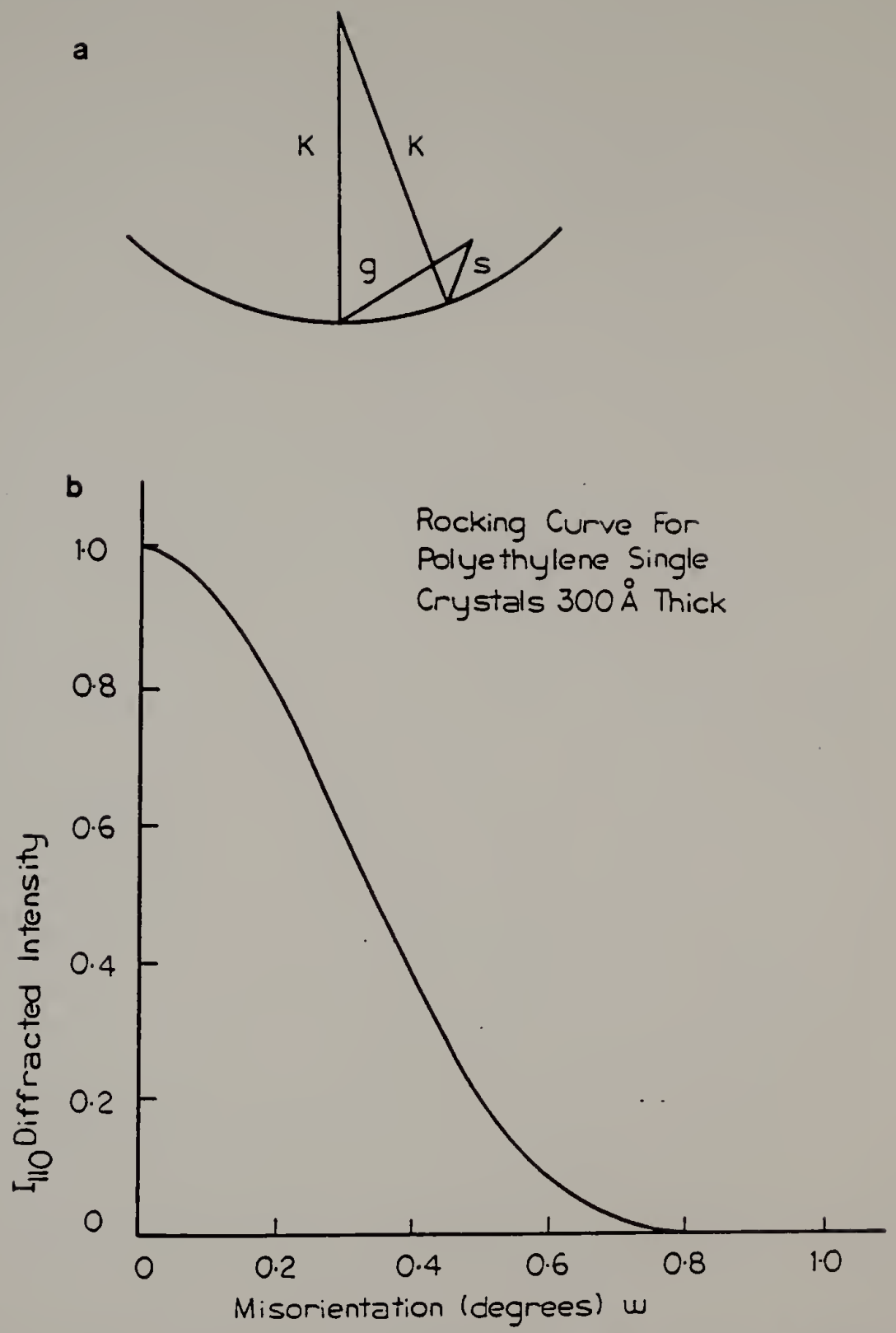

Figure 2.2. (a) Definition of the deviation parameter s in terms of the reciprocal lattice vector g and the unit vectors k and k_0. (b) Rocking curve for diffracted intensity from (110) planes in a 300 Å thick polyethylene crystal at 100 KeV.

the 'rocking'curve for the PE (110) reflection for a lamellar thickness of 300 A°. It is seen that for a 300 A° thick lamella, the intensity of the diffracted beam falls off to zero for one degree of misorientation (ω). A feature of CTEM is that since the incident beam has a very small divergence there is, for a given crystal orientation, essentially just one deviation vector $\underset{\sim}{s}$ defined for each $\underset{\sim}{g}$.

It can be shown that the intensity of a Bragg reflection can be expressed as:

$$I_g = KF_g^2 \frac{\sin^2(\pi N_3 a_3 S_g)}{\sin^2(\pi S_g a_3)} \qquad (2.2)$$

where F_g and S_g are the structure factor and deviation parameter respectively for the reflection considered, N_3 the number of unit cells in the direction of beam, a_3 the magnitude of the unit cell vector in the beam direction and K a constant of proportionality.

For the BF image, the intensity can be expressed as

$$I = I_o - \sum_g I_g \qquad (2.3)$$

where I_o is the incident intensity and the summation is over all the Bragg reflections active for the particular crystal orientation.

Table 2.1 presents calculated structure factors for the prominent PE reflections for 100 KeV electrons. The three strongest reflections are from the (110), (200) and (020) planes. Therefore, regions of crystals with (001) orientation, i.e. with the chain direction parallel to the beam, will generally appear darker in bright field

Table 2.1

Structure Factors for Selected Polyethylene Reflections

$hk\ell$	$d_{hk\ell}$ Å	F(Å)	$F^2(Å)^2$	F^2/F^2_{110}
110	4.10	9.59	91.97	1.00
200	3.69	8.28	68.56	0.74
020	2.46	5.28	27.88	0.30
002	1.27	4.24	17.97	0.19
201	2.09	3.96	15.68	0.17
011	2.25	3.87	14.97	0.16
121	1.72	3.61	13.03	0.14
400	1.85	3.55	12.60	0.14
031	1.38	3.32	11.02	0.12
310	2.20	3.18	10.11	0.11

than crystals in any other orientation (assuming for comparison equal film thickness of each region and all $S_g = 0$ of a particular crystal orientation).

An idealized representation of these two types of regions is shown in Fig. 2.3a. The central lamella is oriented (001) while the other lamellae are oriented (100). In between the lamellae are amorphous regions (shaded). These two orientations belong to the (hoℓ) family of orientations possible for such films since the fast growth direction (b axis) is approximately restricted to the plane of the film [11]. The diffraction patterns for the two orientations are given in Figure 2.3b and the relative intensity profile in BF is shown in Fig. 2.3c.

The attenuation of the beam by the amorphoous sections is given by

$$I = I_o \, e^{-S_p \rho t}$$

where S_p is the scattering cross-section, ρ the density of amorphous polyethylene and t the thickness of film.

The idealized representation of Figure 2.3 explains many of the contrast features in thin film samples, in particular the concentric banding observed in electron micrographs of thin PE films. This rise of contrast may be compared to the similar phenomena of extinction bands in optical microscopy arising due to differing amounts of polarized light rotation by differently oriented PE crystals.

Figure 2.4 explains the origins of bend contours. The central lamella is now curved with just its center oriented exactly (001). Since a misorientation of greater than about 1° places the crystal out

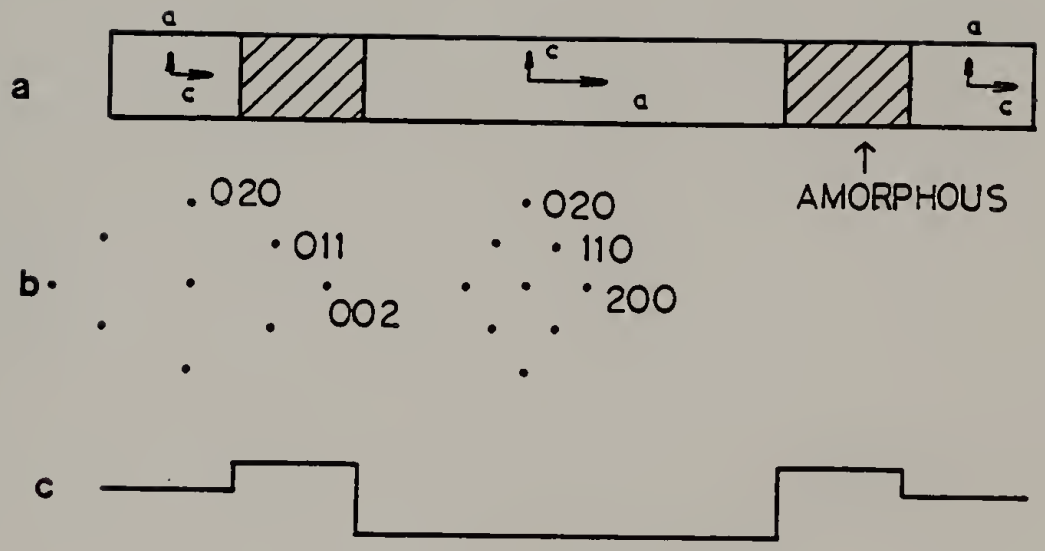

Figure 2.3 (a) Idealized representation of a PE thin film (b) The diffraction patterns for the two crystal orientations and (c) The relative intensity profile in BF for such a film.

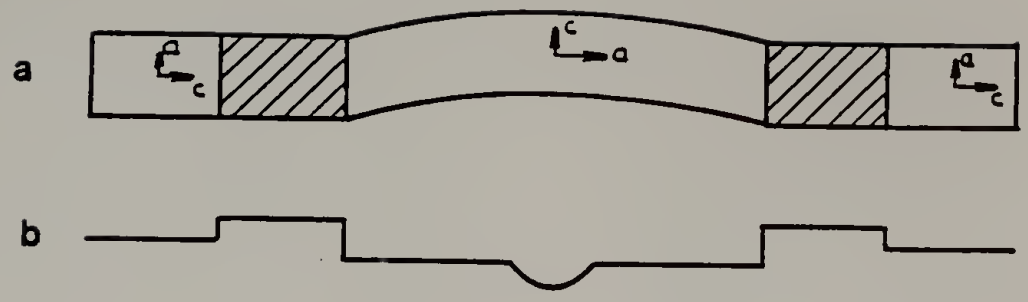

Figure 2.4 (a) Idealized representation of a curved lamella (central lamella) and (b) The effect on relative intensity profile due to curvature.

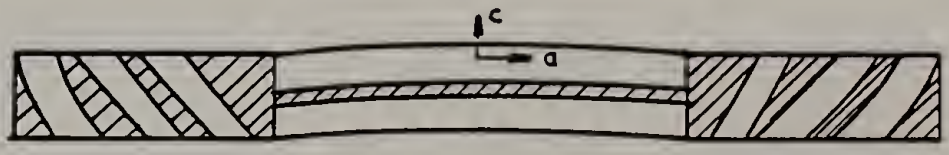

Figure 2.5 A more realistic representation of a section of a PE thin film.

of the diffraction condition, instead of an image of uniform contrast, (110), (200) and (020) bend-contours will be formed (Figure 2.4b). While axially symmetric orientation of curved lamellae with respect to the incident beam will give rise to multiple symmetric bend contours, asymmetric bending and tilting will reduce the number of simultaneously occurring reflections. Symmetric bend contours are shown in Figure 2.1b as well as in the STEM DF micrographs Figures 2.8a and 2.8b.

Lateral dimensions of bend contours range up to approximately 3000 Å. On the other hand continuously imaged contours (along b axis) are approximately a micron long. This would present the structure of lamellae in these films to be ribbon-like. Given the various lamellae and overall film dimensions it is seen that lamellae oriented (001) are likely stacked, while the (100) oriented lamellae span the film thickness and exhibit curvature in the cross-section of the film. Figure 2.5 shows such a representation of the thin film. Figure 2.1c is a 110/200 DF image of PE. Since just a fraction of the total intensity is responsible for the image, the intensity is much lower.

2.5 STEM Imaging of Lamellae

Imaging of radiation sensitive polymers is much easier with STEM primarily because of image intensification and higher collection efficiency of scattered electrons. Another advantageous feature that shall be demonstrated here with advantage is the flexibility of imaging. It is possible to combine various optical parameters on the electron microscope in STEM to permit novel imaging modes. Use of the

sample z-lift and intermediate lens current control permits control of the camera constant. In addition, the use of a modified beam stop tip and various SAD apertures effectively converts the photomultiplier tube detector into a number of detectors with differing geometry and size. The SAD aperture is convenient in this microscope because it is far enough away from the sample for the scattered beam to diverge sufficiently from the transmitted beam.

Figure 2.5a-d shows the different optical arrangements utilized for BF and DF STEM. For BF, diffraction contrast is provided by blocking almost all the scattered electrons with an SAD aperture. For n-beam annular DF, the main beam is blocked by a modified beam stop and all other reflections out to the cutoff (SAD or column) are collected. For 110/200 annular DF, the main beam as well as all outer reflections are blocked using the beam stop and a larger diameter SAD aperture. For 002 annular DF the intermediate lens current is adjusted using the intermediate lens free lens control to effectively decrease the camera constant so as to collapse all the inner reflections into the beam stop effectively allowing 002 and other weaker outer reflections to form the image.

Four consecutively obtained images from the same area are shown in Figure 2.7. The arguments for contrast mechanisms presented in the CTEM discussion hold with two qualifications. Complete azimuthal range of each reflection is imaged contributing to higher intensity and since the incident beam is quite divergent there is a distribution of $\underset{\sim}{S}_g$ and the Bragg condition is effectively relaxed permitting more

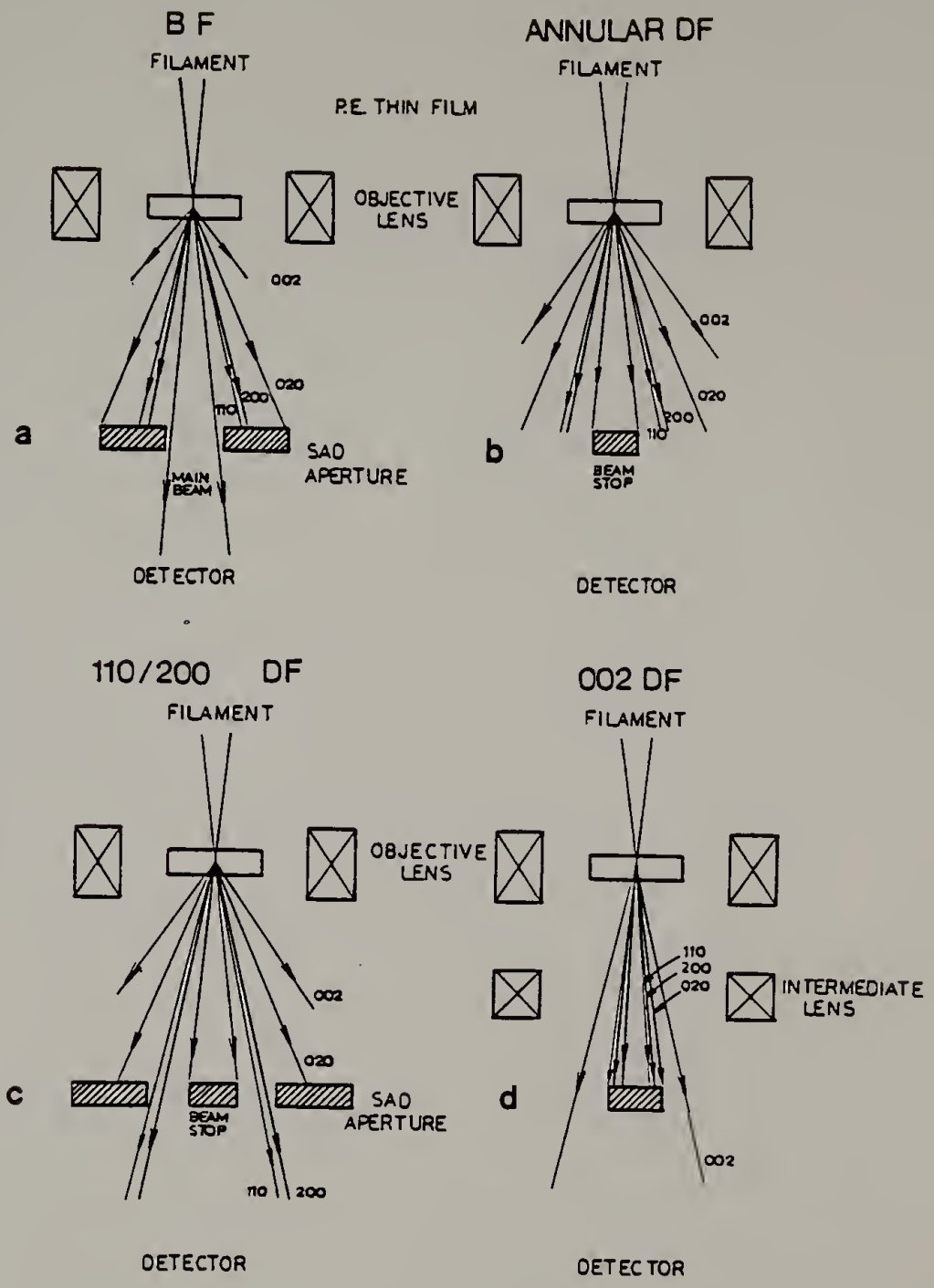

Figure 2.6 Different STEM optical arrangements: (a) BF (b) n-beam annular DF (c) 110/200 annular DF (d) 002 annular DF.

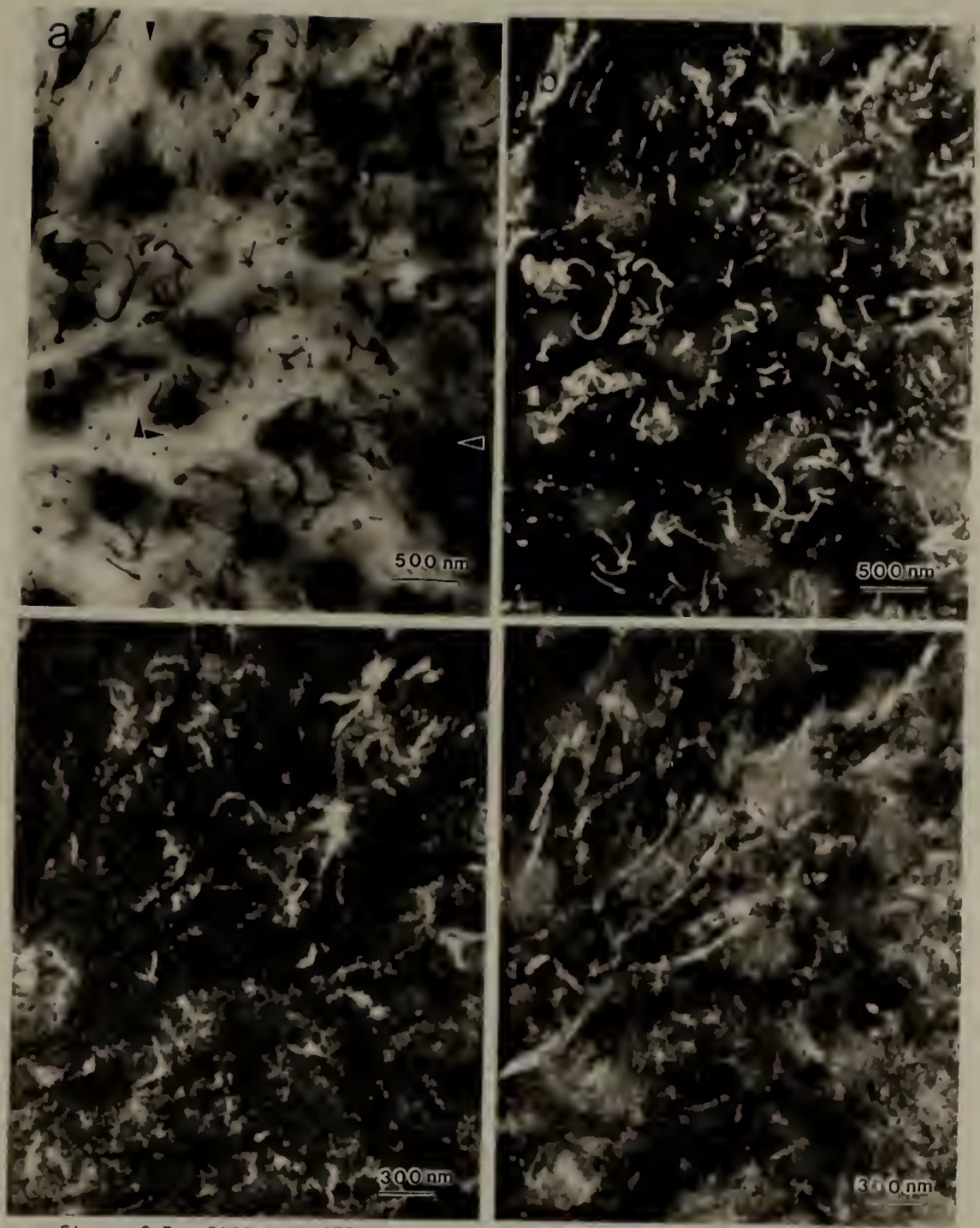

Figure 2.7 Different STEM images of the same region of PE thin film. (a) BF; (b) annular DF; (c) 110/200 annular DF and (d) 002 annular DF. Micrographs 8c and 8d are from area indicated within arrows in 8a.

diffracting regions for each reflection.

In Figure 2.7cis shown the annular 110/200 DF STEM image. The lamellae are clearly imaged as dark regions along their length when oriented approximately (100). This reverse contrast arises because the strong (020), (011) and (002) reflections for this orientation are removed from the image by the SAD aperture and consequently the image exhibits the lowest intensity for these regions.

Figure 2.8a and 2.8b are STEM DF micrographs illustrating "star" band contours arising due to curvature of lamellae, the causes of which have been discussed earlier. The contours in both figures can be labelled consistent with the fact that b axis is the growth direction. The measured angle between the (110) and (200) contours of 60° compares with the calculated value of 56° favorably. In Figure 2.8b, the dark lines imaged correspond to lamella viewed edge-on whereas the extinction contours correspond to lamellae in the plane of the film. From the dimensions of the lamellae, the ratio of the b/a axis is again about 3:1.

2.6 Discussion

It is quite worthwhile to compare this EM investigation utilizing various modes of diffraction contrast to results from studies using staining and replication techniques. An obvious drawback is that diffraction contrast imaging on semicrystalline polymer films is much more limited in quantitative terms. The extensive studies of Bassett et al. [4,12,13] and those of Voigt-Martin et al. [5] investigated a

Figure 2.8 (a) annular DF STEM image of PE lamella (b) 110/200 annular DF STEM of PE thin film illustrating (100) lamellae in reverse contrast (dark lines). Bend contours are labelled consistent with lamellar growth direction.

range of molecular weights and different crystallization temperatures. In both studies thin sections of PE crystallized under conditions similar to those employed in this study were found to exhibit random oriented, highly curved lamellae. While the lamellae are indeed curved, Figure 2.1a indicates that the morphology is not random and this could be ascribed to the fact that the samples in this study were initially solvent cast and remelted.

Bassett [13] has shown the gradual progression of the lamellar structure from ridged sheets to curved lamellae with a decrease in crystallization temperature. These same conclusions have also been arrived at by Voigt-Martin et al. [5] who have noted the independent effects of molecular weight and temperature on the morphological ordering.

The observation of the "star" contours also demonstrates the curvature of lamellae for lamellae lying in the plane of the film (J.-F Revol et al. [14] have also noted the presence of the crossing lines in films of nascent polyethylene which we have now identified as bend contours).

From the measured thickness of the contours and considering the fact that the rocking curve allows a maximum misorientation of 1 degree, the curvature of the lamellae is seen to be about 0.01 °/Å. In Figure 2.8a the lamella has more curvature perpendicular to the b axis than along it. Secondly, the formation of bend contours has another implication. For the samples studied, the contours suggest that the basal plane are of the {00ℓ} family and no molecular tilt

exists. Voigt-Martin et al. have observed molecular tilt to the extent of 18° in lower molecular weight samples crystallized at low undercoolings.

As for the matter of crystallite dimensions as noted earlier, average widths of 0.3 microns, lengths of about 1 micron and thicknesses of 300 - 500 Å are observed. It must be noted that the width of these lamellae is in remarkable agreement to the value of the ratio of the diffusion coefficient of impurities in the melt to the growth rate of the spherulite (δ) predicted by Keith and Padden [15]. This is rather fortuitous because the characteristics of the Hifax® polyethylene considered in our study are quite different from the polyethylenes used by Keith and Padden. Bassett and Hodge [4] have noted wide disagreement between lamellar widths and extrapolated estimates of δ.

It is therefore apparent that the imaging of untreated films have certain important advantages not obtainable by other techniques. In addition to those demonstrated in this study, other largely unrealized advantages exist: dislocation imaging and movement and monitoring of crystal transformation under deformation. It must however be kept in mind that cumulative electron damage with the passage of time will remain a limitation on the use of STEM techniques which will prevent continuous monitoring for long periods of time.

2.7 Conclusions

This chapter investigates features of diffraction contrast imaging of thin films of a high molecular weight polyethylene crystallized at

120°C. While both conventional transmission electron microscopy (CTEM) and scanning transmission electron microscopy (STEM) imaging has been carried out, the advantages of STEM are emphasized including reduced sample damage and flexibility of imaging conditions. In particular the annular 110/200 DF STEM mode has the advantage of clearly delineating lamellae aligned nearly edge-on to the electron beam.

Diffraction contrast analysis explains difference in contrast at differently oriented regions of the film. In addition extinction contours are observed, indicating curvature of lamellae. Average dimensions of lamellae are observed to be 300 - 500 Å thickness, 0.3 micron width and 1 micron length.

2.8 References

1. E.S. Sherman, W.W. Adams, E.L. Thomas, J. Mat. Sci., 16, 1 (1981).
2. D.T. Grubb, J. Mat. Sci., 9, 1715 (1974).
3. G. Kanig, Kolloid Z. und Z. Polymere, 251, 782 (1973).
4. D.C. Bassett and A.M. Hodge, Proc. R. Soc. Lond. A. 359, 121 (1978).
5. I.Y. Voigt-Martin, E.W. Fischer, L. Mandelkern, J. Polym. Sci., Polymer Physics, 18, 2347 (1980).
6. D.T. Grubb and A. Keller, J. Polym. Sci., Polym. Phys, 18, 207 (1980).
7. P. Hirsch et al.,"Electron Microscopy of Thin Crystals", (1965).
8. A. Low, D. Vesely, P. Allan and M. Bevis, J. Mat. Sci. 13, 711 (1978).

9. V.P. Chacko, F.E. Karasz, R.J. Farris and E.L. Thomas, J. Polym. Sci, Polym. Phys., to be published.

10. E.S. Sherman and E.L. Thomas, J. Mat. Sci., 14, 1109 (1979).

11. P. Allan and E.M. Bevis, Philos, Mag. 35, 2, 405 (1977).

12. D.C. Bassett, "Principles of Polymer Morphology", Cambridge (1981).

13. D.C. Bassett and A.M. Hodge, Proc. R. Soc. (Lond.), A 377, 25-71 (1981).

14. J.-F Revol, W. Luk and R.H. Marchessault, J. Crystal. Growth, 48, 240 (1980).

15. H.D. Keith and F.J. Padden Jr., J. Appl. Phys., 34(8), 2409 (1963).

CHAPTER III

THE MORPHOLOGY OF $CaCO_3$-FILLED POLYETHYLENES

3.1 Introduction

In this chapter the morphology of filled and unfilled polyethylenes is investigated by optical and electron microscopy and by calorimetry. This investigation is of primary importance since it is clear that an ideal objective is to relate the mechanical behavior of filled polyethylenes to the morphology.

The morphology of filled polyethylenes is expected to be different from that of the unfilled PE for two prominent reasons. The first is the presence of a crystalline substrate during the crystallization process. The effect of impurities on crystallization is well known; when the impurity has a crystalline character, it may, besides making crystallization thermodynamically favorable, influence the crystal structure of the growing phase.

Another role of the filler is that of a volume filling entity. This would then present a discontinuous space to the crystallizing polymer instead of a continuous melt where, under certain conditions, spherulites are formed.

Transmission Electron Microscopy of such thin composite films offers many advantages in such a study. While the availability of lamellar resolution is perhaps the most important one, it is also possible to obtain diffraction patterns from interfaces, making it possible to study filler polymer interaction.

3.2 Background

Microstructural investigations on filled semicrystalline polymers have been carried out previously. Grigor'ev et al.[1] concluded from their studies on TiO_2 filled PE that the size of both spherulites and crystallites was affected by presence of filler. Dolakova and Hudecek [2] in studies on glass bead and mineral filled PE observed fibrillar links extending from the particles into the matrix in micrographs of impact fracture surfaces. Gahde et al [3] observed lamellar growth perpendicular to the interface upon studying certain silane modified kaolin filled PE.

Much work has been done on the crystallization of various polymers in the presence of heterogeneous surfaces and substrates. The phenomenon of trans crystallinity at high energy surfaces and the properties of the transcrystalline layer have been investigated by Schonhorn [4,5]. Such studies have also been carried out by Fitchmun and Newman [6] and Chatterjee [7].

While Schonhorn stresses the importance of high energy surfaces in order for transcrystallinity to occur, Fitchmun and Newman and Chatterjee found that even low energy surfaces could initiate transcrystallinity and note that thermal conditions can affect transcrystalline growth. Binsbergen [8], Kargin et al. [9] and Chatterjee [7] also investigated the nature of polymer crystallization nucleating agents. Crystallinity of the substrate was found to be a necessary condition for nucleation by Binsbergen and Chatterjee while

Kargin et al. note that close lattice match between the polymer and the substrate was not a criterion for effective nucleation. Most of the above studies used primarily optical microscopy to examine the effect of heterogeneous phase presence in the crystallized polymer while a few used scanning electron microscopy.

In a recent study Rybnikar [10] investigated the effect of talc, kaolin and glass bead filler presence on the morphology of PE by electron microscopy. Single crystals of PE were melted and recrystallized on basal surfaces of filler particles. Ordered lamellae, oriented perpendicular to the filler surface were observed. On the basal surface of talc, pseudohexagonal arrangement of PE lamella was observed implying that rows of equally charged ions in the talc crystal have an effect on ordering molecular segments in the PE chains.

In our study we have primarily used transmission electron microscopy to understand changes in polymer morphology both in the vicinity of and away from the filler particle. This study is part of a wider investigation of the structure and mechanical properties of filled polyethylene.

3.3 Experimental

3.3.1 Materials. The materials used are described in Chapter I.

3.3.2 Sample Preparation. 1. Thin films: Thin films were prepared for transmission electron microscopy by the following method: Dilute solutions of the polyethylene (0.2% by weight of polymer) were

prepared in filtered, dried xylene and drops of the hot solution were introduced onto the surface of glycerol kept in a Petri dish at 140°C. After all the xylene had evaporated, the glycerol and the polyethylene thin film were transferred to a Mettler FP-2 hot stage where the film was remelted at 160°C for fifteen minutes and then cooled to 120-123°C. The crystallized thin films were then transferred into distilled water, washed and then picked up on grids. At all stages of preparation care was taken to avoid oxidation by using a nitrogen blanket. Thin films were prepared from Hifax, the duPont PE/$CaCO_3$ composite (DPCC) and a mixture of 70% Hifax and 30% $CaCO_3$ using the above procedure.

2. Bulk Sections: For scanning electron microscopy, uniform sections less than 1 mm thick were cut from compression molded plaques of filled polyethylenes blended in a two roll mill. These sections were subsequently melted in the temperature range of 150-175°C (depending upon the molecular weight of the polymer) for thirty minutes and then crystallized at 120°C for twenty minutes. These freely crystallized surfaces were sputter-coated with a 15-20 nm layer of gold.

For optical microscopy, microtomed sections were placed on glass slides under cover slips, melted and recrystallized as in the case of bulk sections. Some nucleation by the coverslip and glass slide surfaces occurs but is equally present for all the samples thus examined, and differences between samples are substantial.

Bright field (BF), dark field (DF) and scanning electron microscopy SEM were performed using a JEOL 100 CX "TEMSCAN" in both

the conventional transmission electron microscopy (CTEM) mode and in the scanning transmission electron microscopy (STEM) mode. Annular 110/200 STEM-DF was performed on the thin films (see section on STEM in this chapter for the optical arrangement). Micrographs of specimen areas with minimum electron damage were obtained by focusing to the required area and recording the image using approximately 60% of the measured radiation lifetime.

Optical micrographs were obtained on a Carl Zeiss polarising microscope with a Polaroid attachment. A summary of the experimental methods is given in Table 3.1.

3.4 Results

3.4.1 Optical Microscopy. Figures 3.1a-d are BF transmitted optical micrographs which document the changes in morphology occurring with increasing loadings of filler. In Figure 3.1a the spherulitic nature of Marlex® PE is well developed. However the introduction of as little as 5 wt% $CaCO_3$ filler changes the morphology quite drastically, as seen in Figure 3.1b. Spherulitic ordering disappears and in its place there is a rather "grainy" morphology. The arrows point to the larger $CaCO_3$ particles (particles as large as 45 μm are present in this grade of $CaCO_3$). This granularity increases with filler loading as seen in Figure 1c of 40 wt% $CaCO_3$ filled Marlex®. DPCC (Figure 3.1d, 63.5 wt% $CaCO_3$) is quite similar to the filled Marlex® samples. These features were found to be quite general for the polyethylenes examined and are typical of such mixtures [11].

TABLE 3.1

SUMMARY OF MICROSCOPY TECHNIQUES

Experimental Method	Optical Microscopy	TEM, STEM Micro-diffraction	SEM	DSC
Sample Description	Microtomed Sections	Very Thin Films	Sections	Sections
Sample Preparation	Optical Microtomy, Melt Recrystallized on Glass Slide	Solution Casting, Melt, Recrystallized on Glycerol	Melt, Recrystallized Free Surface, Gold Coated	Annealed 80-85°C for Two Hours
Sample Types	Marlex 6003 Marlex 6003 + 10% Atomite Marlex 6003 + 40% Atomite duPont PE/$CaCO_3$ composite (63% $CaCO_3$)	Hifax duPont PE/$CaCo_3$ Hifax + 30% Atomite	Marlex 6003 Alathon 7050 + 40% treated Atomite Marlex 6003 + 40% treated Atomite duPont PE/$CaCO_3$	All Unfilled Polyethylenes Alathon 7050 + 40% Atomite Marlex 6003 + 40% Atomite duPont PE/$CaCO_3$

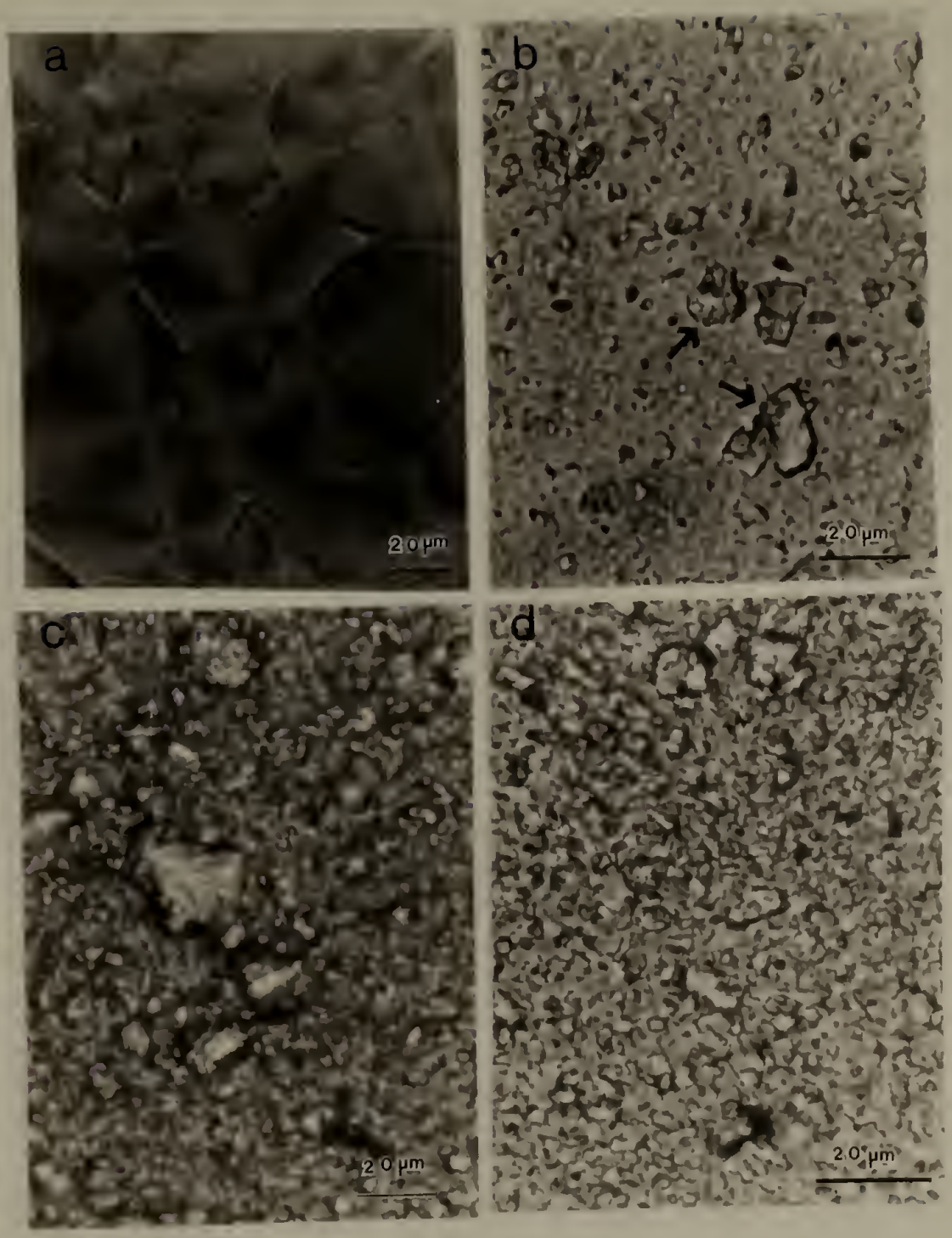

Figure 3.1 BF transmission optical micrographs of unfilled and filler polyethylene: a) Marlex 6003 unfilled; b) Marlex 6003 with 5 wt% $CaCO_3$ ATOMITE; c) Marlex 6003 with 40 wt% $CaCO_3$; d) duPont PE/$CaCO_3$ composite. Arrows indicate $CaCO_3$ particles.

3.4.2 Transmission Electron Microscopy. Figure 2 is a low magnification BF CTEM image of an unfilled Hifax® thin film. The micrograph reveals parts of two spherulites (their centers are marked A). This low dose exposure was made with slight objective lens underfocus to delineate the lamellae more clearly. One notices the usual periodic banding observed in spherulitic growth (see regions B1 and B2). Figure 3 is an in focus higher magnification view of the spherulitic morphology. This micrograph is quite remarkable in that it succeeds in resolving the relatively undamaged lamellae without resorting to staining or defocus techniques as usually employed [12-15]. Such clarity is achieved only with ultra high molecular weight PE (UHMWPE) and very likely reflects its high amorphous content (see Discussion).

The effect of the presence of the fillers on the morphology of polyethylene is seen in Figure 3.4a. The micrograph is of a region of a thin film of DPCC composite. Figure 4b is a schematic representation of the cross section indicating the particles embedded in the polymer. In Figure 4a the particles are the dark, irregular, randomly-spaced regions and are totally opaque to the electron beam because of their size and density. It is quite apparent that the presence of these particles has destroyed ordering at the spherulite level. More careful observation reveals that the morphology has a radial ordering evident around some of the filler particles (see arrows). Moreover the banding observed in Hifax is absent in the filled polymer.

Figures 3.5a and b are a pair of CTEM images of the duPont composite illustrating the effect of electron damage on contrast mechanisms from

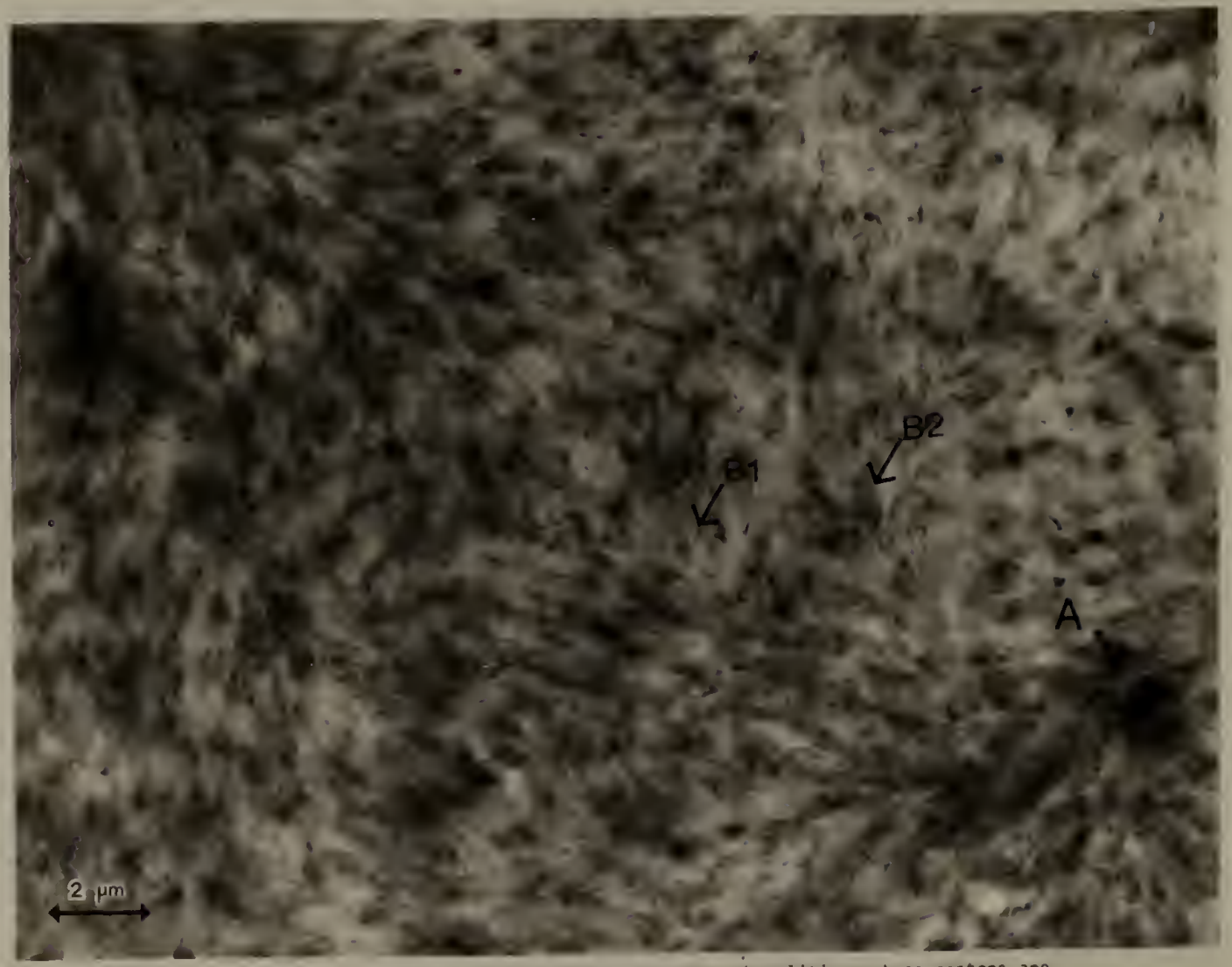

Figure 3.2 BF CTEM of Hifax 1900 thin film. The two spherulitic centers centers are at top right and bottom right corners (marked A). Regions B1 and B2 are successive bands of the bottom right spherulite.

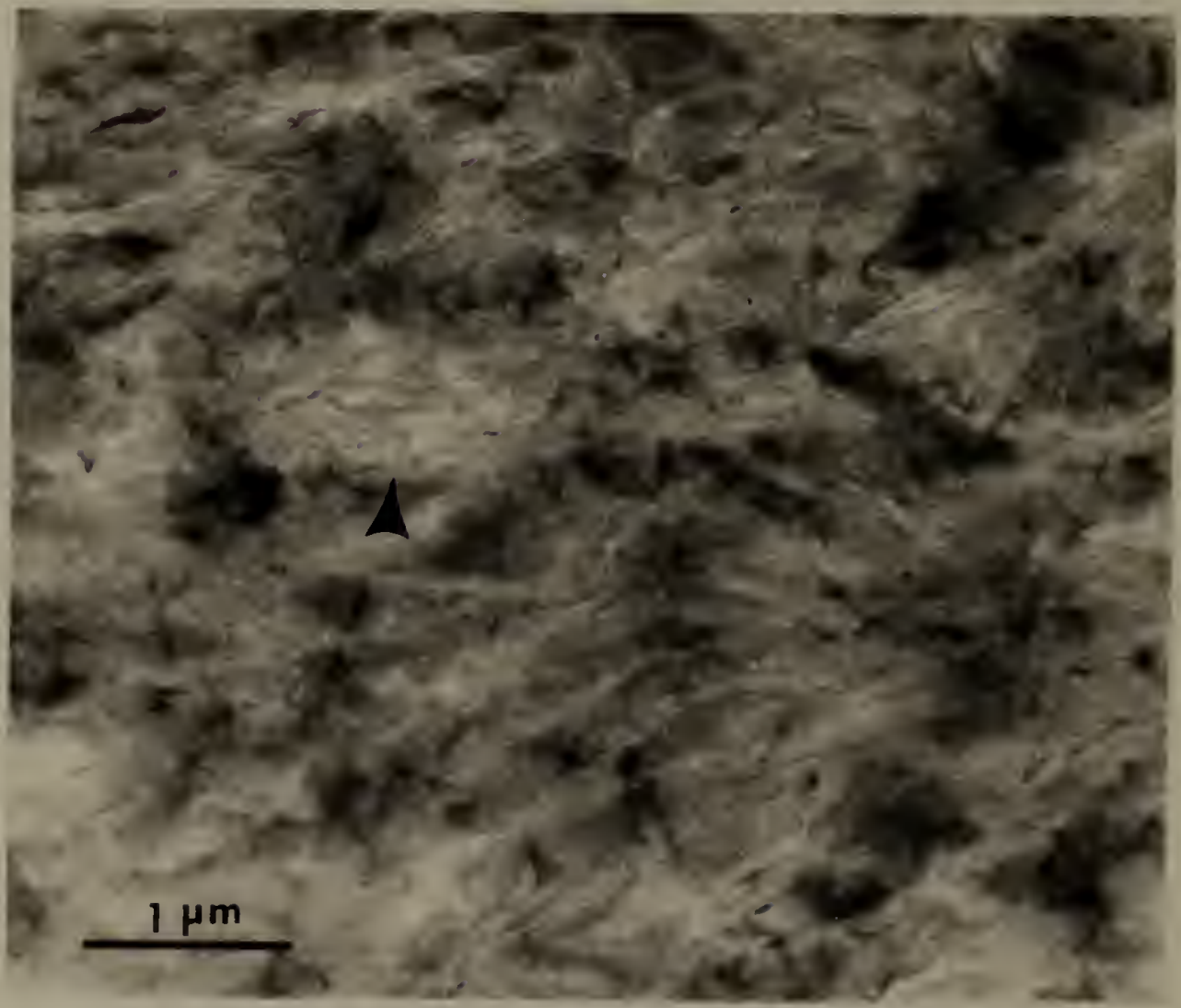

Figure 3.3 BF CTEM of Hifax. Note clearly resolved lamellae in region of arrow.

thin films. In Figure 3.5a diffraction contrast (see A) is present indicating that sample crystallinity is still preserved. However, after considerable electron damage has occurred, no diffraction contrast is seen in Figure 3.5b and only mass thickness contrast from distortion of the film is present. While the state of the specimen with respect to diffraction contrast is easily determined by inspection of the electron diffraction pattern, changes in the overall morphology in routine BF investigations may be overlooked because the rather high doses employed may cause changes long before the operator has adjusted the microscope for a particular area. Thus, Figure 3.5b is a "normal" appearing BF micrograph similar to many in the literature of lamellae in a PE spherulite. Figure 3.5a, on the other hand, shows the actual morphology. The effect of radiation damage in polymer electron microscopy has been well reviewed by Grubb [16]. Low dose images such as Figure 3.5a serve as a check on erroneous conclusions from radiation damage electron micrographs (see also Ref. 17). A scrutiny of the corresponding areas in Figures 3.5a and b reveals the same structure present in both micrographs.

In these micrographs lamellae are seen originating on the faces of the particles and radiating outward. There is yet another interesting feature - that of a highly curved lamellar configuration in region D. These "defect lamellar configurations" are revealed in most of our micrographs and occur almost exclusively at the interface.

Figures 3.6a and b are a similar pair of low and high dose micrographs of the Hifax®/$CaCO_3$ mixture. The general features noticed

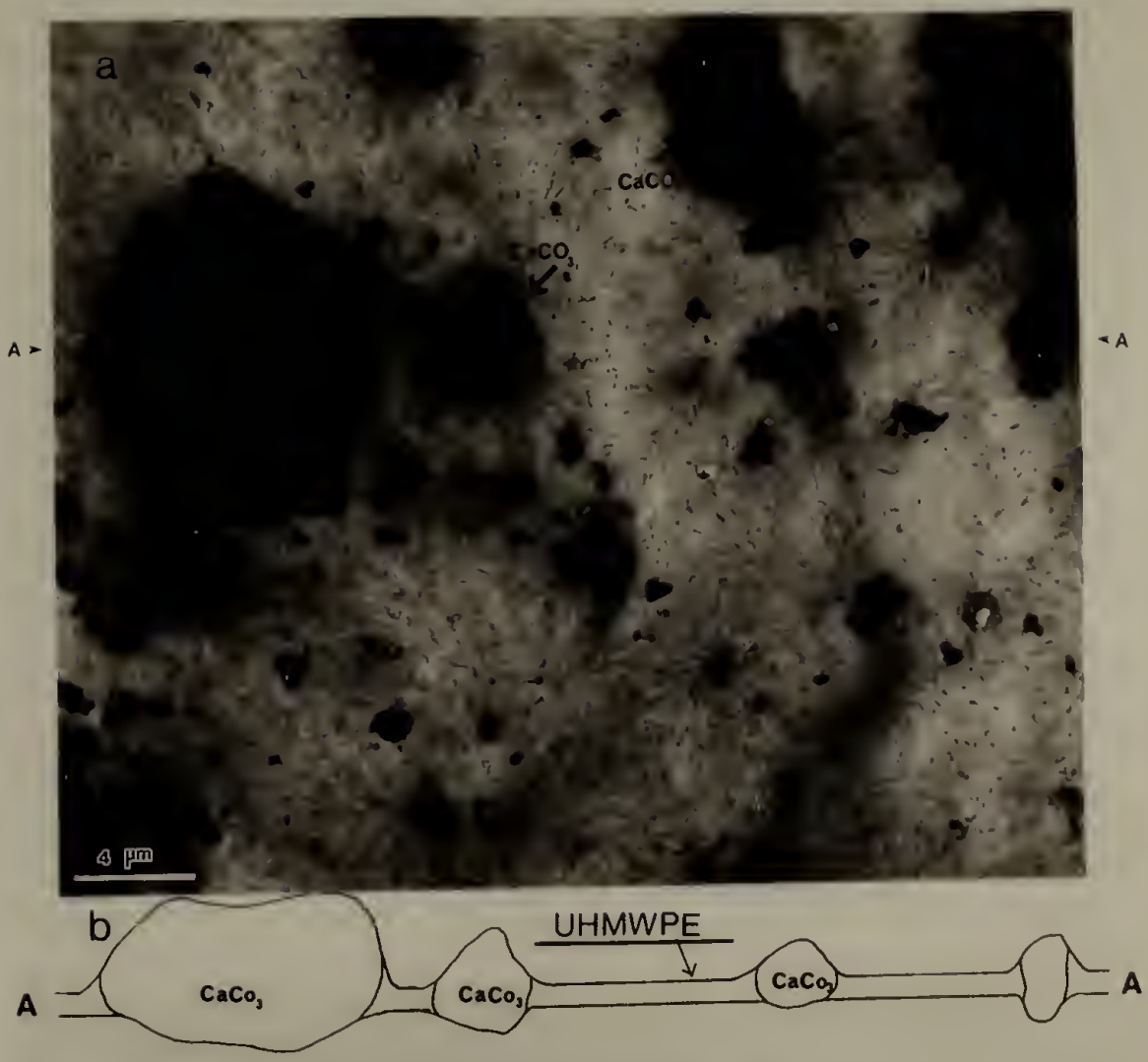

Figure 3.4 a) BF CTEM of duPont PE/$CaCO_3$ composite. Note radial patterns originating from particles at arrows; b) Schematic of a cross-section of such a film.

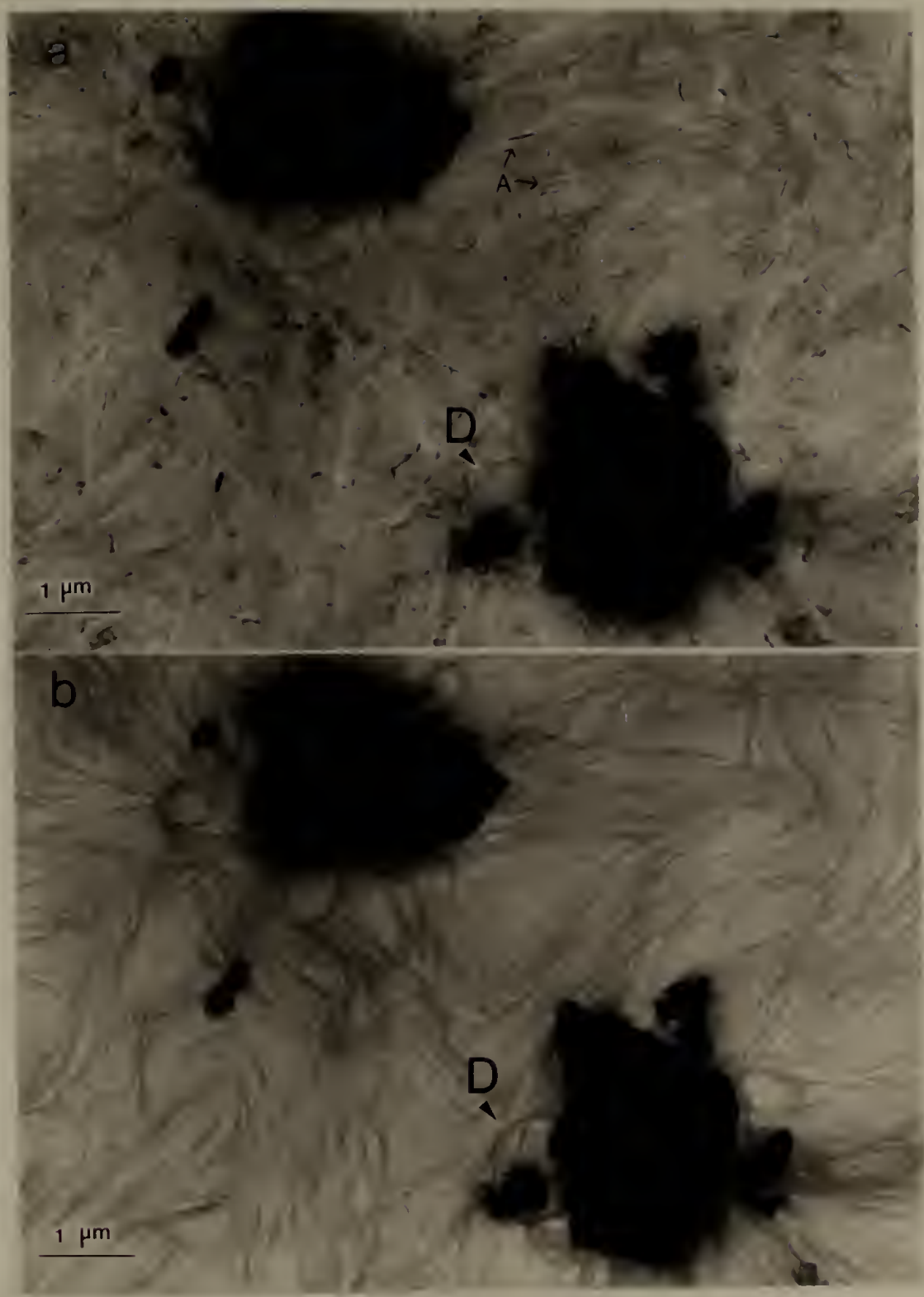

Figure 3.5 BF CTEM of duPont PE/$CaCO_3$ composite before (a) and after damage by electron beam (b). Defect configurations are marked D. Arrows (A) point to diffracting crystallites.

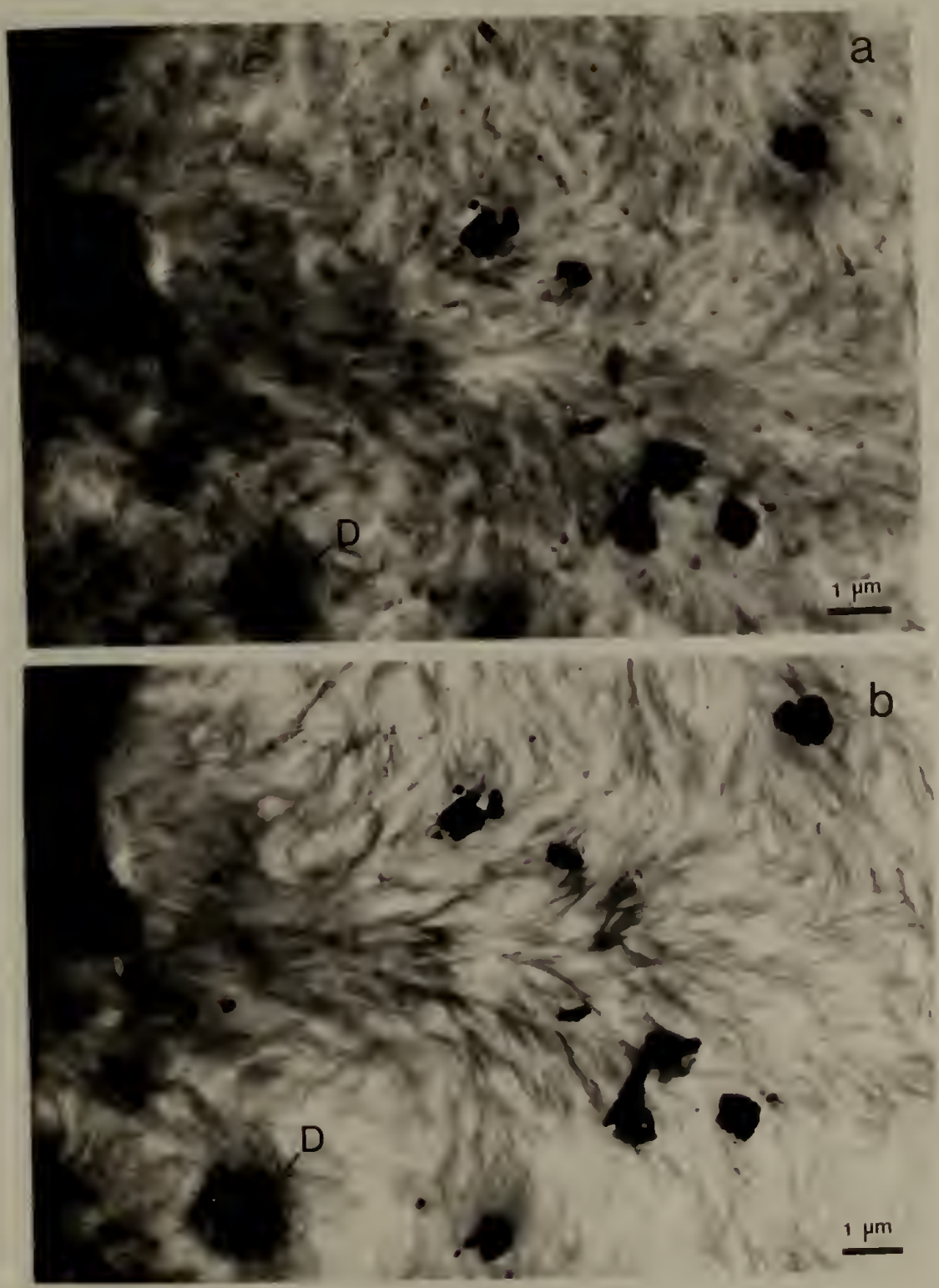

Figure 3.6 BF CTEM of Hifax/$CaCO_3$ mixture as in Figure 5.

earlier are again observed as are the defect lamellar configurations.

Figures 3.7 and 3.8 are high magnification micrographs of the polyethylene - $CaCO_3$ interface. At this magnification the crystallinity has, of course, been destroyed due to electron beam damage. However, while the lattice itself has been destroyed, the gross local morphology is relatively intact, and is in fact rather striking. The lamellae are seen to radiate perpendicular to the interface and appear laterally well ordered near the interface. The ordering while evident in both micrographs, is especially clear in the duPont composite and may reflect inherent characteristics arising from the method of preparation of the composite. This interfacial ordering must arise during the process of crystallization and reflects on the relative nucleating ability of the various $CaCO_3$ crystal faces.

3.4.3 Scanning Transmission Electron Microscopy. To investigate the polymer-filler interface more thoroughly and to obtain information about undamaged crystal orientation, STEM was utilized. STEM, with its inherent image intensification and higher collection efficiency enables work with much lower electron beam currents. The use of STEM for radiation sensitive polymers has been well illustrated by Sherman et al. [18] and condenser aperture settings and lens currents for the JEOL 100CX similar to those used in that work were employed in our study. For BF imaging all electrons not part of the main beam were blocked out with a selected area diffraction (SAD) aperture which acts as the objective aperture for BF STEM. For DF imaging the main beam was blocked with a beam stop and in addition the outer reflections

Figure 3.7 BF CTEM of Hifax/$CaCO_3$ interface at high magnification. Defect configuration is marked D.

Figure 3.8 BF CTEM of duPont PE/$CaCO_3$ interface at high magnification.

(020, 011 and 002 included) were blocked using a SAD aperture. This made possible a reverse contrast where edge-on lamellae show up as dark lines in the DF micrograph and only the diffracting regions (110/200 type reflections) remained bright. This kind of contrast mechanism is useful for imaging all lamellae in the nearly edge-on position.

Figures 3.9a and 3.9b are STEM BF micrographs of the DPCC composite and the Hifax/$CaCO_3$ composite respectively. Mass thickness effects are seen in Figure 3.9a (compare regions A and B). This is due to the nature of the preparation of the duPont composite with polymer associated with each filler particle. This is not seen in the solution mixed Hifax/$CaCO_3$ composite. Figure 3.10a is a higher magnification STEM BF micrograph of the DPCC composite while Figure 3.10b is a 110 annular DF of the same area. A comparison of the two micrographs reveals the advantages of the 110 annular DF imaging technique. While in the BF micrograph it is difficult to resolve the lamellae, in the DF micrograph the lamellae are clearly evident as the long, dark regions. Figure 3.11 is another 110 annular DF micrograph showing quite clearly the influence of $CaCO_3$ particles on the crystallization of polyethylene. The lamellae are observed radiating outward up to a distance of 300-400 nm away from the particle.

3.4.4 Scanning Electron Microscopy. To confirm our observations using CTEM and STEM and also to investigate molecular weight effects in these filled systems, secondary electron imaging (SEI) studies were carried out on samples of filled and unfilled polyethylenes. Figure

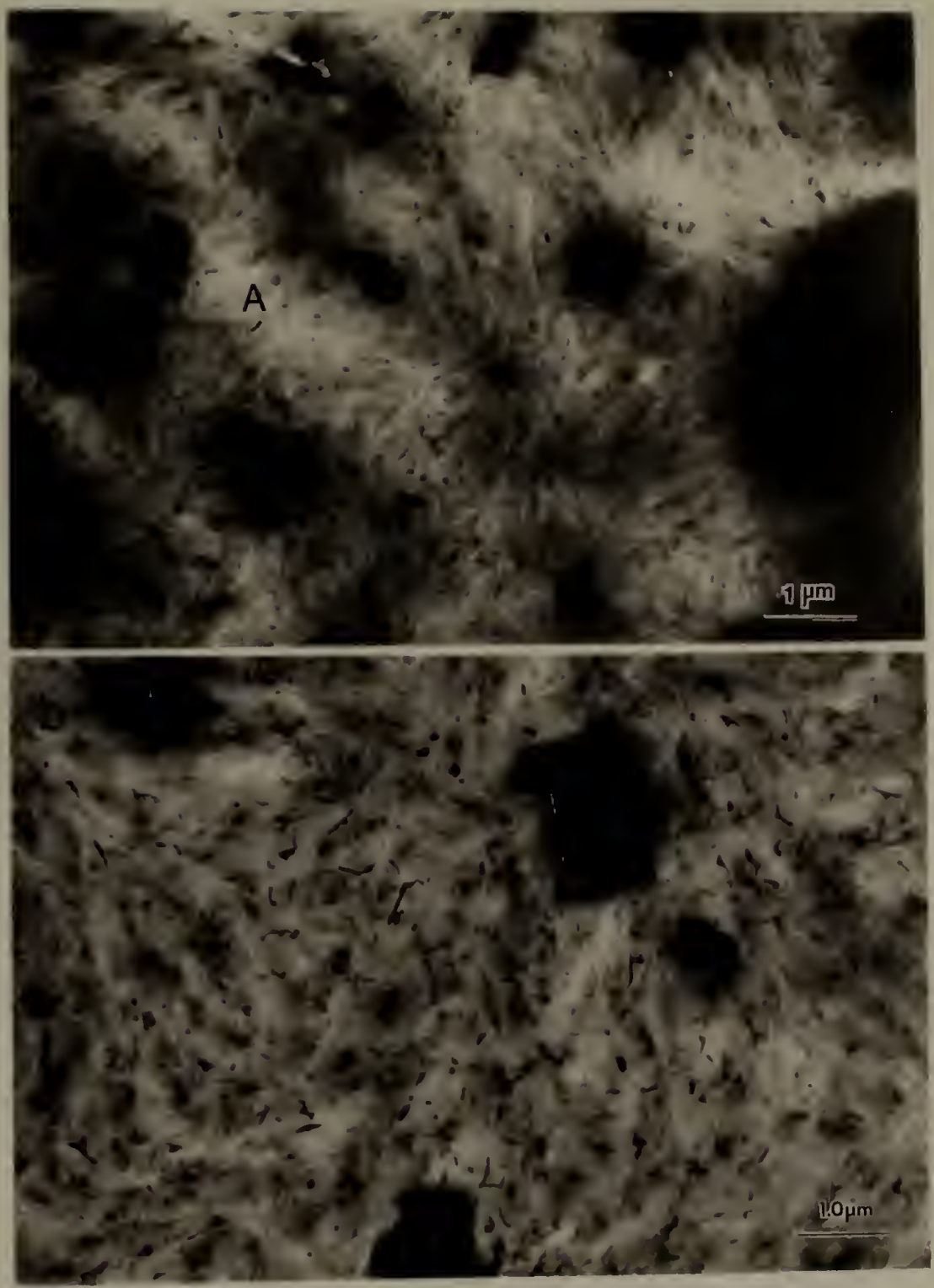

Figure 3.9 BF STEM micrographs of a) duPont + PE/$CaCO_3$ composite and b) Hifax/$CaCO_3$ mixture.

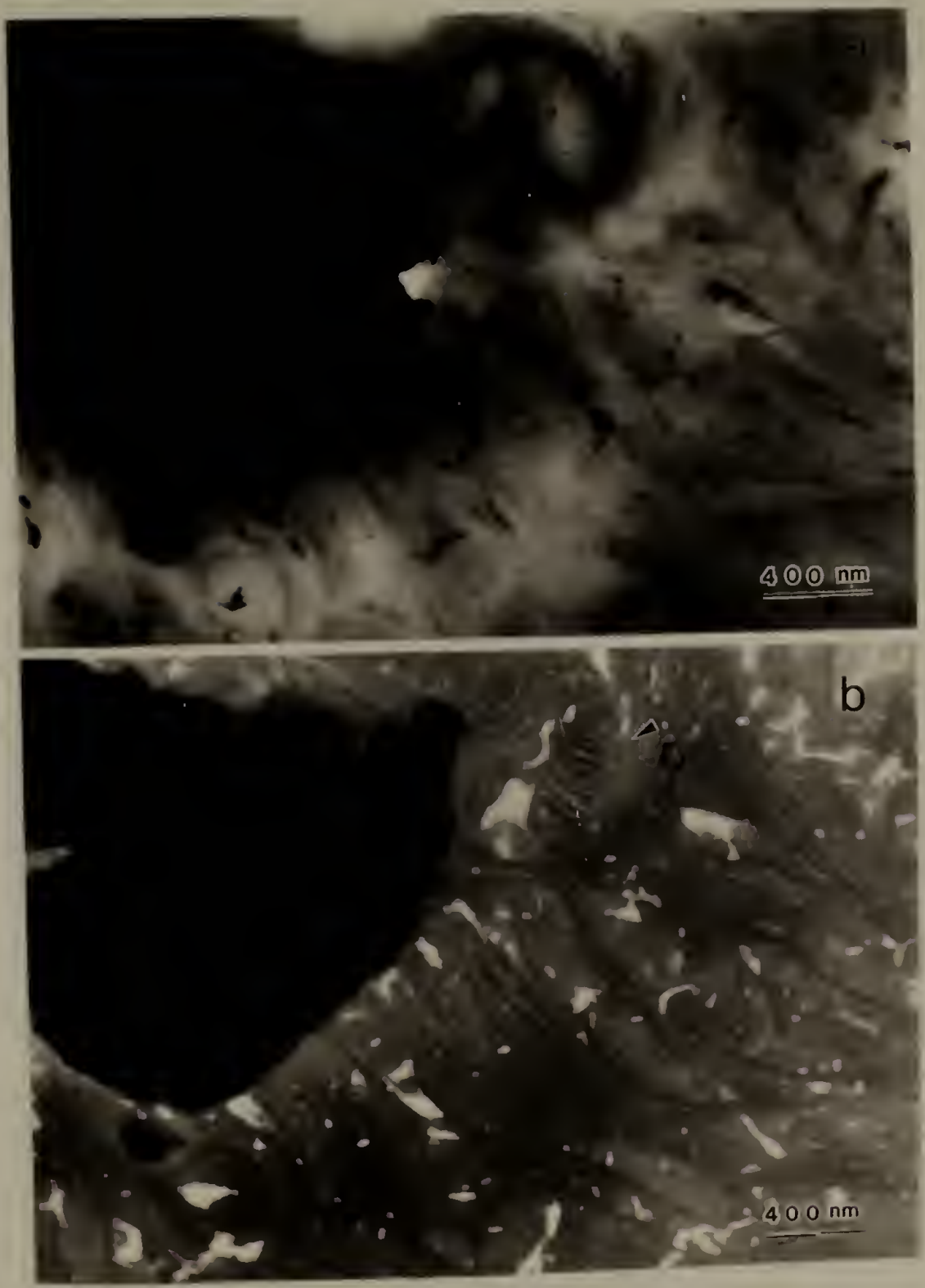

Figure 3.10 STEM images of the same region of the duPont PE/$CaCO_3$ composite a) BF image and b) hk0 annular DF image (see text). Defect configuration is marked D.

Figure 3.11 STEM 110/200 annular DF image of duPont PE/$CaCO_3$ composite.

3.12a is an SEM-SEI of melt crystallized Marlex® 6003 and shows the well developed spherulitic morphology of the unfilled polymer. Figure 3.12b is a high magnification view of the banding in the spherulite. Contrast is provided by the relatively high yield of secondary electrons from lamellar edges. The small dark lines in Figure 3.12b are due to the cracking of the gold coating due to dimensional changes of the underlying polymer from the electron beam. Figures 3.13a, b and c are SEM-SEI micrographs of filled Alathon® 7050, filled Marlex® 6003 and the DPCC composite. This sequence of pictures has three important features. In all three cases it is seen that the nucleation and oriented growth of lamellae occur at the selected regions of the particle surface. Also quite striking is the ease of resolution of lamellae for increased molecular weight. While the lamellae are tightly packed in the case of Alathon®, the structure becomes progressively more open so that individual lamellae are clearly discernible in the duPont composite. Also evident is the disorder in the lamellar configuration in the polymer matrix with increasing molecular weight. In Figure 3.13a for example, one sees that the lamellae possess little curvature. However, in Figure 3.13c, the lamellae exhibit much more disorder in their packing and tend to exhibit high curvature.

Figure 3.14 is a higher magnification micrograph of the neighborhood of a single $CaCO_3$ particle in region A of Figure 3.13c. The regular stacking of the lamellae at the interface corresponds to both the CTEM and STEM results.

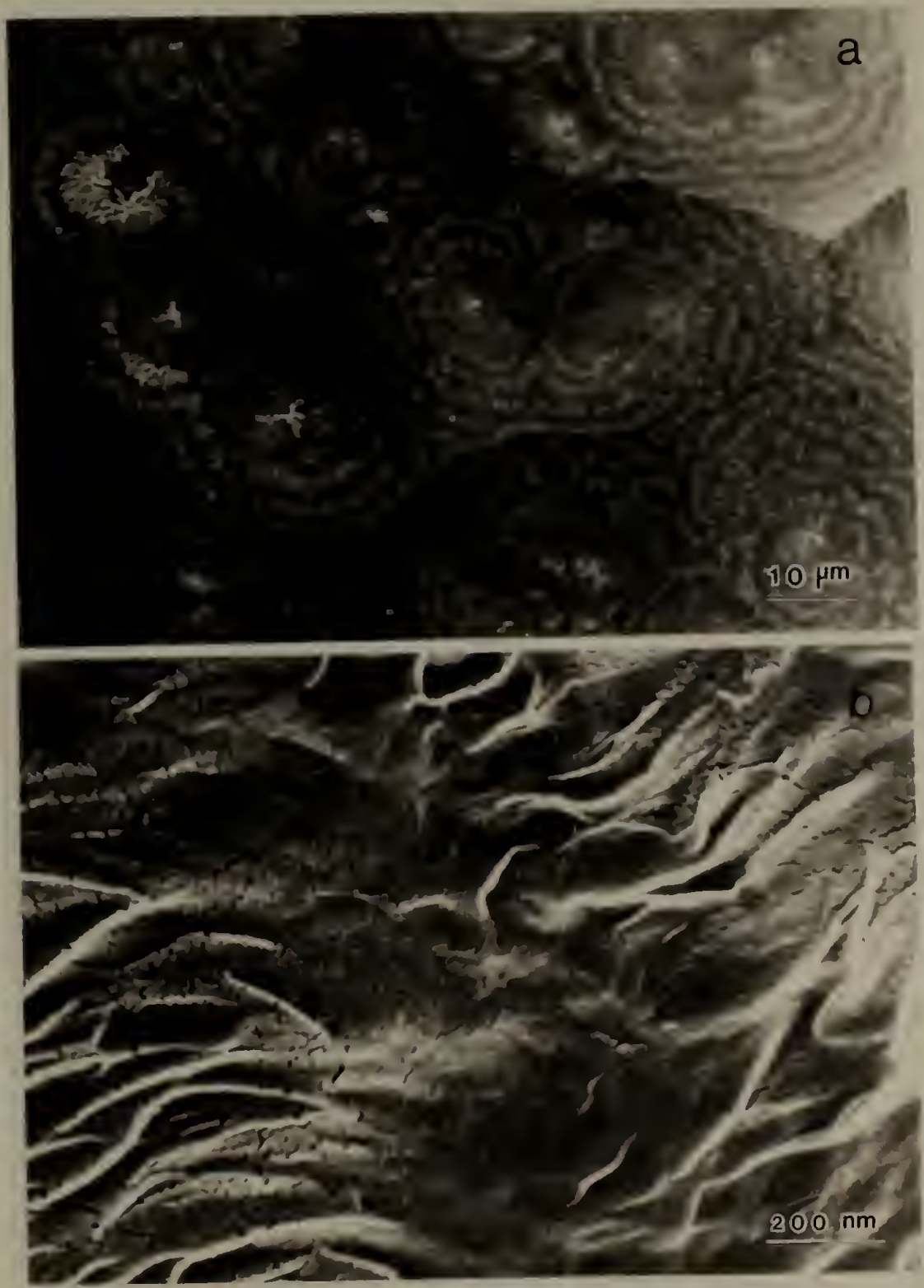

Figure 3.12 SEM-SEI of freely crystallized surface of Marlex® 6003 a) low magnification image showing banded spherulites and b) higher magnification view of a banded region.

Figure 3.13 SEM-SEI images of filled polyethylenes a) Alathon®/40% treated $CaCO_3$ and b)Marlex®/40% treated $CaCO_3$.

Figure 3.13 c) SEM-SEI image of duPont PE/$CaCO_3$ composite.

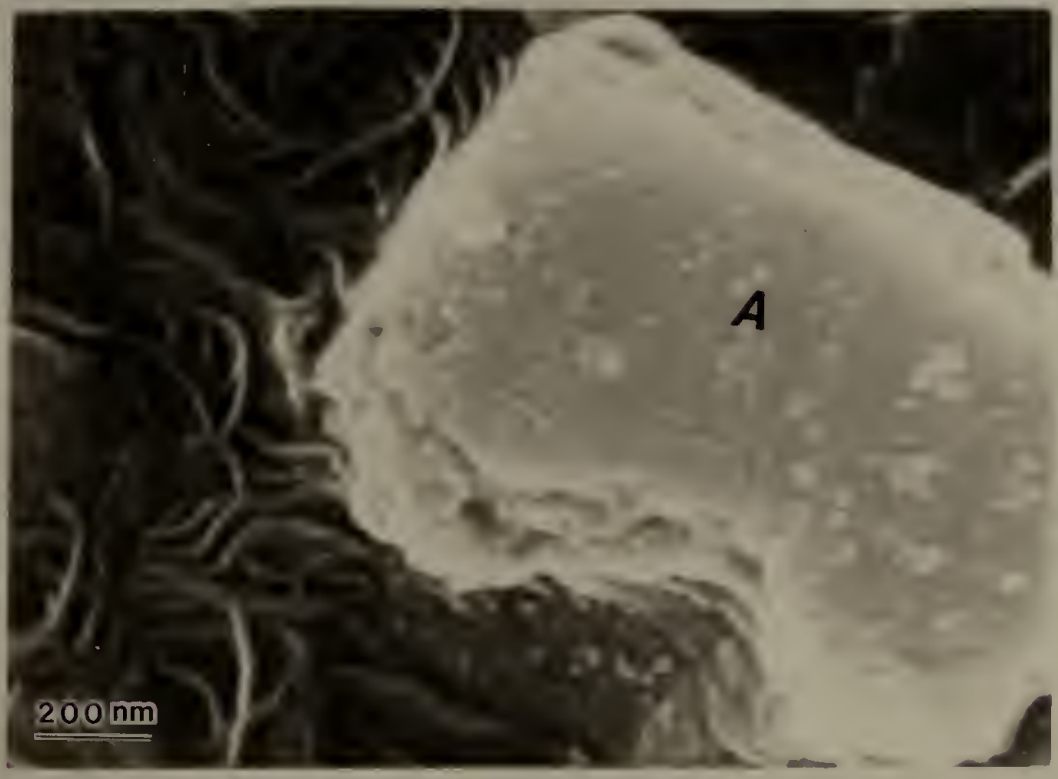

Figure 3.14 High magnification SEM-SEI of region A of Figure 13.

3.5 Discussion

3.5.1 Effect of Filler on Long Range Ordering. At the outset consideration must be given to the effects of introducing fillers into a crystallizing polymer. Firstly, the volume occupied by fillers presents a discontinuous space for polymer crystallization. A simple calculation shows that for a 30% volume filled polymer with 2μm monodisperse spheres the average distance between particles is of the order of 2.0μm. For smaller particles at constant filler loading the average particle to particle distance is much less. Secondly, the surface of the particle can act as a nucleation site for crystallization. The large amount of available surface would necessarily imply that nearly all nucleation be heterogeneous. Thirdly, the interface of polymer and filler is a region of discontinuity for all properties (thermal, mechanical, etc.) because of the wide disparity in properties of the two materials. For instance, the difference in the thermal expansion coefficients will result in uneven stresses in the polymer matrix surrounding the filler particle. All this means that lamellar ordering (of which spherulitic growth is one case) is not expected. This has been observed earlier in the optical studies of Cole and St. Pierre [11], Kargin et al. [9] and Binsbergen [8]. While in the unfilled case, spherulitic ordering could take place until two spherulites impinged, the presence of filler and the simultaneous nucleation by some facets of the filler particles precludes such long range organization.

3.5.2 Local Ordering of Lamellar Growth. While long range ordering on the scale of spherulites is not observed, almost all the micrographs show evidence of local lamellae orientation at the $CaCO_3$ interface. The high magnification CTEM micrographs and the STEM micrographs illustrate this for composite films of the DPCC composite and Hifax/$CaCO_3$. It is apparent that lamellae nucleate on the surface of the $CaCO_3$ particle and grow normal to the surface to lengths of about 300-400 nm. However, a careful examination of a large number of interfaces indicates that such lamellar growth is neither uniform in extent nor evident from all facets of the $CaCO_3$ particle. Figure 3.7 shows one such region centered around a discontinuity in the particle surface and Figure 3.10 shows another such region where from the micrographs it is not evident if the surface was active in nucleating crystallization.

The nature of the nucleation process has been the objective of many studies [7,8,9]. While the process of heterogeneous polymer crystal nucleation is, as yet, incompletely understood, most studies point to various phenomena which include epitaxy, interfacial stresses and substrate wettability. The thermo dynamic criterion is of course a reduction in the activation energy for nucleation.

The phenomenon of oriented overgrowth of a crystalline phase upon the surface of a substrate which is also crystalline is known as epitaxy [19]. Most polymer epitaxial studies involve crystallization from solution onto the substrate surface [20]. While in general it is believed that only a certain amount of lattice mismatch is possible

for oriented overgrowth, Koutsky et al. [21] demonstrated in a study of PE epitaxial growth on alkali halides that this is not a requirement for overgrowth of PE on halide surfaces. On the other hand, Wellinghof et al. [22] noted the presence of the monoclinic crystal form in PE layers less than 40 thick grown on halide surfaces and ascribed this change of unit cell to the closer lattice match.

The case of polymer melt crystallization in the presence of a heterogeneous phase such as the $CaCO_3$ particles in this study is rather different because the polymer chain mobility is much less. Transcrystallinity is perhaps more pertinent to the present study in that the nucleating sites are constrained to simple mold surfaces [5,6,7]. However, as indicated in the Introduction, it is not quite clear what the characteristics of the surface have to be. The studies of Binsbergen [8] and Kargin et al. [9] are perhaps closest to this study since solid nucleating agents were dispersed in the polymer phase. Binsbergen concludes that crystallinity of the substrate is necessary and also argues for adsorption of polymer segments onto the surface of the substrate which then assists crystal nucleation. Kargin et al. [9] emphasize the role of stresses in the polymer at the interface contributing to nucleation.

It is evident that examination of the polymer-substrate interface would yield useful information about the nucleation process. Microbeam diffraction (MBD) is one such technique. Microbeam diffraction (MBD) has been used by Sherman et al. [18] and Low et al. [23] to investigate the microstructure of small (300 nm diameter) regions of

polyethylene thin films. In a study of heterogeneous phase systems such as PE/$CaCO_3$, MBD can ideally be used not only to study crystal orientation in the polymer phase in the neighborhood of the interface, but also to evaluate the efficiency of various substrate faces in nucleating crystallinity. This was indeed one of the objectives of the present study. However, the thickness of the $CaCO_3$ particles and the polyfaceted nature of the surface prevented acquisition of any useful diffraction patterns from the $CaCO_3$ phase. Moreover, obtaining diffraction patterns from PE at the interface was often difficult because of increased thickness of the PE film at the interface. Therefore, for the type of information ideally sought, much thinner and more perfect calcite crystals will have to be utilized. A limited number of microdiffraction patterns obtained from 500 nm diameter regions close to the $CaCO_3$ surface exhibit arcing of the PE 002 reflection but no useful information on the specific $CaCO_3$ orientation has been obtained. All the diffraction patterns obtained revealed only crystal structure of the orthorhombic form.

3.5.3 Effect on Crystallinity. While growth of spherulites is essentially prohibited by presence of filler, it is also seen that the overall sample crystallinity is also affected. DSC measurements of crystallinity show for low and medium molecular weight polyethylenes a reduction of 15% and 8%, respectively (see Table 3.2). For the ultrahigh molecular weight polymer, the reduction in crystallinity is only about 2%. The ultrahigh molecular weight polyethylene has an inherent crystallinity of 57%.

TABLE 3.2

CRYSTALLINITY AND MELTING TEMPERATURES OF FILLED AND UNFILLED POLYETHYLENES BY DSC

Sample	Crystallinity X_c (a)	T_{max} °K (b)
Alathon 7050	0.83	410.9
Marlex 6003	0.75	412.2
Hifax 1900	0.57	413.7
Alathon/40% $CaCO_3$	0.68	408.5
Marlex/40% $CaCO_3$	0.67	409.5
duPont PE/63.5% $CaCO_3$	0.55	413.8

a scanning rate @ 20°C/min.

b peak maximum temperature

The peaks of the melting curves are similarly affected, shifting relative to the pure polymer toward lower temperatures for the low molecular weight (by 2.4°C) and for the medium molecular weight (2.8°C) samples while remaining constant for the ultrahigh molecular weight polyethylene. Therefore, crystallite size and/or perfection is evidently also affected by presence of filler.

3.5.4 Effect of Filler Treatment. The role of filler treatment is not obvious from microscopy at least in a quantitative fashion. It is seen in DSC isothermal crystallization studies that treated $CaCO_3$ in Marlex® reduces half time of crystallization more significantly than untreated $CaCO_3$ does (unpublished). This is taken to imply that the dispersion of such treated filler is superior to untreated $CaCO_3$.

3.5.5 Schematic for Composite Morphology. On the strength of the microscopy data a simple schematic of filled PE microstructure is given in Figure 15. The particles are surrounded by an interlayer of radially oriented polymer lamellae. This layer is not uniform around the particle depending upon the nucleation characteristics of the particular filler surface. Defect lamellar configurations also exist near the filler particles. These may arise because rapid crystallization from two non-adjacent sites would force polymer in between to adopt distorted configurations. Further from the interface, lamellae order in the rod-like morphology or random morphology as described by Go et al. [24].

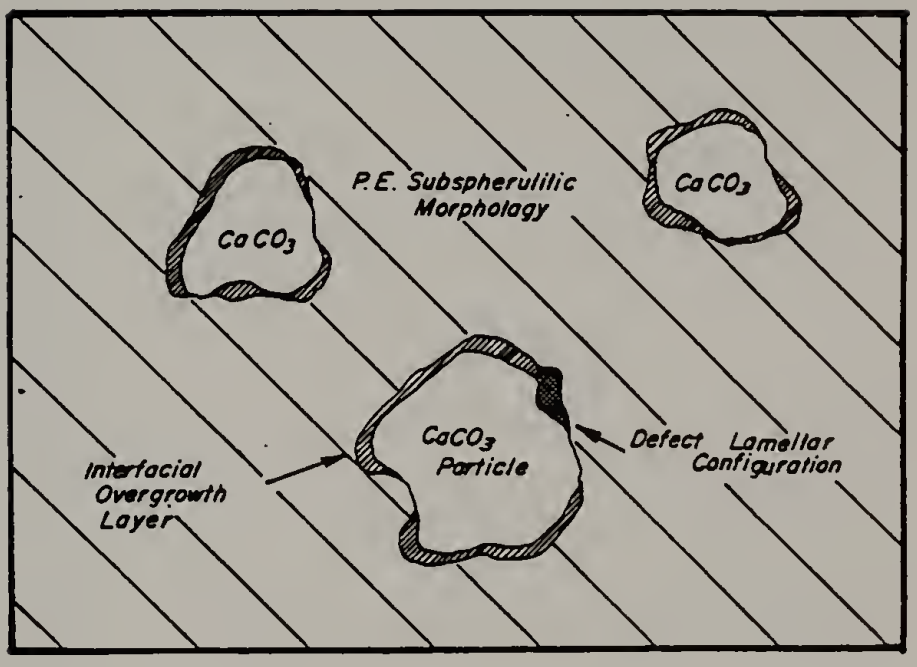

Figure 3.15 A schematic for filled polyethylene microstructure.

3.5.6 Molecular Weight Effects. While this study concerns itself with the morphology of filled systems an important aspect of the wider investigation of the behavior of filled polyethylenes are molecular weight effects. These effects are succinctly illustrated in Figure 3.13. It was noticed that the ease of lamellar resolution increased with increasing molecular weight of the polyethylene. An explanation for this effect may be found in the crystallinity data which are shown in Table 3.2. While the Alathon® sample has a crystallinity of 82%, the Hifax® polymer has crystallinity about 25% lower, indicating a major noncrystallizing fraction in UHMWPE. It is well known that the amorphous fraction is present to a major extent in between lamellae and this explains the greater separation of lamellae in UHMWPE resulting in clearer visualization of the lamellae.

The molecular weight effect also manifests itself in increased curvature of lamellae (see Figure 3.13). This effect was previously noted by Voight-Martin et al. [25] in their study on microstructure of fractionated polyethylenes. In our study also it is seen that the long linear lamellae evident in Alathon® (Figure 3.13a) degenerate into a disordered spaghetti-like mass in UHMWPE. An increase in molecular weight results in increased viscosity of the melt and an increase in entanglements at the crystal-melt interface. It is logical to assume that these effects manifest themselves in the noticeable morphological differences discussed above.

3.6 Conclusions

This study has investigated the effect of presence of $CaCO_3$ ($\overline{D}w$ =

2.5 μm) filler particles on the microstructure of a range of molecular weights of polyethylene.

It is found that for the concentration of $CaCO_3$ particles studied, long range organization of the polymer microstrusture (e.g. spherulites) is not observed irrespective of molecular weight and nature of polymer-filler attachment. Radially oriented lamellar growth is characteristic of the polymer-filler interface. At the interface the ordered layer is not uniform. It is postulated that this reflects on the differing nucleating ability of the different facets of the crystalline $CaCO_3$ particle.

Changes in polymer molecular weight results in easily observed differences in morphology with increasing curvature of lamellae and increasing disorder in lamellar arrangement for higher molecular weight.

3.7 References

1. V.I. Grigor'ev, V.P. Gordienko and A.N. Tynnyi, Soviet Mater. Sci., 9 (6), 672-676, 1973.
2. V. Dolakava and F. Hudecek, J. Macro. Sci., Phys., B15(3), 337-346, 1978.
3. J. Gahde, V. Muller, Y.V. Lebedev and Yu.S. Lupatov, Polym. Sci. USSR, 10(6), 1446-1452, 1977.
4. H. Schonhorn, J. Polym. Sci. B, 5, 919, 1967.
5. H. Schonhorn, Macromolecules, 1, 145, 1968.
6. D. Fitchmun and S. Newman, J. Polym. Sci. B7, 301, 1969.

7. A.M. Chatterjee, Ph.D. Thesis, Univ. of Massachusetts, Amherst, 53, 1974.

8. F.L. Binsbergen, Polymer, 11, 253, 1970.

9. V.A. Kargin, T.I. Sogolova and N.Ye. Rapoport, Dokl. Phys. Chem., 163, 600, 1965.

10. F. Rybnikar, J. Macromol. Sci. 1319(1), 1, 1981.

11. J.H. Cole and L.E. St. Pierre, J. of Polym. Sci., Polym. Symp. 63, 205-235, 1978.

12. "Polymer Single Crystals" by P.H. Geil, Wiley-Interscience, New York, 1963.

13. 15. A.M. Hodge and D.C. Bassett, J. Mater. Sci., 12, 2065, 1977.

14. M.J. Miles and J. Petermann, J. Macro. Sci., Phys, B16, 243, 1979.

15. E.J. Roche and E.L. Thomas, Polymer, 22, 333, 1981.

16. D.T. Grubb, J. Mater. Sci., 9, 1715, 1974.

17. G. Kanig, Kolloid Z.u.Z. Polym., 251, 782-783, 1973.

18. E.S. Sherman, W.W. Adams and E.L. Thomas, J. Mater. Sci., 16, 1, 1981.

19. K.E. Mann, E. Baer, A.J. Hopfinger, J. Polym. Sci., Macromol. Rev., 13, 1-61, 1978.

20. E.W. Fischer, Kolloid Z., 159, 108, 1958.

21. J.A. Koutsky, A.G. Walton and E. Baer, J. Polym. Sci., A-2, 4, 611-629, 1966.

22. S.H. Wellinghof, F. Rybnikar and E. Baer, J. Macromol. Sci., Phys., B10, 1, 1974.

23. A. Low, D. Vesely, P. Allan and M. Bevis, J. Mater. Sci., 13, 711-721, 1978.

24. A. Go, L. Mandelkern, R. Prud'homme and R.S. Stein, J. Polym. Sci., A-2, 12, 1185, 1974.

25. I.G. Voight-Martin, E.W. Fischer, L. Mandelkern, J. Polym. Sci., Polym. Phys. Ed., 18, 2347-2368, 1980.

C H A P T E R I V

DYNAMIC MECHANICAL BEHAVIOR OF FILLED POLYETHYLENE AND MODEL COMPOSITES

4.1 Introduction

In Chapter III the morphology of filled polyethylene was investigated. In this chapter the determination of the mechanical properties is approached with studies of mechanical response of filled and unfilled polyethylene in the linear viscoelastic region. The dynamic behavior of filled and unfilled polyethylenes is determined over the temperature spectrum 100°K to 400°K using a Rheovibron (Direct Reading Dynamic Viscoelastometer). The strains imposed on the materials are small enough that it is safe to assume that no micro-failure is occuring during a test.

The prediction and determination of the dynamic behavior of composites is of undeniable importance. While addition of rigid inorganic particulates to polymers results in desirable reinforcement, other material properties are altered and one such property is the behavior under time dependent loads or deformations. Since the viscoelasticity of the polymeric component is generally an important attribute, it is necessary to determine and understand changes in viscoelastic behavior brought about by presence of the essentially elastic inclusions.

The knowledge of the dynamic properties of materials is useful not only when the material is considered for use when dynamic loads are

present, but can also be used to estimate their time dependent behavior. Hence, this makes the dynamic modulus and tan δ important properties of the material.

In this study the intent has been to determine the effect of inorganic particulate filler inclusion and polymer-filler coupling on the dynamic mechanical properties of polyethylene and to compare this to the behavior of model composite systems.

4.2 Background

Rather expectedly, there is a sizable volume of literature dealing with dynamic behavior of heterogeneous systems where the dispersed phase is a relatively rigid inclusion. Of general relevance is the large amount of work dealing with carbon black presence in elastomers due to its obvious importance to tire performance. This has been reviewed by Gessler *et al*. [1]. In these systems the particles are considered rigid while the matrix is incompressible which considerably simplifies the modeling of such materials. However, the high surface area of typical blacks leads to occlusion and non-ideal behavior.

Perhaps of immediate relevance to the stated objective of this work are studies of filler presence on the dynamic behavior of glassy and semicrystalline thermoplastics. Nielsen [2] and Bohme [3] investigated the effect of filler presence in polyethylene. Other studies, among them those by Hirai and Kline [4], Kardos *et al*. [5], Lee and Nielsen [6] and Lewis and Neilsen [7], have addressed the problem of explaining the behavior of filled composites in relation to

deviations from expected behavior. It may be concluded from these studies that the dynamic behavior of filled polymers is not only dependent on the nature of polymer and filler but often strongly influenced by the character of the polymer-filler interface.

To investigate interface effects, different kinds of PE-$CaCO_3$ coupling were investigated. Both untreated $CaCO_3$ particles and $CaCO_3$ particles coated with a titanate coupling agent (KR-TTS)® were dispersed in polyethylene. In addition a third kind of polymer-filler coupling (the duPont PE/$CaCO_3$ composite, see below) was also studied.

4.3 Experimental

Table 1.2 details the origins and relevant properties of the PE and $CaCO_3$ fillers used in this study.

4.3.1 Sample Preparation. Mixing of polyethylene and $CaCO_3$ for the Alathon® and Marlex® composites was performed on two roll mills for 5-7 minutes in the temperature range 140- 160°C depending on molecular weight of polyethylene. The milled sheets were then cut and thin sheets (thickness ~ 0.2 mm) were compression molded in a picture frame mold according to ASTM procedure D1928.

Hifax® 1900, the ultra high molecular weight polyethylene, is not melt processible by conventional techniques. Mixing of Hifax® and $CaCO_3$ was carried out by preparing a slurry of the two powders in acetone and slowly evaporating the acetone in a Büchi rotary evaporator. The mixture was compression molded as above but using higher temperatures [12]. A blend of Hifax® and the duPont composite (DPCC) was prepared

along the same lines to result in a 20 wt% PE/$CaCO_3$ composite. The DPCC composite was compression molded similarly.

4.3.1 Dynamic Testing. Thin strips of length 5.5 cm and maximum cross-sectional area 0.004 cm^2 were cut from the compression molded sheets, annealed for 1 hour at 80°C, and tested on a Rheovibron DDV-II at 11 Hz over the temperature range 100°K to 400°K with an average scanning speed of 1.25°/min. Complex modulus and tan δ values determined are related thus:

$$E^* = E' + iE''$$

$$\tan \delta = E''/E'$$

A smooth curve was fit through the data points. Since the use of a constant correction for system compliance and sample yielding within the grips resulted in modulus overprediction at low temperatures a variable error constant was assumed for each sample in the expression for complex modulus using the method of analysis suggested by Massa [13] and this resulted in improved determination of low temperature behavior.

4.4 Results

Figures 4.1-4.4 show the dependence on temperature for the storage modulus E' and the loss tangent tan δ for the filled and unfilled polyethylenes. In Figure 4.1a is plotted the storage moduli E' of the three polyethylenes. The difference in moduli reflects their different crystallinity (see Table 3.2), varying by as much as 26% as determined by DSC. Hifax® registers a sharp drop in modulus at around

Figure 4.1 a) Storage modulus vs. temperature and b) loss tangent vs. temperature for Alathon, Marlex and Hifax.

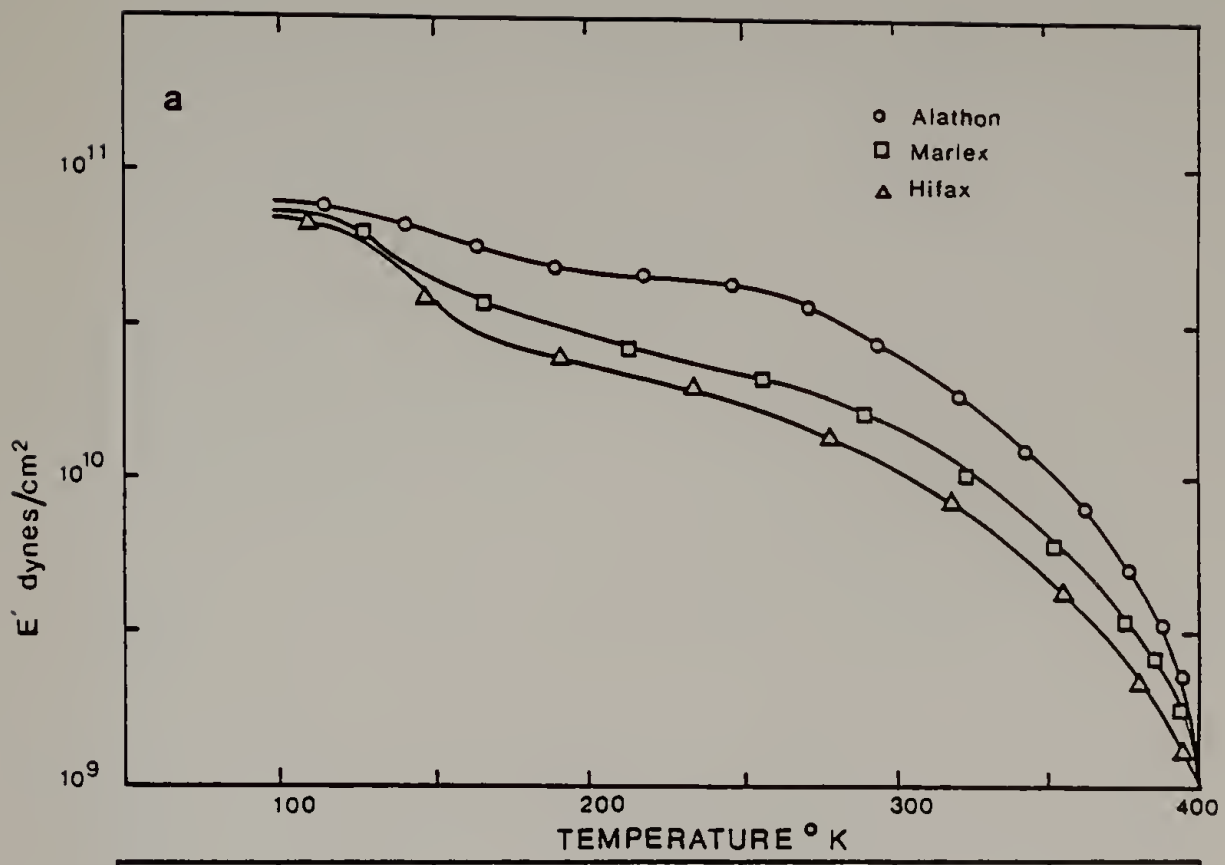
a
Alathon
Marlex
Hifax
10^{11}
10^{10}
10^{9}
E' dynes/cm^2
100
200
300
400
TEMPERATURE ° K

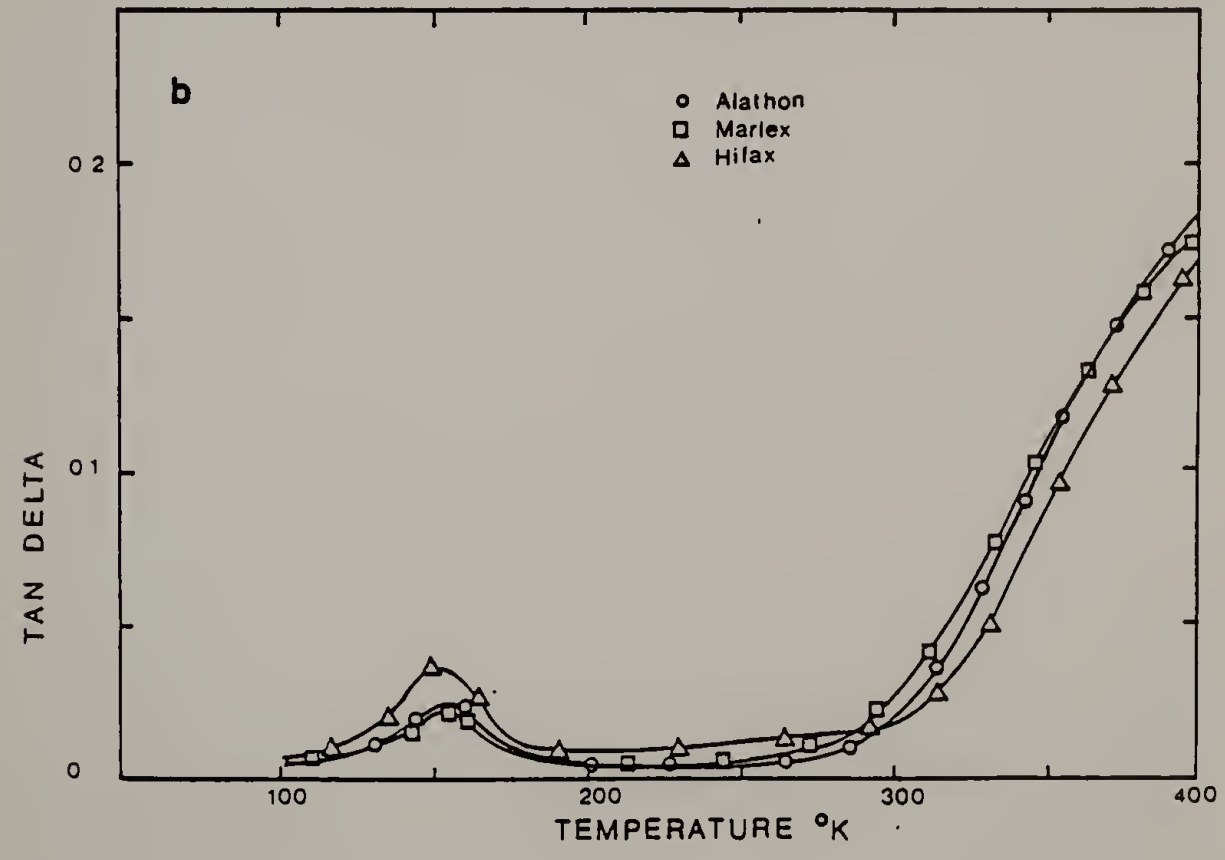
b
Alathon
Marlex
Hifax
0 2
0 1
0
TAN DELTA
100
200
300
400
TEMPERATURE °K

150°K and reflects the behavior of its high amorphous fraction passing through its glass transition temperature. This phenomenon is seen in the tan δ curves (Fig. 4.1b) at 150°K, with the highest peak observed for the least crystalline Hifax® and the lowest peak for the highly crystalline Alathon®.

Figures 4.2, 4.3 and 4.4a and b display the effect of presence of filler on the E' and tan δ spectra, respectively, for each of the three polyethylenes studied. In general it is seen that filler presence results in an increase in E' because of the reinforcing effect of a relatively rigid inorganic inclusion. The reinforcing effect is not as prominent at temperatures below the γ transition at 150°K and is possibly due to the role of thermally induced stresses in the polyethylene matrix [6,14,15]. The storage modulus spectra also display a broad transition at 150°K when the $CaCO_3$ is coated with coupling agent when compared to the untreated $CaCO_3$. It is noticed (see Figure 4.1a) that the broadening of the transition is associated both with higher crystallinity and with well dispersed $CaCO_3$ particle presence (coupling agent presence on inorganic particles results in better dispersion in the hydrophobic polymer during milling). A similar effect is noticed in the ultrahigh molecular weight polyethylene composites. Broad transitions of the E' spectra and higher modulus characterize the well dispersed and well bonded DPCC composite as well as the blend of Hifax® with the DPCC composite.

The loss tangent spectra reveal complementary information about the role of the PE-$CaCO_3$ interface. In all cases it is seen that in

Figure 4.2 a) Storage modulus vs. temperature and b) loss tangent vs temperature for Alathon, Alathon + 40 wt% $CaCO_3$ and Alathon + 40 wt% treated $CaCO_3$.

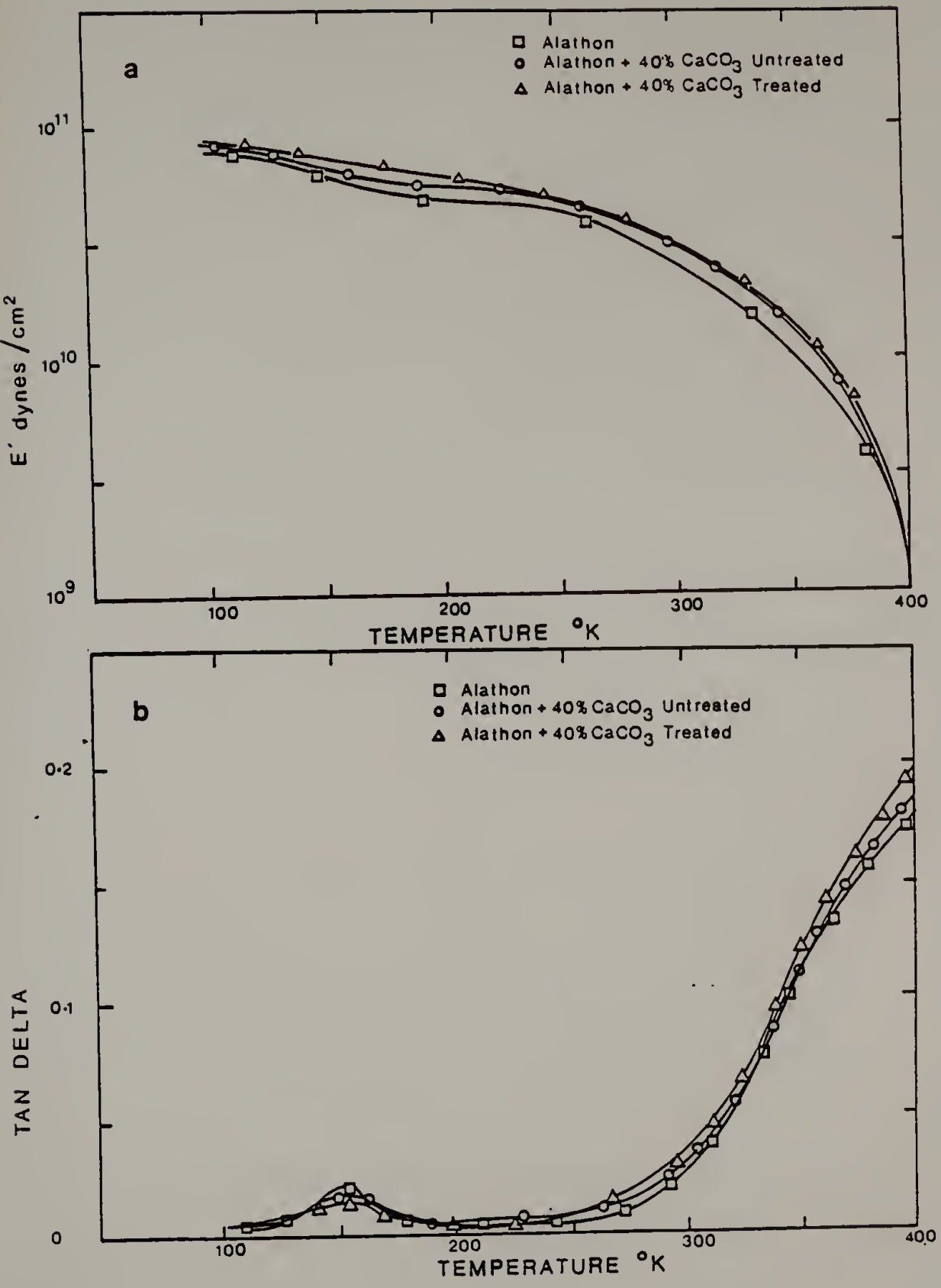
a
Alathon
Alathon + 40% $CaCO_3$ Untreated
Alathon + 40% $CaCO_3$ Treated
10^{11}
10^{10}
10^{9}
E' dynes /cm^2
100
200
300
400
TEMPERATURE °K
b
Alathon
Alathon + 40% $CaCO_3$ Untreated
Alathon + 40% $CaCO_3$ Treated
0·2
0·1
0
TAN DELTA
100
200
300
400
TEMPERATURE °K

Figure 4.3 a) Storage modulus vs. temperature and b) loss tangent vs. temperature for Marlex, Marlex + 40 wt% $CaCO_3$ and Marlex + 40 wt% treated $CaCO_3$.

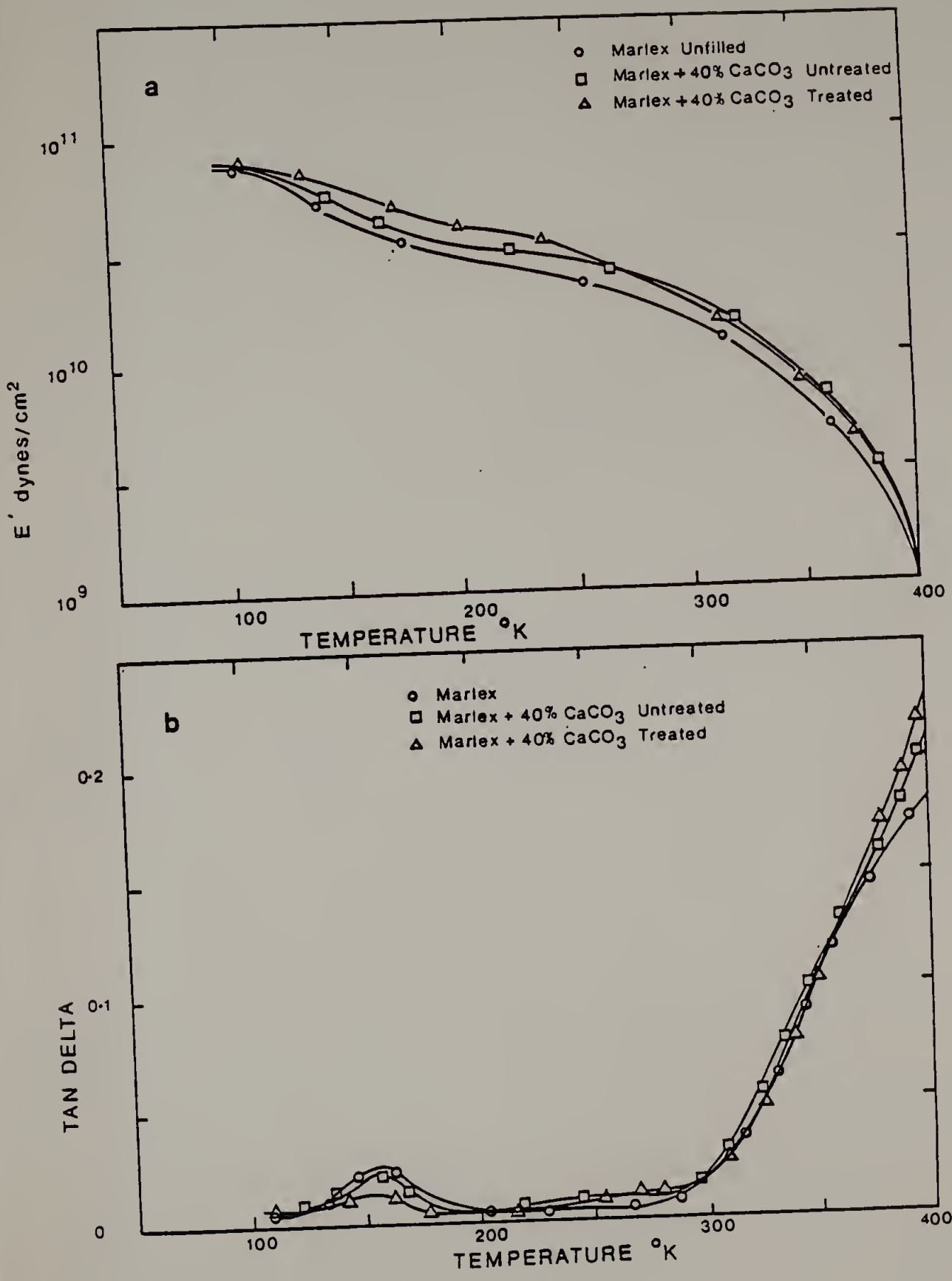
a
Marlex Unfilled
Marlex + 40% CaCO3 Untreated
Marlex + 40% CaCO3 Treated
10^11
10^10
10^9
E' dynes/cm^2
100
200
300
400
TEMPERATURE °K
b
Marlex
Marlex + 40% CaCO3 Untreated
Marlex + 40% CaCO3 Treated
0·2
0·1
0
TAN DELTA
100
200
300
400
TEMPERATURE °K

Figure 4.4 a) Storage modulus vs. temperature and b) loss tangent vs. temperature for Hifax, Hifax + 40 wt% $CaCO_3$, Hifax + duPont PE/$CaCO_3$ blend (20 wt% $CaCO_3$ and duPont PE/$CaCO_3$ composite.

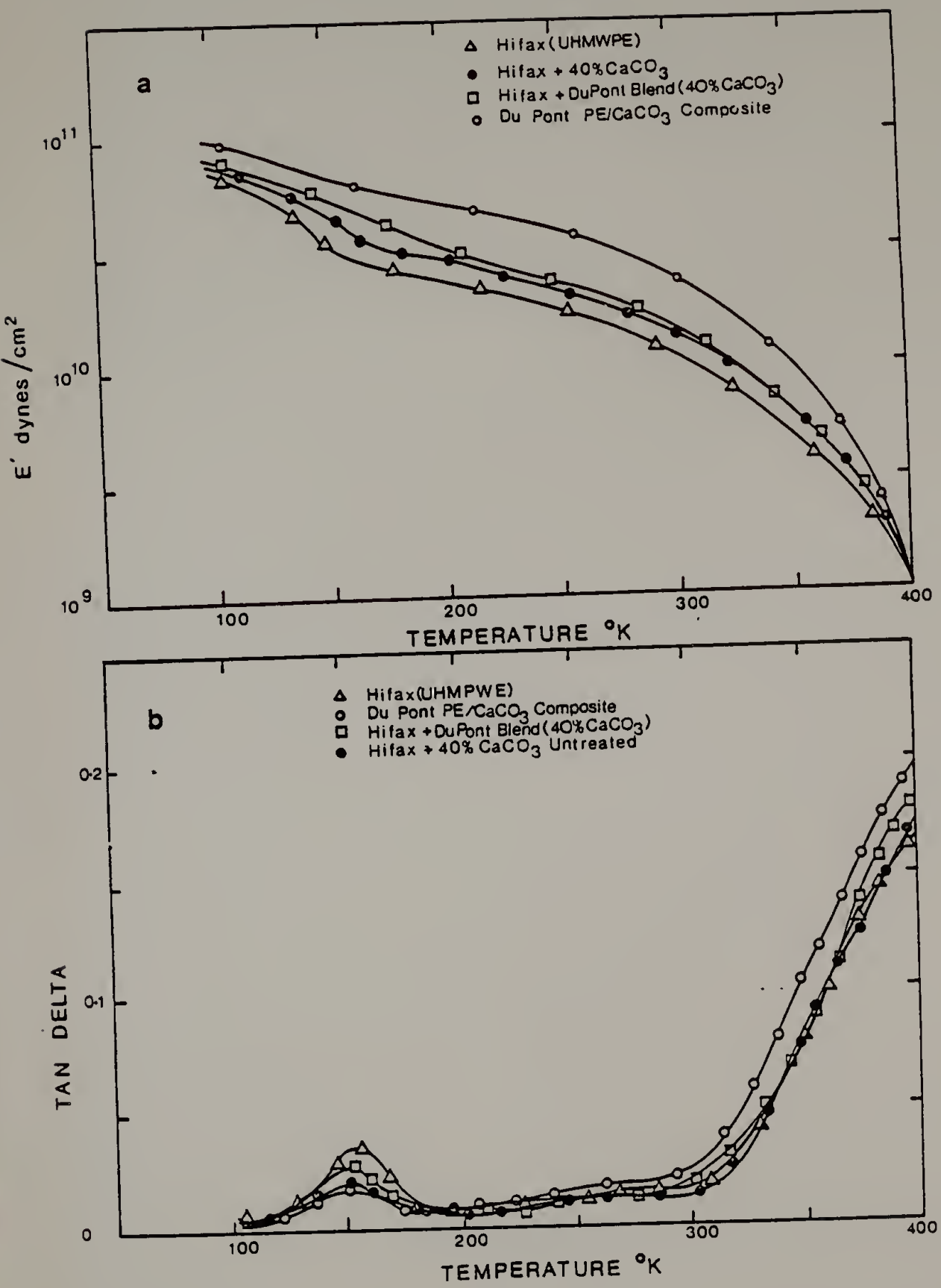
a
Hifax(UHMWPE)
Hifax + 40% $CaCO_3$
Hifax + DuPont Blend(40% $CaCO_3$)
Du Pont PE/$CaCO_3$ Composite
E' dynes /cm^2
10^{11}
10^{10}
10^9
100
200
300
400
TEMPERATURE °K
b
Hifax(UHMPWE)
Du Pont PE/$CaCO_3$ Composite
Hifax + DuPont Blend(40% $CaCO_3$)
Hifax + 40% $CaCO_3$ Untreated
TAN DELTA
0·2
0·1
0
100
200
300
400
TEMPERATURE °K

the low temperature region the damping decreases in presence of filler and this is found irrespective of molecular weight of the polyethylene. Furthermore the damping is dependent upon the nature of the interface with reduced damping when coupling agent is present at the interface. Again the DPCC composite exhibits the lowest damping at 150°K and this probably reflects the good dispersion of the $CaCO_3$ particles and improved polymer filler adhesion. However, at temperatures above 250°K the damping exhibited by the filled samples is more typically greater than that of the unfilled polymer. The duPont composite similarly exhibits higher damping at temperatures above 250°K.

It is necessary to determine the dynamic behavior of model viscoelastic composites so as to place the experimental data in proper perspective.

4.5 Dynamic Behavior of Model Viscoelastic Composites

While many expressions for composite moduli, exact and empirical, are available in the literature [16,17] just four will be considered in the analysis that follows:

The Voigt model is the theoretical lower bound on composite modulus irrespective of configuration of the component phases:

$$E_c = \frac{E_f\ E_p}{(1-c)E_f + c\ E_p} \qquad (1)$$

Similarly the Reuss model is the theoretical upper bound [19]:

$$E_c = c\,E_f + (1-c)E_p \qquad (2)$$

where E is the Young's modulus, c volume concentration of filler and subscripts c,f and p refer to composite, filler and polymer, respectively. Two other exact models will be considered.

The Dewey-Goodier model (DG model) is the analytical solution to the case where elastic inclusion concentration in matrix is low, $c \ll 1$. The Christensen Lo Kerner Model (CLK Model) is the exact solution to the composite configuration first proposed by Kerner [20]. The expression for the elastic moduli for these models is given in Table 4.1.

To proceed from the elastic to the viscoelastic problem, the correspondence principle is invoked. The correspondence principle equates solutions of Laplace (or Fourier) transformed viscoelastic problems to the solutions of the corresponding elastic problem. For steady state harmonic excitations, the correspondence is even more straight forward as shown by Hashin [21]. An abbreviated version of this proof is given in Appendix I.

For the two phase composite of relevance hence, it is seen that in general the elastic composite tensile modulus is expressed as below (assuming both phases are isotropic):

$$E_c = E_c\,(c,\ E_p,\ E_f,\ \upsilon_p,\ \upsilon_f) \qquad (3)$$

For the viscoelastic composite, the composite complex tensile modulus is given by

$$E_c^* = E_c^*\,(c,\ E_p^*,\ E_f,\ \upsilon_p,\ \upsilon_f) \qquad (4)$$

TABLE 4.1

Expressions for Elastic Modulus and Loss Tangent for Model Composites

Model (Remarks)	Tensile Modulus of Composite E_c	Loss Tangent of Composite ($\tan \delta_c$)
Voigt (Theoretical Lower Bound on Modulus)	$E_c = E_p E_f / [cE_p + (1-c)E_f]$	$\tan \delta_c = \dfrac{(1-c) \tan \delta_p}{(1-c) + c\dfrac{E_p'}{E_f} + c\left(\dfrac{E_p'}{E_f}\right) \tan^2 \delta_p}$
Reuss (Theoretical Upper Bound on Modulus)	$E_c = (1-c)\, E_p + c\, E_f$	$\tan \delta_c = \dfrac{(1-c) \tan \delta_p}{(1-c) + c\, E_f / E_p'}$
Dewey-Goodier (DG) (Dilute Suspension Case, see ref. 15)	$E_c = 9K_cG_c/(3K_c + G_c)$ where $K_c = K_p + \dfrac{(K_f - K_p)c}{1 + K_f - K_p)/(K_p + \frac{4}{3} G_p)}$ and $G_c = 1 - \dfrac{15\,(1-\nu_p)\,[1 - G_f/G_p]c}{7 - 5_p + 2(4 - 5_p)\, G_f/G_p}$	$\tan \delta_c$ evaluated numerically using equation 4.

TABLE 4.1 (cont'd)

Model (Remarks)	Tensile Modulus of Composite E_c	Loss Tangent of Composite $\tan \delta_c$
Christensen-Lo-Kerner Model (CLK) (see Ref. 19)	$E_c = 9 K_c G_c/(3K_c + G_c)$ where $K_c = \dfrac{(K_f - K_p)c}{1 + [(1-c)(K_f - K_p)/(K_p + \frac{4}{3} G_p)]} + K_p$ and G_c given by solution of quadratic equation $A(G_c/G_p)^2 + 2B(\frac{Gc}{Gp}) + C = 0$ A, B, C are functions of G_p, G_f, ν_p, ν_f and are explicitly stated in Ref. 19 or 20.	evaluated numerically

E,K,G Tensile, Bulk and Shear Modulus, respectively

ν Poisson's Ratio

c Volume fraction filler

c,p,f Subscripts for composite, polymer and filler, respectively

where E, and E^* (= E' + iE") stand for elastic and complex tensile modulus, υ for Poisson's Ratio and subscripts c, p, and f have their usual meaning. The Poisson's ratio for the polymer, while in general complex [18], is assumed here to be real.

For the Voigt model, chosen here for illustration, the loss tangent evaluated using the correspondence principle, is expressed as:

$$\tan \delta_c = \frac{(1-c) \tan \delta_p}{(1-c) + c\, E_p'/E_f + c(E_p'/E_f) \tan \delta_p^2} \qquad (5)$$

where $\tan \delta_p$ is loss tangent of the polymer phase, E_p' the storage modulus of polymer, and the other terms have their usual meaning. Considering the limits, when $E_p \sim E_f$ which is appropriate for polymer below its glass transition, temperature and assuming $\tan \delta_p^2 << 1$ which is generally true,

$$\tan \delta_c = (1-c) \tan \delta_p \qquad E_p \sim E_f \qquad (6)$$

Interestingly this is the result obtained empirically by Nielsen [2].

The other limit considered Ep << Ef gives the result

$$\tan \delta_c = \tan \delta_p \qquad Ep << Ef \qquad (7)$$

and this limit is also considered in the literature [20,21]. Appendix II lists the computer program used for the calculation of model complex moduli using the four models discussed above. In Figures 4.5a and 4.5b are plotted the relative composite modulus at various filler loadings

for the two cases when E_f/E_p = 10 and E_f/E_p = 75 as predicted by the models considered. The Poisson's ratio υ for $CaCO_3$ and Polyethylene have been assumed to be 0.3 and 0.4, respectively, and E_f, the tensile modulus of $CaCO_3$ inclusion to be 4.7×10^{11} dyne/cm^2 [22] in both cases. It was found that the two cases considered were appropriate for all the filled polyethylenes at the temperatures 125°K and 350°K irrespective of initial crystallinity of the polyethylenes. It is noticed that at the higher temperature (350°K) the storage modulus is well predicted by the theoretical models (the Reuss model is seen to be meaningless for spherical inclusions). However, at the lower temperature (125°K) the samples have lower than expected storage moduli.

In Figures 4.6a and 4.6b are similarly plotted the predicted relative loss tangent of composite at various filler loadings for the two cases E_f/E_p = 10 and E_f/E_p = 75. It is seen that the loss tangent as predicted by the Voigt model is the theoretical upper bound on the loss tangents exhibited by model viscoelastic composites. Also shown for comparison between theory and experiment are experimentally determined loss tangent values. Again the low temperature (T = 150°K) relative tan δ is overpredicted by the models. Conversely, the high temperature (T = 350°K) damping exhibited by the filled samples is consistently higher than expected. It is apparent that the non ideal behavior of these samples must arise due to the vastly different chemical nature of the two components since agreement between prediction and experiment for heterogeneous polymer-polymer blends is much better [23].

Figure 4.5 Comparison of predicted dynamic modulus by various models with experiment a) E_f/E_p = 10 (T = 125°K), (b) E_f/E_p = 75 (T = 350°K). The symbols in Figures 4.5 and 4.6 represent: Alathon + 40 wt% $CaCO_3$ (o) and 40 wt% treated $CaCO_3$ (Δ); Marlex + 40 wt% $CaCO_3$ (Ⓞ) 40 wt% of treated $CaCO_3$ (●); Hifax + 40 wt% $CaCO_3$ (•); and Hifax + duPont composite (40 wt% $CaCO_3$) (▲) and duPont PE/$CaCO_3$ composite.

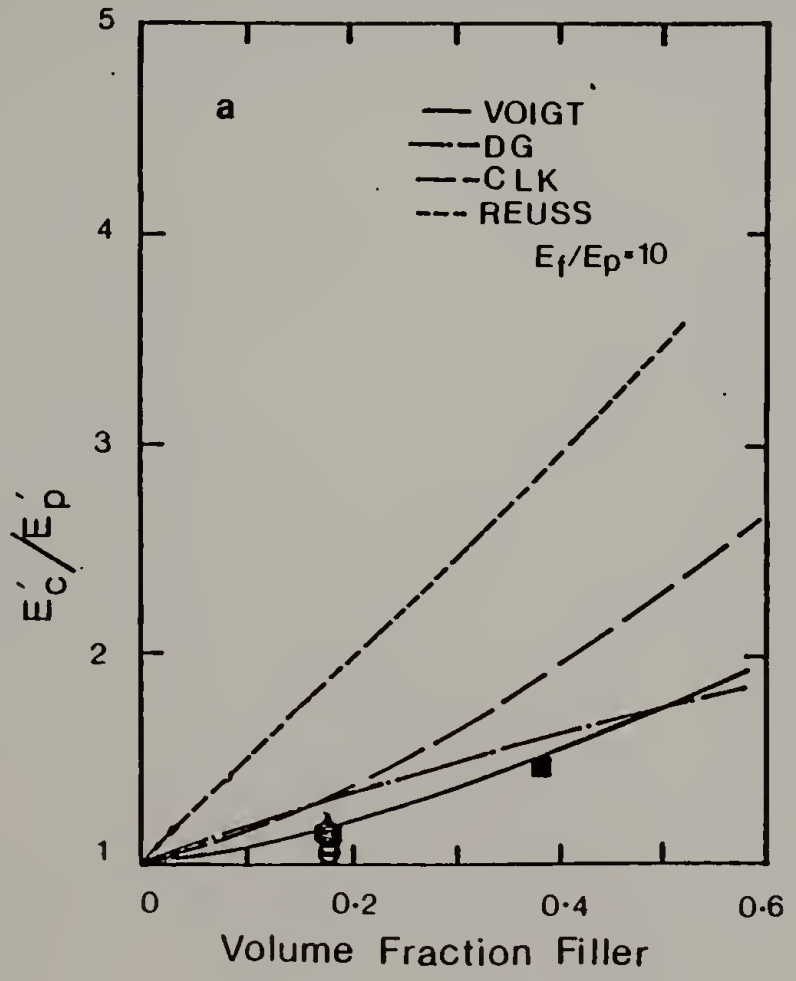
a
VOIGT
DG
CLK
REUSS
E_f/E_p=10
E_c'/E_p'
5
4
3
2
1
0
0·2
0·4
0·6
Volume Fraction Filler

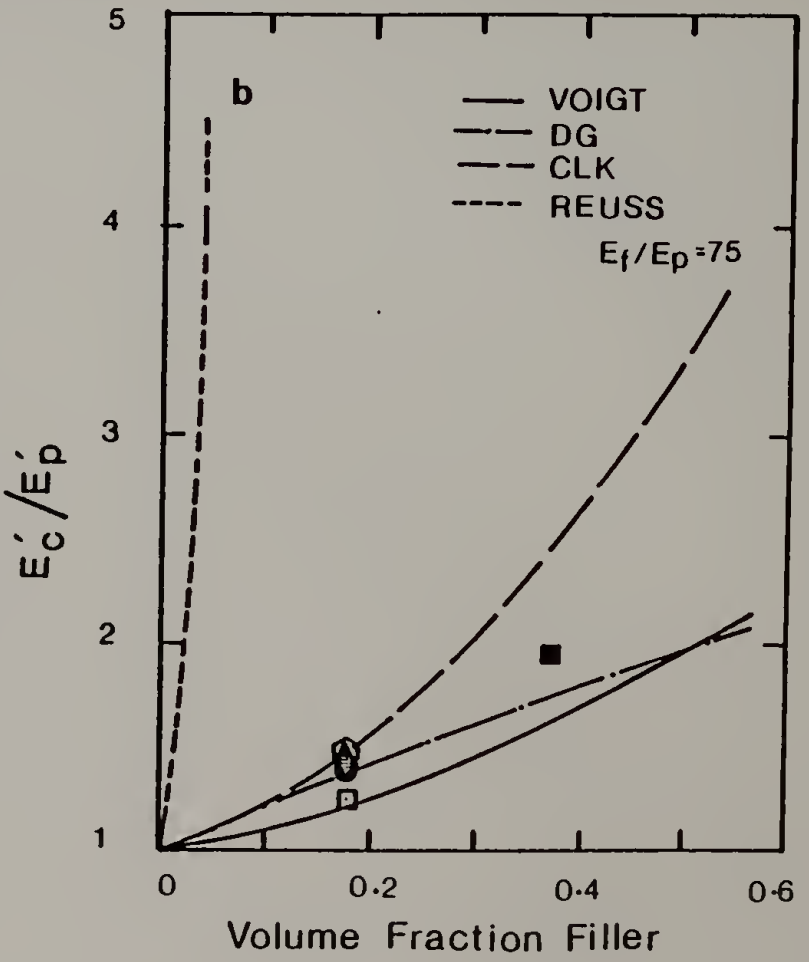
b
VOIGT
DG
CLK
REUSS
E_f/E_p=75
E_c'/E_p'
5
4
3
2
1
0
0·2
0·4
0·6
Volume Fraction Filler

Figure 4.6 Comparison of predicted loss tangent by various models and experiment a) E_f/E_p = 10 (T = 150°K), (b) E_f/E_p = 75 (T = 350°K). Data representation as in Figure 5.

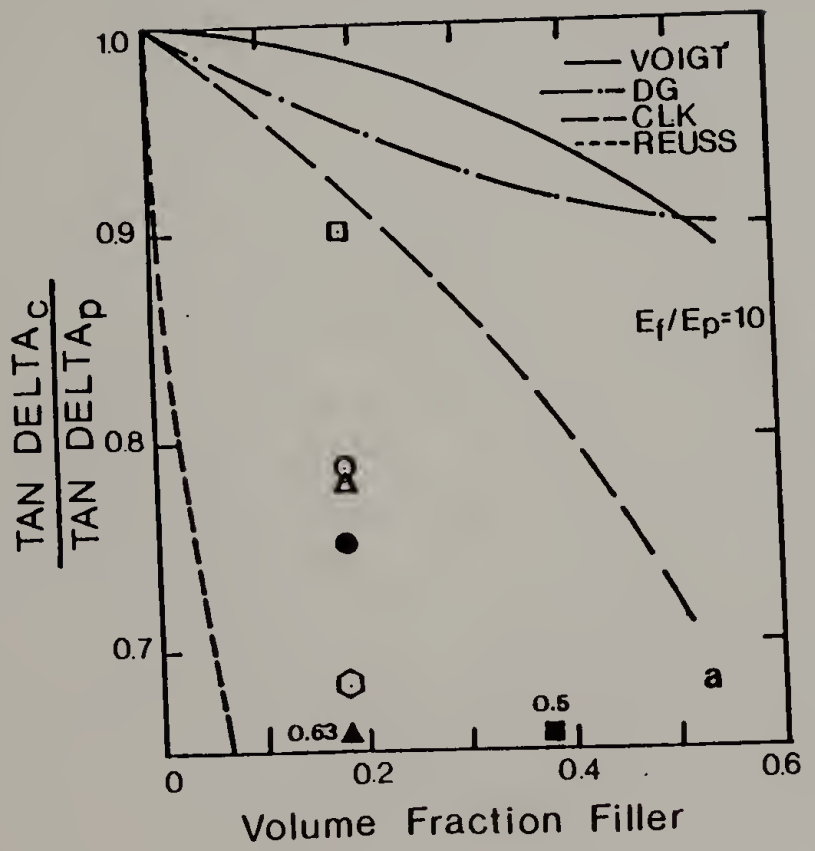
TAN DELTA$_c$ / TAN DELTA$_p$
1.0
0.9
0.8
0.7
VOIGT
DG
CLK
REUSS
E_f/E_p=10
a
0.63
0.5
0
0.2
0.4
0.6
Volume Fraction Filler

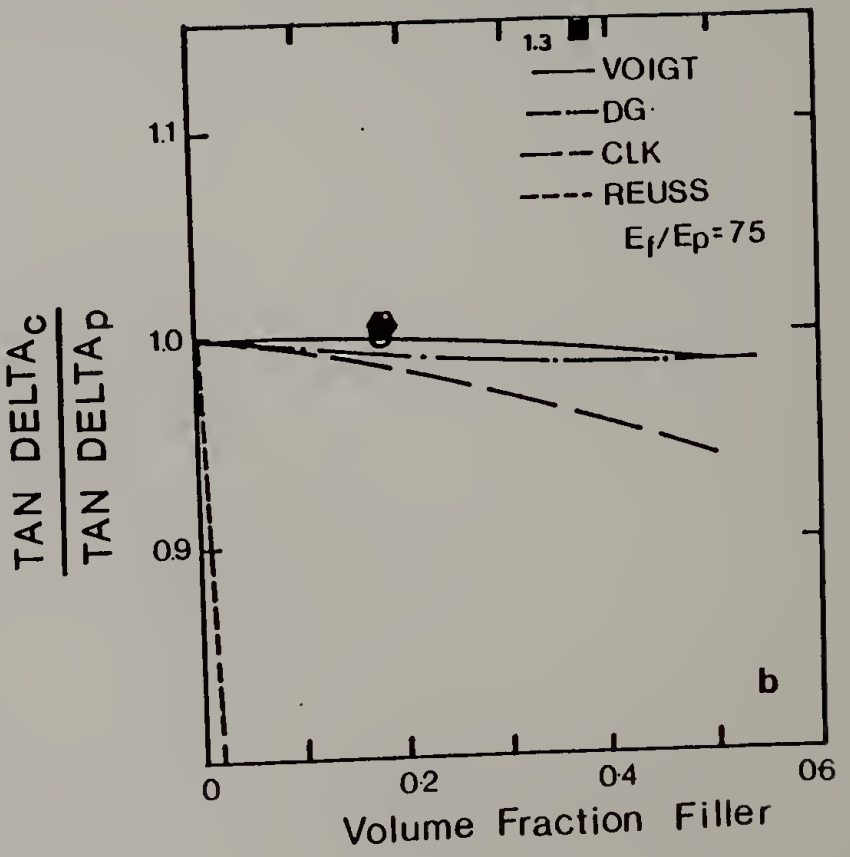
TAN DELTA$_c$ / TAN DELTA$_p$
1.1
1.0
0.9
1.3
VOIGT
DG
CLK
REUSS
E_f/E_p=75
b
0
0·2
0·4
0·6
Volume Fraction Filler

4.6 Discussion

The discrepancy between predictions of both modulus and damping of polymer-filler composites and experimentally obtained values has been of some concern and possible reasons and corrections have been suggested in the literature [6,14]. This problem is usually severe at high volume concentration of dispersed phase (at low concentration of dispersed phase it must be noted that the Voigt, DG and CLK Model predictions are extremely close).

If one were to seek causes of lack of correspondence between the models and real materials, at least three distinct reasons for the lack of perfection of real materials may be noted: 1) agglomeration of filler phase due to a vastly different chemical nature from the matrix phase; 2) lack of adhesion at the polymer filler interface and 3) thermal effects due to different coefficients of thermal expansion of the two phases. Each of these reasons have been considered to explain the failure of theoretical models to accurately predict moduli. In cases where the matrix is semicrystalline, the presence of filler will influence not just overall crystallinity but also the morphological character of the matrix and this phenomenon was observed in the present study.

These causes may also be responsible for the increased damping of filled polymers at higher temperatures beyond even that predicted by the theoretical upper bound (the Voigt Model tan δ). Particle-particle friction and particle polymer friction are generally assumed to be responsible for increased damping [6,24].

The increased damping is thus seen to be an interfacial term since for most inorganic fillers the relatively low surface area would prevent presence of filler from affecting the environment of a large volume of polymer. To be able to quantitatively study this for steady state harmonic excitation, the energy loss per cycle per unit sample volume is considered:

$$L = \pi \gamma_o^2 E''$$

Where γ_o is the strain amplitude imposed on sample and E" the loss modulus. In general the measured energy loss differs from theory by

$$I = \frac{\pi \gamma_o^2}{v_p} (E''_{meas} - E''_{model})$$

Where I is the interface energy loss per cycle per unit volume of polymer and E" model is the loss modulus predicted by an appropriate model. In Figure 4.7 the mechanical energy loss spectra for Marlex® filled with 40% untreated $CaCO_3$ is compared with the DG model of Marlex® filled with 40 wt% $CaCO_3$. The difference in the two spectra at higher temperatures (shaded region) can be attributed to interfacial energy losses. Given relatively more ideal systems, this expression may be utilized to study effect of filler concentration and surface properties on interfacial energy loss.

4.7 Conclusions

Differences in dynamic mechanical spectra of three polyethylenes

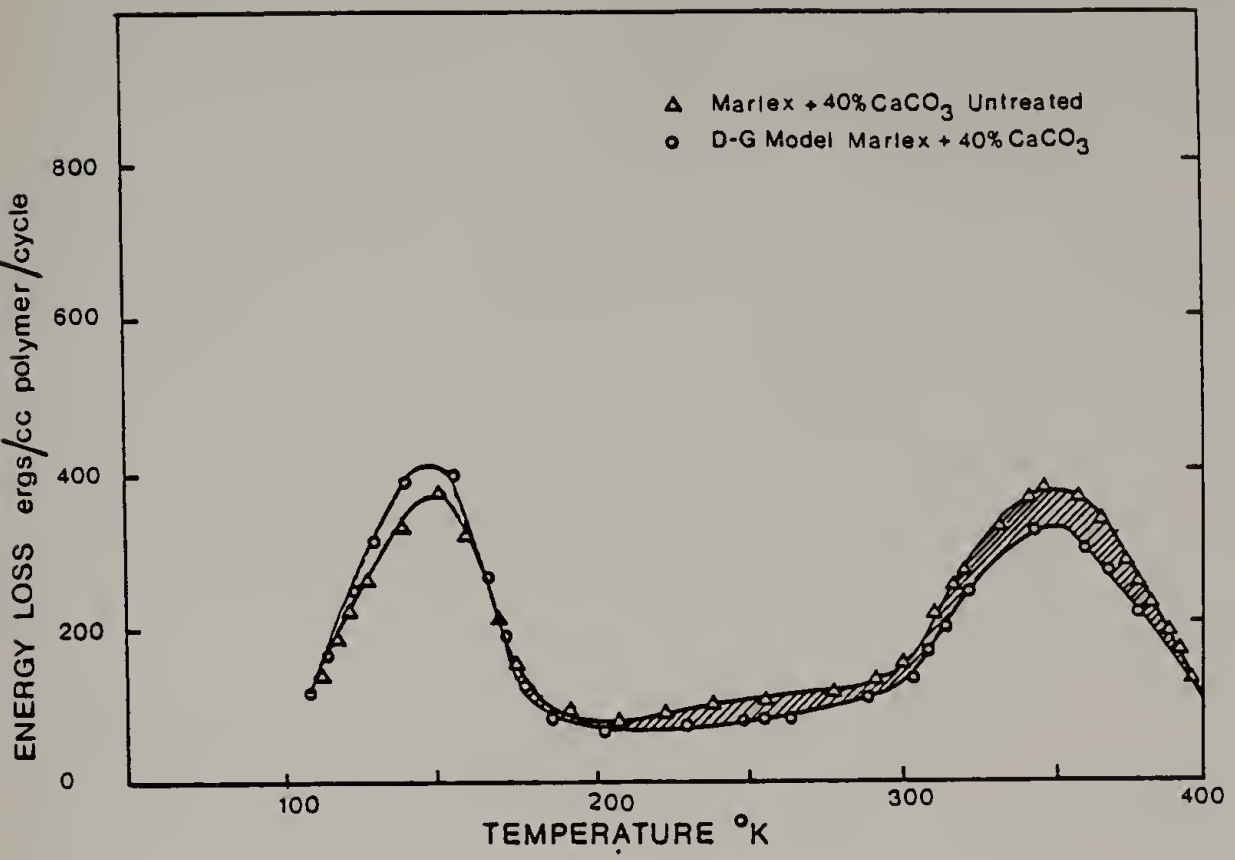

Figure 4.7 Energy loss per cycle for Marlex + 40 wt% untreated $CaCO_3$ compared to the D-G model prediction. Shaded area indicates interfacial energy loss estimate.

filled with $CaCO_3$ can be attributed to polymer crystallinity and differences in polymer filler coupling.

Certain elastic moduli expressions have been used to generate complex moduli of model viscoelastic composites and these have been compared to experiment. Differences between prediction and actual values are attributed to particleparticle and particle-polymer interactions arising at the interface of the materials.

An interfacial energy loss estimate is proposed which can be used to determine the causes of increased damping at high temperatures in presence of filler.

4.8 References

1. A.M. Gessler, W.M. Hess and A.I. Medalia, Plast. Rubber Process. 3, 3, 109, 1978.
2. L.E. Nielsen, Trans. Soc. Rheol., 13 (1), 141, 1969.
3. R.D. Bohme, J. Appl. Polym. Sci., 12, 1097, 1968.
4. T. Hirai and D.E. Kline, J. Compos. Mat., 7, 160, 1973.
5. J.L. Kardos, W.L. McDonnell and J. Raisoni, J. Macromol. Sci., B6, 397, 1972.
6. B-L Lee and L.E. Nielsen, J. Polym. Sci., B15, 683, 1977.
7. T.B. Lewis and L.E. Nielsen, J. Appl. Polym. Sci., 14, 1449, 1970.
8. U.S. Patent #4,097,447 issued June 27, 1978 to E.G. Howard of E.I. duPont de Nemours and Co.
9. U.S. Patent #4,950,303 issued April 13, 1976 to R.D. Lipscomb of E.I. duPont de Nemours and Co.

10. E.G. Howard, B.L. Glazar and J.W. Collette, I & E.C., Prod. Res. Dev., 20, 421 (1981).

11. E.G. Howard, R.D. Lipscomb, R.N. MacDonald, B.L. Glazar, C.W. Tullock and J.W. Collette, I & E.C., Prod. Res. Dev., 20, 429 (1981).

12. Hercules Powder Co., Hifax 1900 product literature.

13. D.J. Massa, J. Appl Phys., 44, 6, 1973.

14. L.E. Nielsen and T.B. Lewis, J. Polym. Sci., A2, 7, 1795, 1969.

15. J. Kolarick, J. Janacek and L. Nicolais, J. Appl. Polym. Sci., 20, 841, 1976.

16. "Polymer Blends and Composites" by J.A. Manson and L.H. Sperling, Plenum, New York, 1976.

17. Z. Hashin, Appl. Mech. Rev., 17, 1, 1964.

18. M.T. Takemori, Poly. Engr. and Sci., 18, 16, 1193, 1978.

19. "Mechanics of Composite Materials" by R.M. Christensen, Wiley-Interscience, New York, 1979.

20. R.M. Christensen and K.H. Lo, J. Mech. Phys. Solids, 27, 4, 1979.

21. Z. Hashin, Int. J. Solid Structures, 6, 539, 1970.

22. G. Jarzebski, S. MeGee and P. Mroz, Univ. of Delaware, Report CCM-79-11.

23. R.A. Dickie, J. Appl. Polym. Sci., 17, 45, 1973.

24. "Dynamic Mechanical Analysis of Polymeric Material" by T. Murayama, Elsevier, New York, 1978.

CHAPTER V

TENSILE PROPERTIES OF $CaCO_3$-FILLED POLYETHYLENES

5.1 Introduction

In the previous chapter the small strain behavior of filled polyethylenes was investigated with a view to determine the changes in the viscoelastic behavior of PE brought about by presence of higher modulus elastic inclusions. In this chapter the large strain behavior of filled polyethylenes is investigated. The objective is to understand the differences which exist, if any, in the deformation behavior of filled and unfilled polyethylenes in the nonlinear regions of the stress-strain curve.

The determination of sample dilatation upon deformation was also performed on filled and unfilled polyethylenes. Dilatation is especially significant in multiphase materials because dilatational stresses are present at the numerous internal interfaces, leading to cavitation, crazing or like phenomena which initiate at the interface. Such dilatational failure is generally considered deleterious, but may have advantages as evidenced in the superior impact properties of ABS or high impact thermoplastics where crazing is an important non critical microfailure mode.

5.2 Experimental

Table 1.2 details the origins and relevant properties of the

polyethylenes (PE) and $CaCO_3$ fillers used in this study.

5.2.1 Sample Preparation. The mixing of $CaCO_3$ with Alathon® and Marlex® was carried out in a two roll mill in the temperature range 140°C to 160°C for 5 to 7 minutes (depending upon the polymer molecular weight). Prior to mixing the $CaCO_3$ was dried and stored in air tight containers. Compression molding of the milled composite was carried out according to ASTM D1928-70 procedure C in a picture frame mold. Blends of DPCC with Marlex® and Alathon® were prepared as above. It must be noted that the melt behavior of Alathon®, the low molecular weight PE, in the milling step revealed that it was unsuitable for such operations.

Hifax®, the high molecular weight PE, is not melt processible by conventional techniques. Mixing of Hifax® and $CaCO_3$ was carried out by preparing a slurry of the two powders in acetone and slowly evaporating the acetone in a Buchi rotary evaporator. Blends of Hifax® and DPCC were prepared similarly. The high molecular weight PE composites were compression molded using higher temperatures [3].

From the 3 mm thick compression molded sheets, ASTM D638 Type C specimens were punched out. All specimens were annealed for 1 hour at 80°C prior to testing. All stresses and strains are engineering quantities.

5.2.2 Testing. Tensile test: Stress strain tests till break were carried out on an Instron testing machine at 5 mm/min stroke rate.

Determination of tensile stress at yield (σ_y), tensile stress at break (σ_b), strain at yield (ε_y) and strain at break (ε_b) are according to the ASTM D638 procedure.

Dilatation Test: Stress-strain-dilatation testing was carried out in a Farris gas dilatometer [4]. A brief description of its operating principle is given below.

Figure 5.1 is a schematic of the dilatometer shown in profile. The specimen S is introduced into a constant volume chamber C and held by the grips UG and LG. The lower grip (LG) is attached to a traveling shaft (TS) which passes through a leak proof O-Ring assembly (ORA). To compensate for the volume changes due to TS displacement, an identical compensating shaft (CS) is rigidly attached to the TS. When the sample dilates, the resulting compression of gas in C is measured by a pressure transducer (PT). The transducer is previously calibrated for precise volume changes using a piston micrometer.

The dilatometer as described above was mounted in an Instron servo-hydraulic testing system (Model 1321). Testing was performed with the tester in stroke control at a stroke rate of 5 mm/min. Sample strain (based on specimen gage length) was limited to 0.50.

Specimens were prepared thus: previously annealed ASTM D638 C specimens were dipcoated in an ammoniated natural latex for 5 minutes. They were then dried in air for 30 minutes, transferred to an air oven maintained at 45°C and dried overnight. The dried samples were lightly coated with grease prior to testing. The latex dipcoating prevented any diffusion of gas into the specimen

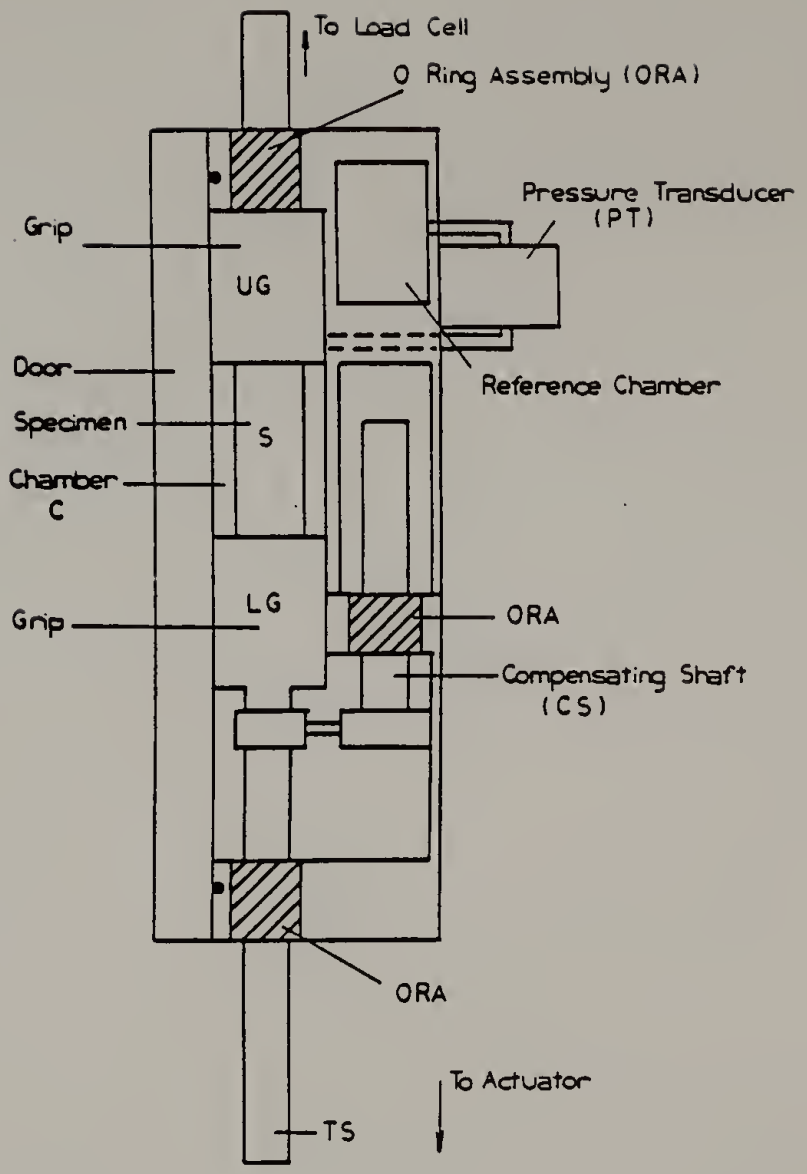

Figure 5.1 Schematic of gas dilatometer.

while the grease reduced heat transfer between sample and chamber.

Deformation microscopy: Small dogbone shaped specimens of dimensions (0.75 mm x 1 mm x 0.1 mm) were mounted on specially prepared copper deformation grids coated with gold and stretched in an electron microscope (JEOL 100 CX Temscan) using a deformation grid holder. The specimens were observed in the secondary electron imaging mode.

5.3 Results

The results of tensile tests are shown in Table 5.1.

5.3.1 Comparison of Tensile Behavior Unfilled Polyethylenes. The polyethylenes under investigation were chosen to represent a wide range of molecular weight and were chosen so as to determine the role of matrix molecular weight on the ultimate properties of the filled polymer.

Alathon®, once annealed under conditions described above, is quite brittle and has negligible extension after yield. Marlex® specimens exhibit a neck and the samples extend to 530% by drawing. In Hifax® specimens necking and consequent drawing is not observed. Instead, after yielding, the slope of the stress-strain curve remains positive and the samples extend by uniform reduction of cross-sectional area. It may be expected that such differences in mechanical behavior are a result of morphological differences in the sample which result from the variation of molecular weight. Alathon®

Table 5.1

TENSILE PROPERTIES OF FILLED POLYETHYLENES

	σ_y MN/m^2			ε_y %			σ_D MN/m^2			ε_b %		
	U	T	B	U	T	B	U	T	B	U	T	B
Alathon	19.1			6			13.3			9		
+2% $CaCO_3$							22.6	23.5	21.4	9	23	8
+4% $CaCO_3$						13	22.0	22.2	24.6	7	15	16
+8% $CaCO_3$						10	14.7	19.8	22.5	4	15	12
+19% $CaCO_3$							12.68			3	3	
Marlex	24.6			22			12.9			530		
+2% $CaCO_3$	25.6	24.6	23.9	20	20	20	8.6	12.3	14.7	140	290	410
+4% $CaCO_3$	23.4	21.4	22.4	25	18	18	7.5	16.8	17.9	92	394	120
+8% $CaCO_3$	22.2	20.4	28.3	14	15	20	7.0	13.3	18.5	100	300	106
+19% $CaCO_3$	17.9	14.9		6.4	14		18.2	13.0			42	
Hifax	21.5			28			28.1			820		
+2% $CaCO_3$	17.0		16.4	20		13	21.2		22.7	595		344
+19% $CaCO_3$	13.5	11.6	14.7	12	12	10	13.7	12.1	20.0	20	20	614
DuPont PE/$CaCO_3$ Composite (38% $CaCO_3$)	12.4			4			12.6			410		

U = Untreated $CaCO_3$
T = $CaCO_3$ + 2% KR-TTS
B = Blend of PE and DuPont Composite

samples exhibit visually flat fracture surfaces while Marlex® fractures with the creation of jagged fibrillated surfaces. Hifax® fracture surfaces are also quite flat. However, there is substantial recoil of the two halves of the Hifax sample upon breaking indicating a distinct entropic character in the deformation of high molecular weight polyethylene.

5.3.2 Comparison of Tensile Behavior of Filler Polyetheylenes.

duPont PE/$CaCO_3$ Composite (DPCC): DPCC has a sharp yield at a relatively low strain of 4%. Beyond this it extends with no necking until break (410%). The stress-strain curve resembles that of an impact modified glassy thermoplastic.

Filled Alathons: Since the unfilled low molecular weight Alathon® was itself quite brittle, it is not surprising that the filled specimens exhibited brittle behavior. Treatment of the $CaCO_3$ surface with KR-TTS® improved elongation at break as did blending of Alathon® with DPCC composite.

Filled Marlex®: In general yield stress and elongation at break decreased with increasing amount of filler. The treatment of $CaCO_3$ with KR-TTS® (treated $CaCO_3$) had a significant effect. The yield stress of treated $CaCO_3$ filled PE's is less than that of the untreated case at the same filler loading. On the other hand the elongation at break improves greatly when the $CaCO_3$ is treated at all filler loadings investigated. Filled Marlex® specimens also exhibit some necking, though that becomes less pronounced at higher

filler loadings. With DPCC composite blends the yield stress and elongation at break are not consistent with the above results though elongations at break are lower than treated $CaCO_3$ filled specimens. This is believed to be due to imperfect mixing of DPCC with Marlex®.

Filled Hifax: Blends of Hifax® with DPCC display very good mechanical properties with high elongations at break. However, in blends of Hifax® with treated and untreated $CaCO_3$, properties rapidly deteriorated with increased filler loading and there is little doubt that this deterioration is due to filler agglomeration.

5.3.3 Dilatation Measurement of Unfilled and Filled Polyethylenes.

Figures 5.2, 5.3, 5.4 and 5.5 give the dilatation behavior of the filled polyethylenes tested. Alathon® and its composites gave negligible dilatation before break and hence test results are not reported. Figure 5.2 compares the stress-strain and dilatation-strain behavior of $CaCO_3$ filled Marlex® at 0%, 2%, 4%, 8% and 19% by volume of filler. Dilatation commences at about the yield point of the specimen and increases with filler content. The dilatation curves change slope at strains between 0.3 and 0.4. Similar results are seen for KR-TTS® treated $CaCO_3$, for $CaCO_3$ filled Hifax® and for blends of Hifax® and DPCC.

5.4 Analysis and Discussion

5.4.1 Yielding. For filled glasses (with filler well dispersed in matrix) Nicolais and Narkis [3] proposed a criterion based on

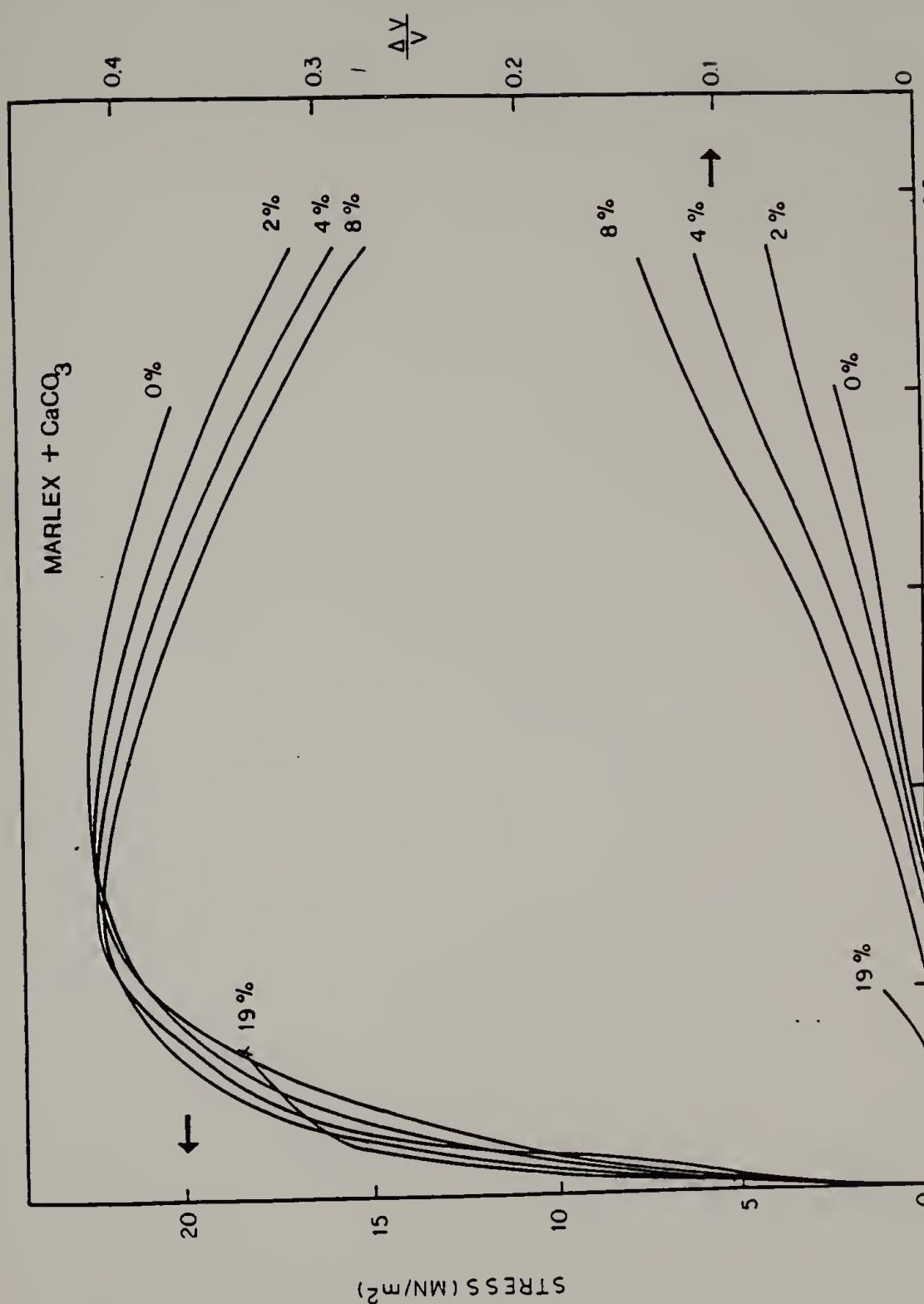

Figure 5.2 Stress-strain-dilatation curves for Marlex filled with 0, 2, 4, 8 and 19 volume % $CaCO_3$.

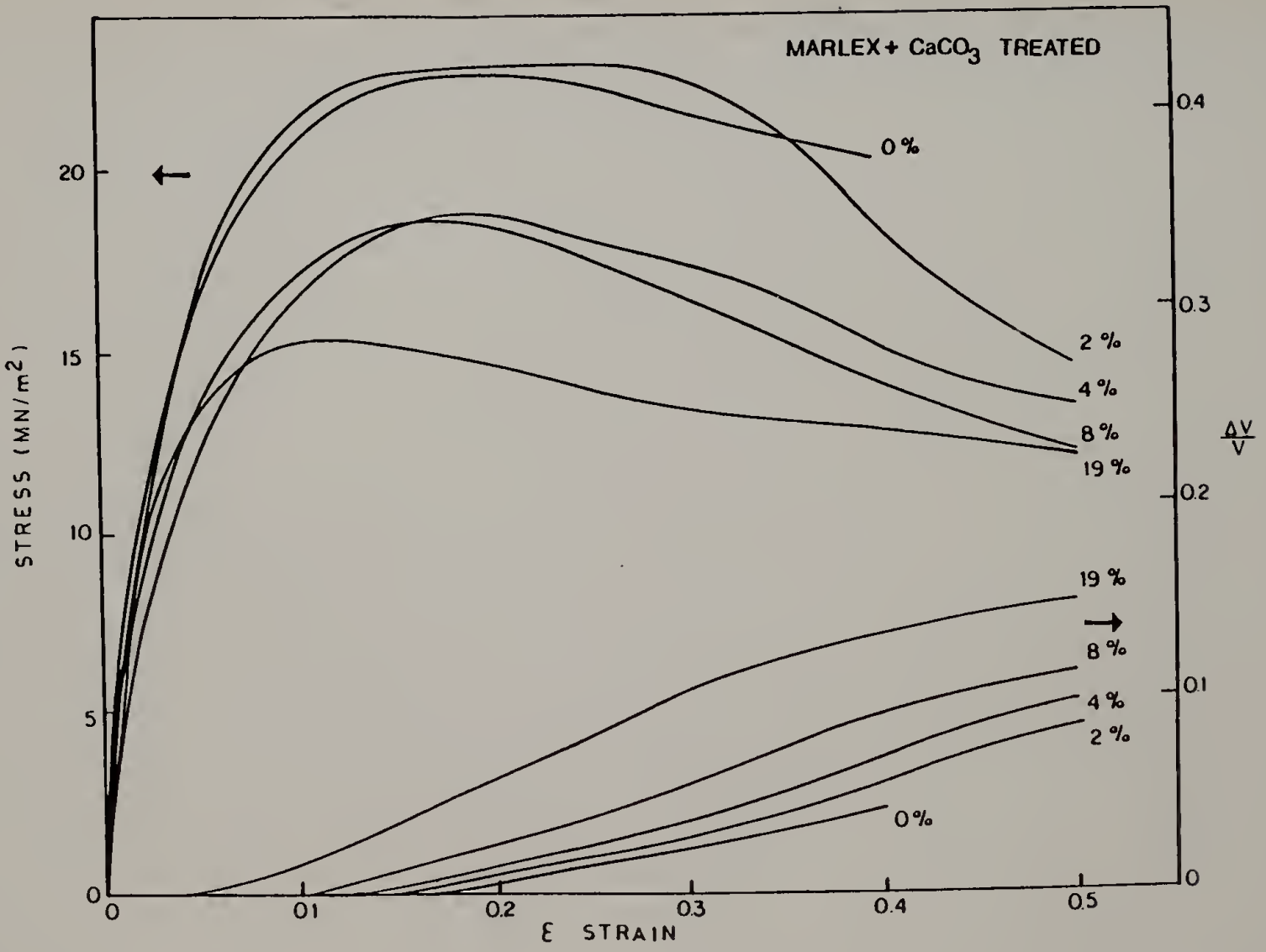

Figure 5.3 Stress-strain-dilatation curves for Marlex filled with 0, 2, 4, 8 and 19 volume % treated $CaCO_3$.

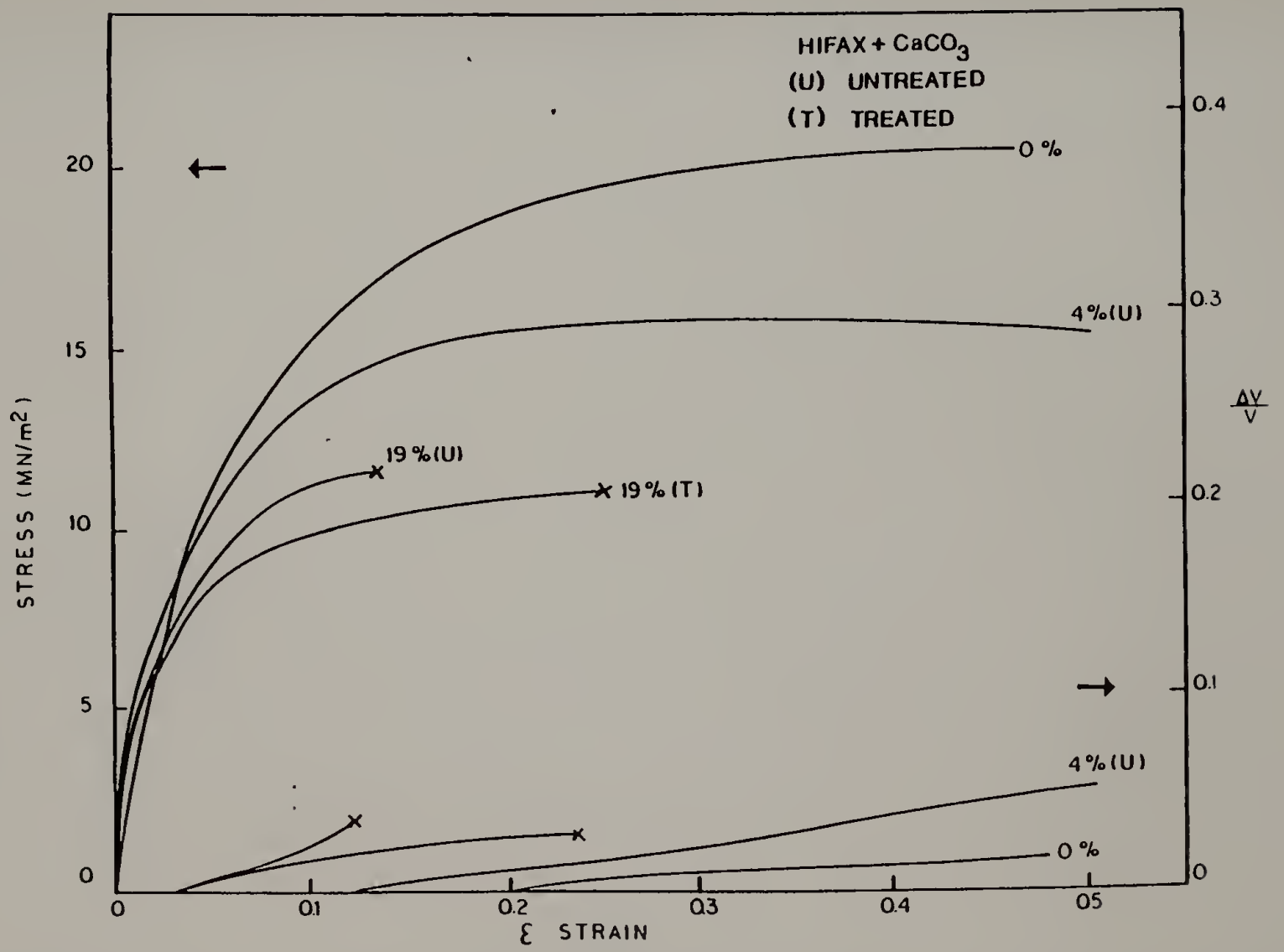

Figure 5.4 . Stress-strain-dilatation curves for Hifax filled with 0.4 and 19 volume % $CaCO_3$ (U) and 19 volume % treated $CaCO_3$ (T).

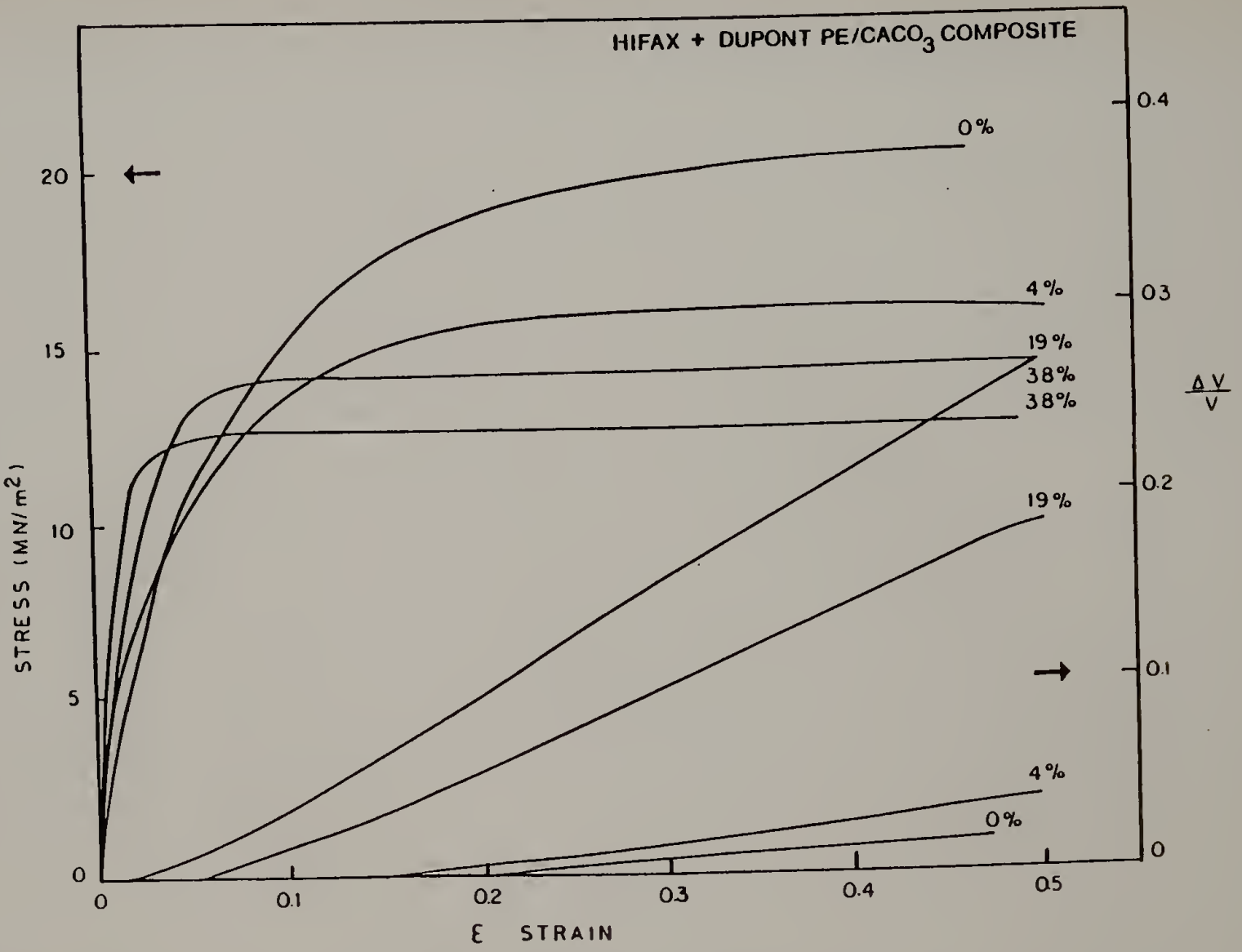

Figure 5.5 Stress-strain-dilatation curves for Hifax blended with DPCC. The blends contain 0.4 and 19 volume % $CaCO_3$. Also shown is DPCC (38 volume % $CaCO_3$).

dewetting reducing effective load bearing cross-sectional area:

$$\sigma_{yf} = \sigma_{yp} (1 - 1.21 \phi^{2/3}) \qquad (1)$$

where σ_{yf} and σ_{yp} are the yield stresses of filled and unfilled polymer respectively and ϕ is the volume fraction of filler. In Figure 5.6 is shown the plot of σ_{yc}/σ_{yp} versus volume fraction filler (ϕ) for filled Marlex®. Better agreement with equation (1) is exhibited by Marlex® filled with treated $CaCO_3$. The result may be rationalized as follows: the surface treatment of $CaCO_3$ results in much better dispersion of $CaCO_3$ in the matrix. The better dispersion of particles leads to a greater reduction of load bearing area upon dewetting as compared to the poorly dispersed case. The reduction of yield stress upon treatment of filler surface has been observed in other studies on $CaCO_3$ filled polyethylene and polypropylene [4,5].

5.4.2 Dilatation. The effect of $CaCO_3$ surface treatment with KR-TTS is shown in Figure 5.7 of the stress-strain-dilatation curves of Marlex® filled with 4% and 8% $CaCO_3$ both untreated and treated. The dilatation curves coincide at low strains; however at higher strains the specimens filled with untreated $CaCO_3$ exhibit higher dilatation.

Volume creating microfailure modes are observed at large strains in polymer blends and composites where phase boundaries exist. Two models of dilatational behavior are considered, the first of which was developed to account for dilatational behavior in filled elastomers, and the second developed for rubber modified thermoplastics.

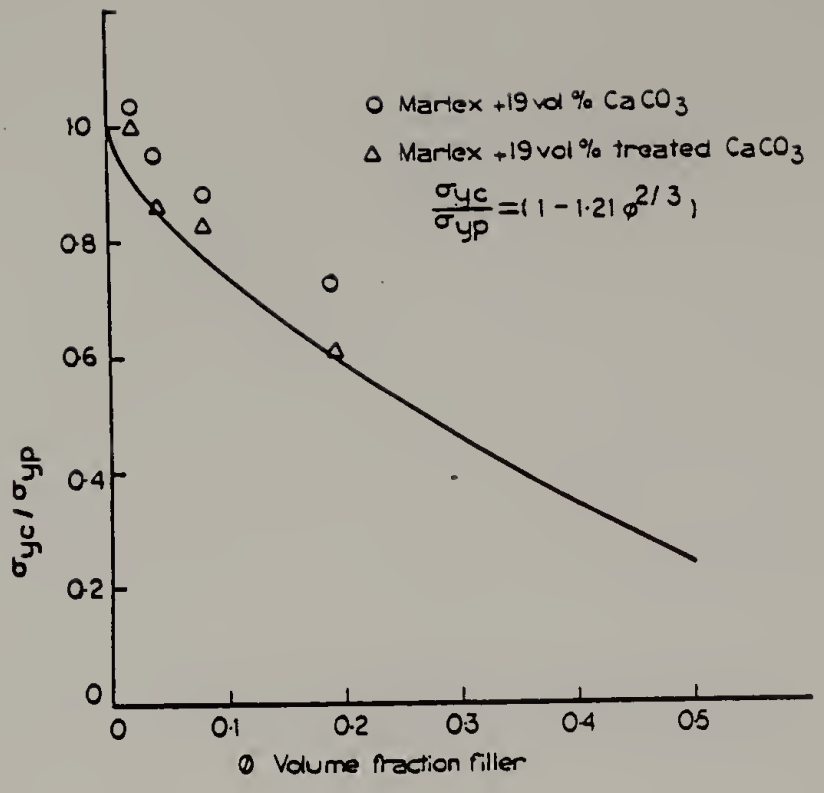

Figure 5.6 Comparison of experimental data with Nicolais-Narkis expression for yield point determination.

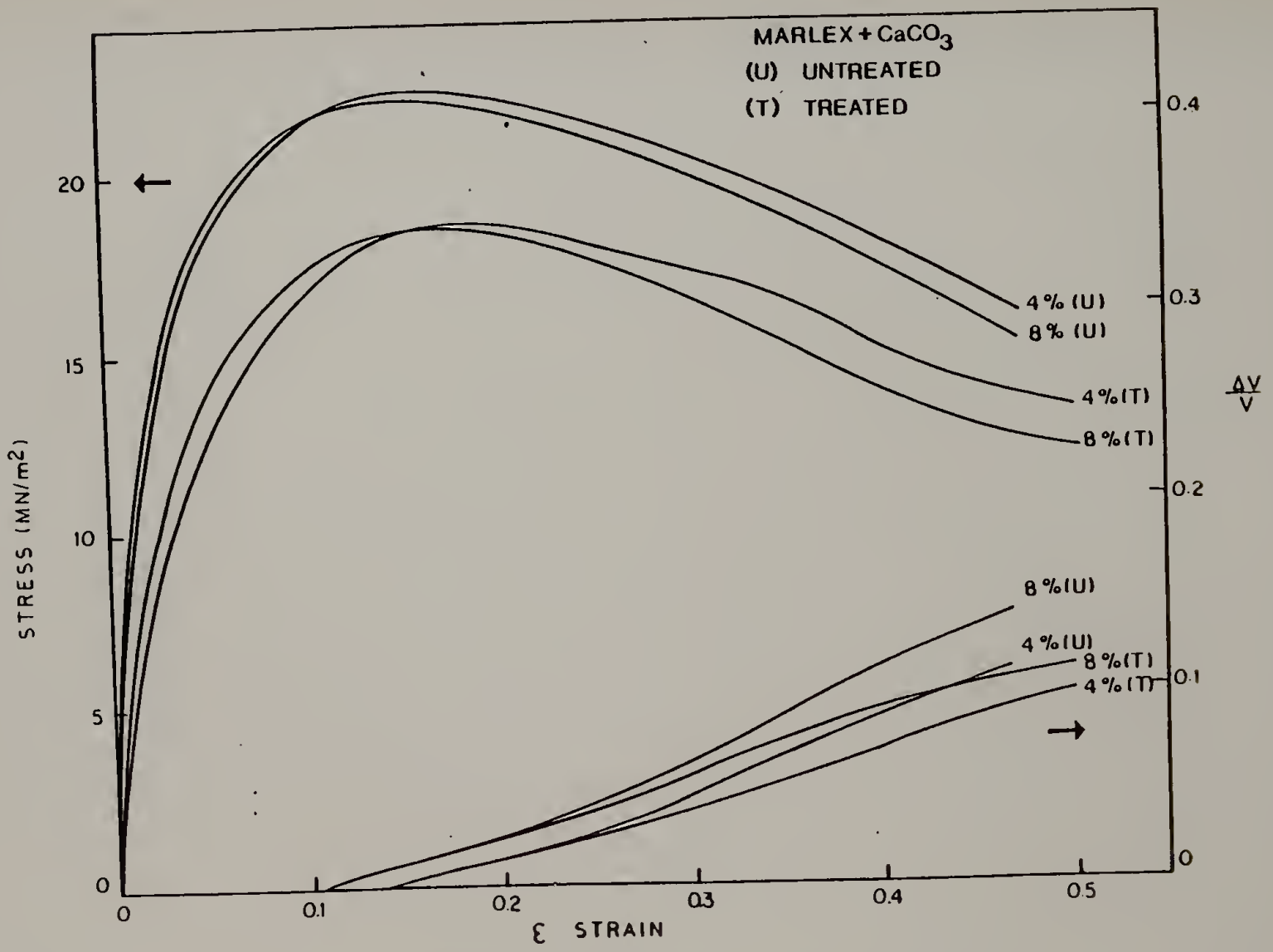

Figure 5.7 Effect of filler treatment on stress-strain-dilatation curves. Shown are Marlex filled with 4 and 8 volume % $CaCO_3$ untreated (U) and treated (T).

Farris [6] proposed a stochastic theory to account for dilatation in filled elastomers based on the fact that ellipsoid shaped vacuole formation was observed around spherical filler particles. It is shown that the maximum slope of the dilatation-strain curve is proportional to volume fraction of filler around which vacuoles exist.

$$\frac{1}{v_0}\left(\frac{d(\Delta v)}{d\varepsilon}\right) = C\, v_f$$

where v_0 is the volume of sample undergoing dilatation, ε the longitudinal strain and v_f the volume fraction of filler present. At steady state the constant C was experimentally evaluated in filled elastomers to be 1.

Bucknall has measured dilatation in rubber modified thermoplastics utilizing the Darlington and Saunders extensometer arrangement [7]. By making the assumption that just crazing and shear yielding are the mechanisms responsible for deformation (beyond the elastic region) and considering shear yielding to be essentially a volume conserving mode of deformation, the slope of the dilatation-strain curve is related to the extent of crazing:

$$\frac{1}{v_0}\left(\frac{d\Delta v}{d\varepsilon}\right) = 1 + 2\,\frac{\partial \varepsilon_2}{\partial \varepsilon_1}$$

where ε_2 is lateral strain and the other symbols have their usual meaning. Hence if there is no shear yielding, the slope of the

curve would be 1, and if shear yield totally dominates mean failure the slope would equal zero. While no assumption is made regarding the geometry of the craze in the above equation, morphological investigations reveal crazes in impact modified thermoplastics to develop and grow normal to the stress direction. Bucknall has modeled the kinetics of growth of crazes with reasonable success [ref. 7, page 201].

In Table 5.2 are given values for the slopes of the dilatation-strain curves of Marlex® filled with $CaCO_3$. It is noticed that the slopes of the curves indicate increasing amounts of dilatational microfailure in the steady state regions (the slope of the curve is independent of the sample gage length). A maximum value of 45% dilatational failure is observed at 19 vol% filler loading. Hence dilatational failure greatly exceeds vacuole theory prediction.

In order to investigate the type of dilatational failure mode present in rigid particle filled semicrystalline polymer the deformation morphology of filled and unfilled polyethylenes was investigated. While the conclusions of the entire study will be discussed in the next chapter a few pertinent results are indicated here. Figure 6.5 (refer to Chapter 6) shows three consecutive scanning electron micrographs using a secondary electron detector (SEM-SEI) of a region of the specimen Marlex® with 4 vol% $CaCO_3$. Figure 6.5a is the region before deformation. In Figure 6.5b is seen the nucleation of a flaw in the region A. At higher strains (Fig. 6.5c) more crazes have appeared. The craze, like the character of the flaws is seen more

Table 5.2

Slopes of Dilatation-Strain Curves for Filled Marlex® Specimens

Sample	Maximum Slope	
	Untreated $CaCO_3$	Treated $CaCO_3$
Marlex	0.17	
+ 2%	0.20	0.20
+ 4%	0.30	0.25
+ 8%	0.35	0.30
+19%	0.60	0.50

clearly in Figure 6.6. Figures 6.9a and b show the critical craze in 19 vol % filled Marlex®. Fully dewetted particles are evident in the midsection of the craze. It is also noticed that shear yielding has occurred in region S. The angle the shear bands make is in the range 20° to 45° to the loading direction. While most crazes are approximately normal to the stress direction, a significant fraction exhibit deviation from normality.

It is easier to visualize dewetting and failure when the inclusions in a composite are rigid relative to the matrix since the stress concentrations occur at the poles and subsequently the matrix separates from the filler in that region. For crazes to occur however the stress concentration must occur in the equatorial regions and this is possible when the modulus of the inclusion is less than that of the matrix as in impact modified thermoplastics.

A possible explanation for crazing in filled semicrystalline thermoplastics could indeed visualize both mechanisms operating and this is shown in Figure 5.8. Initially particles could dewet (Fig. 5.8b). Subsequently the stress concentrations would shift to the equatorial region since the void is nonreinforcing. Given the irregular shape of the particles a profile of the void in the equitorial region would accelerate formation of a craze (Fig. 5.8c). After the crazes attain certain dimensions, their growth would dominate over the dewetting process in the dilatational response of the specimen.

It is expected that improved dispersion would lead to a greater number of localized crazes. However their dimensions would be

Figure 5.8 Schematic for proposed craze formation process in filled PE. (a) Initial configuration (b) Dewetted particle (c) Craze formation normal to stress direction.

smaller than crazes initiated by regions of agglomerated particles and their dilatation would also be less. This has been noted by Farris earlier [8]. This would explain the differences in dilatational behavior of untreated and treated $CaCO_3$ filled polyethylene.

5.5 Conclusions

The mechanical properties and dilatational behavior of three polyethylenes filled with $CaCO_3$ was found to be dependent upon filler content, polymer-filler interface and polymer molecular weight. Treatment of $CaCO_3$ with KR-TTS® improved the elongation at break. However, the yield stress was reduced in the treated specimens and this is attributed to improved dispersion.

Dilatation of specimens increased with $CaCO_3$ loading. Dilatation was suppressed at strains above 30% when the $CaCO_3$ was treated. Electron microscopy study of the deformation of unfilled and filled specimens revealed that crazing is prevalent in polyethylene in presence of filler.

5.6 References

1. Hercules Powder Co., Hifax 1900 product literature.
2. R.J. Farris, J. Appl. Polym. Sci., 8, 25 (1964).
3. L. Nicolais and M. Narkis, Polym. Eng. Sci., 11(3), 194 (1971).
4. S.J. Monte and G. Sugemann, Kenrich Petrochemicals Bulletin KR-1079-9, 1979.

5. Thompson, Weinman & Co., Technical Bulletin T-5-6,8, 1981.

6. R.J. Farris, Trans. Soc. Rheol., 12(2), 315 (1968).

7. "Toughened Plastics" by C.B. Bucknall, Applied Science Publishers Ltd., London, 1977.

CHAPTER VI

MICROFAILURE MODES IN PARTICULATE FILLED POLYETHYLENE

6.1 Introduction

In Chapter V the stress-strain dilatational behavior of unfilled and filled PE's revealed that the mode of deformation was altered because of filler presence in polyethylene. Specifically, it was seen that the dilatational mode of deformation increased in importance with increasing amount of filler.

A microscopy investigation is the simplest and most direct method of studying the physical nature of the deformation process. Accordingly, in this chapter the results of an electron microscopy investigation of the deformation modes in filled and unfilled PE specimens are reported.

6.2 Background

It is well known that the failure behavior of polymer composites is quite different from that of the unfilled polymer [1,2,3]. This is due to the differing nature of internal stress fields in these two classes of materials. The inhomogeneous nature of the stresses in composites results from the discontinuity in material properties at the interfaces of the two materials. Irrespective of the nature of the inhomogeneity, stresses are amplified at the interface and

consequently failure is usually initiated there.

The mode of failure depends upon the nature of matrix and inclusion. The inclusion may possess a higher tensile modulus (hard) or a lower tensile modulus (soft) relative to the matrix. Three types of polymer matrix types may be identified; rubbery, glassy or semicrystalline. When the inclusion is hard and the matrix rubbery, cavitation or dewetting occurs (see Fig. 6.1) resulting in ellipsoidal vacuoles formed about the inclusion [1,4]. Such a mode of microfailure occurs because the stress concentration is highest at the poles of the inclusion. When the inclusion is soft and the matrix is a glassy polymer, a void-fibril formation known as a craze develops in the equitorial regions of the particle (Fig. 6.1b). The microfailure mechanisms in operation for the other combinations of inclusion and matrix indicated are not well understood. However Freidrich and Karsch[5] observed cavitation in silicon oxide filled polypropylene.

The incorporation of a rigid mineral filler results in a deterioration in the impact properties and elongation at break of semicrystalline polymers. This deterioration may be partly attributed to the agglomerating character of the usually hydrophilic inclusion with inherent flaws contributing to early failure. More important perhaps is the reduced ability of these filled materials to deform substantially in a ductile mode.

In the light of this discussion, the objective of this work is

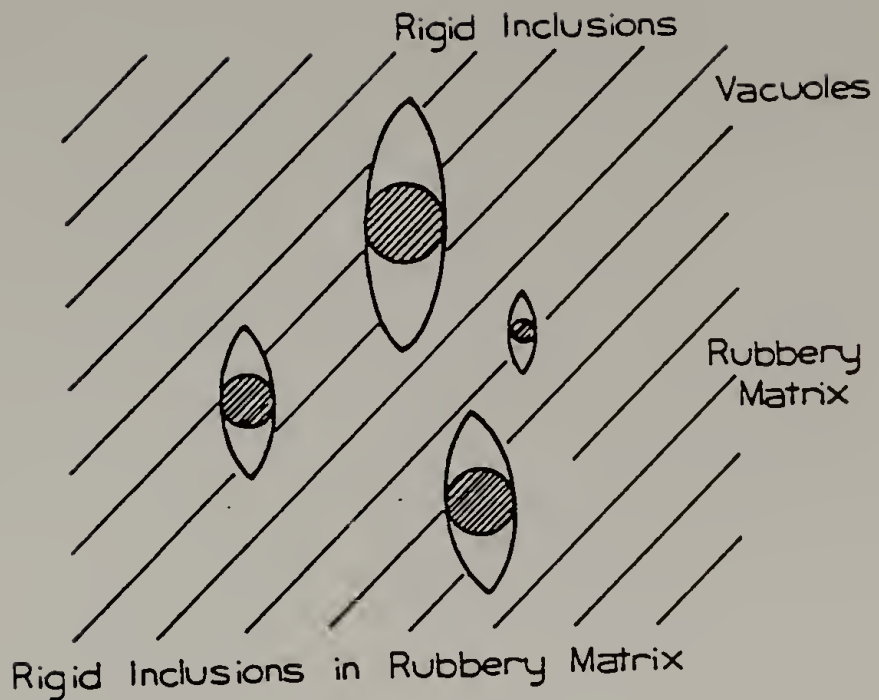

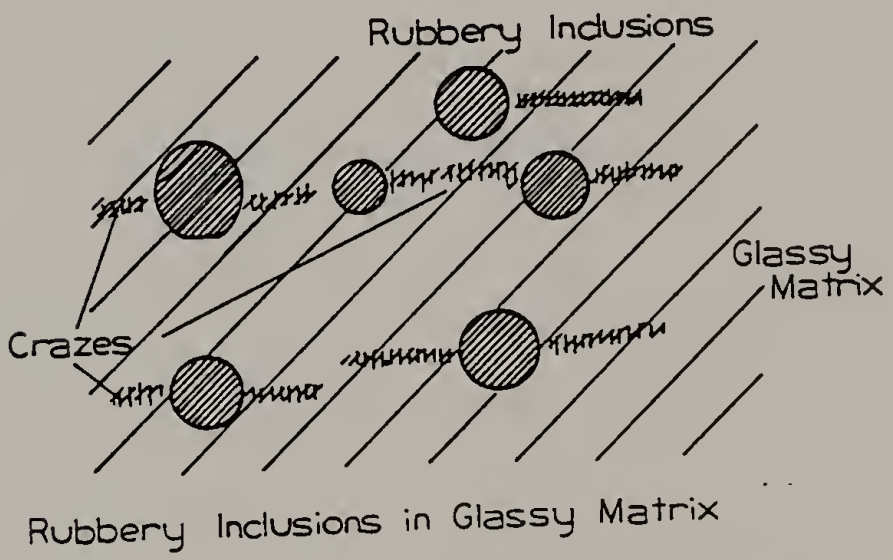

Figure 6.1 Schematic of failure modes in polymer composites (a) ellipsoidal vacuole formation in rigid particle filled elastomer; (b) craze formation in rubber modified glassy polymer.

to investigate microfailure mechanisms in $CaCO_3$-filled polyethylene and to evaluate the role of polymer molecular weight on these failure modes. The results of this study will be evaluated in the light of the dilatometric investigations of filled and unfilled polyethylene of Chapter V.

6.3 Experimental

Table 1.2 details the origins and relevant properties of the polyethylenes (PE) and $CaCO_3$ fillers used in this study.

6.3.1 Sample Preparation. Melt compounding of polyethylene and $CaCO_3$ for the Alathon® and Marlex® composites was performed on two roll mills. The milled material was compression molded in a picture frame mold according to ASTM procedure D1928.

Hifax®, the ultrahigh molecular weight PE is not melt processible. Mixing of Hifax® and $CaCO_3$ was performed by preparing a slurry of the two powders in acetone and slowly evaporating the solvent in a Buchi rotary evaporator. The mixture was compression molded as above but at higher temperatures. The thickness of the compression molded sheet ranged from 0.04 mm to 0.10 mm. A few samples were polished using a series of sandpapers of increasing fineness to almost consistent thickness. Specimen inhomogeneity was noticed in Hifax/$CaCO_3$ specimens as a result of the poor dispersion of $CaCO_3$. With careful selection of the film, however, it was possible to obtain thin film samples which deformed substantially

during a test. All samples were annealed for 1 hour at 80°C.

Miniature tensile bar replicas suitable for mounting on specially prepared copper deformation grids were prepared with width of narrowest section 1 mm. They were glued to the grids and mounted on the electron microscope deformation stage. Such a sample is shown in Figure 6.2. Specimens were gold coated prior to deformation in the microscope.

6.3.2 Electron Microscopy. Deformation microscopy of unfilled and filled polyethylenes was performed on a JEOL 100 CX using a deformation grid holder. The samples were imaged with a secondary electron detector. Strains specified in the text are assuming a deforming length of 1 mm.

The rate of elongation was 3×10^{-4} mm/sec. The deformation grid holder attachment on this microscope is provided with a micro meter to measure elongations with an accuracy of 0.01 mm. However, no real significance could be attached to these measurements since it was observed that no proportional relationship could be established between localized strain and overall strain. Moreover, in general during the process of plastic deformation different regions of sample with field size of interest to this study were in different states of deformation. Hence, specific values of strains mentioned in the text must be treated with caution and are provided to give a relative measure between stages of deformation. For consecutive micrographs, estimate of relative strain can be gauged from the micrographs themselves.

Figure 6.2 SEM-SEI of specimen (δ) mounted on deformation grid (G) for deformation microscopy study.

6.4 Results

6.4.1 Unfilled Polyethylenes. The three linear polyethylenes in this study behave quite differently in tensile tests at 5 mm/min stroke rate of ASTM D638 Type C specimens in an Instron, shown in Figure 6.3a. Alathon®, the low molecular weight PE, fractures in a brittle manner at strains of 9%. Marlex®, the intermediate molecular weight PE, behaves in a ductile manner with a sharp yield and subsequent necking. The strain hardened fibrillated section grows at the expense of the initial morphology to about 500% strain. Hifax®, the high molecular weight sample, does not draw; instead the stress strain curve continues to exhibit a positive, though lower, slope after yield.

In Figure 6.3b are dilatation-strain curves forthe two unfilled polyethylenes and for DPCC (38 Vol% $CaCO_3$), 4 vol% Marlex® filled $CaCO_3$, 19 vol% Marlex® filled $CaCO_3$ and 19 vol% filled Hifax®. The increase in dilatation with increasing $CaCO_3$ content is quite evident. The slope of the dilatation curve is an indication of the relative importance of volume creating failure mechanisms as compared to volume conserving failure mechanisms (a slope of 0.6 indicates that 60% of the deformation is of a dilatation nature).

In Figure 6.4 are comparative views of Marlex® and Hifax® at low (~ 30% strain, 6.4a,b) and high elongation (~ 150% strain, Figures 6.4c and d), respectively. It is seen that at the low deformation the overall morphology looks quite similar. The dark blocks of

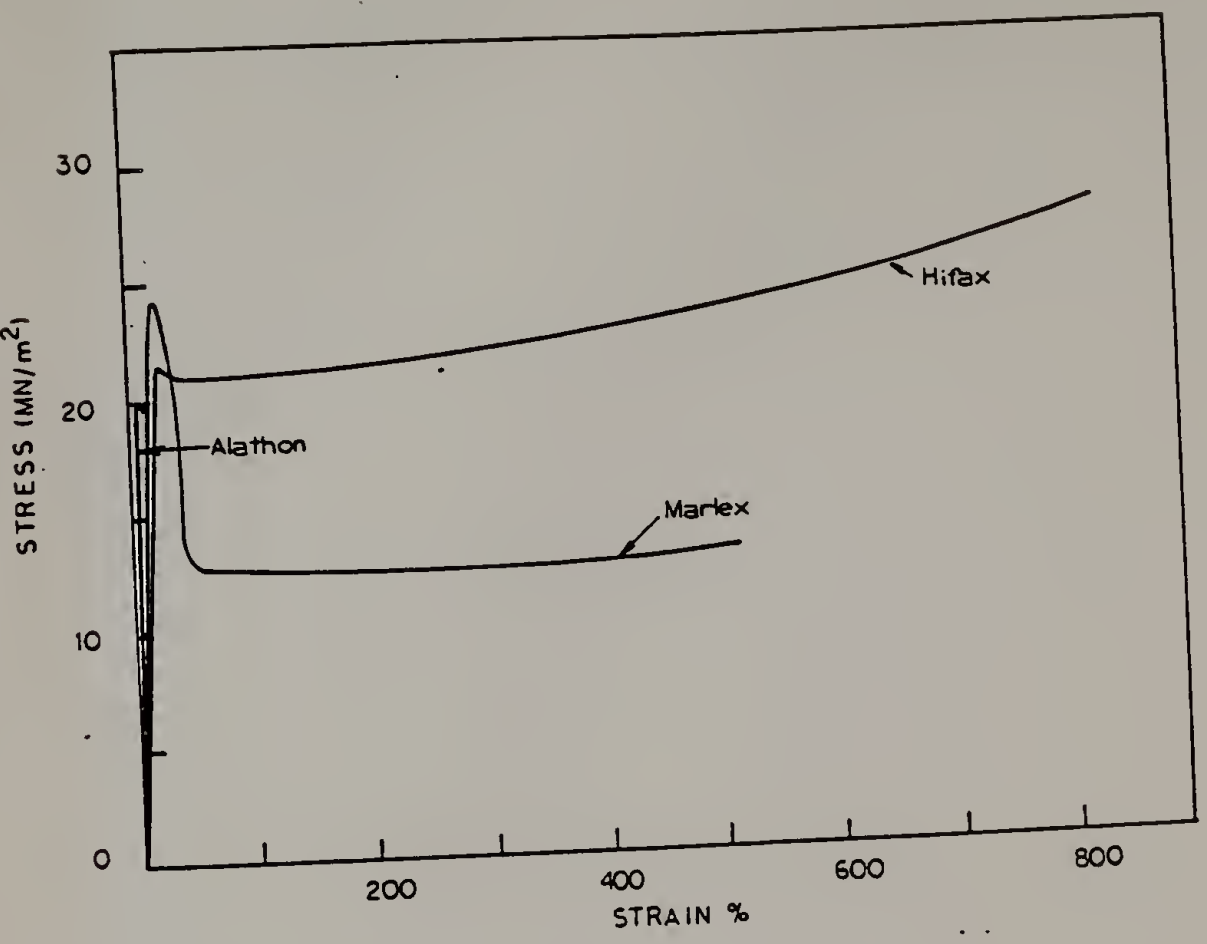

Figure 6.3 (a) Stress strain curves for Alathon, Marlex and Hifax. Stroke rate 5 mm/min.

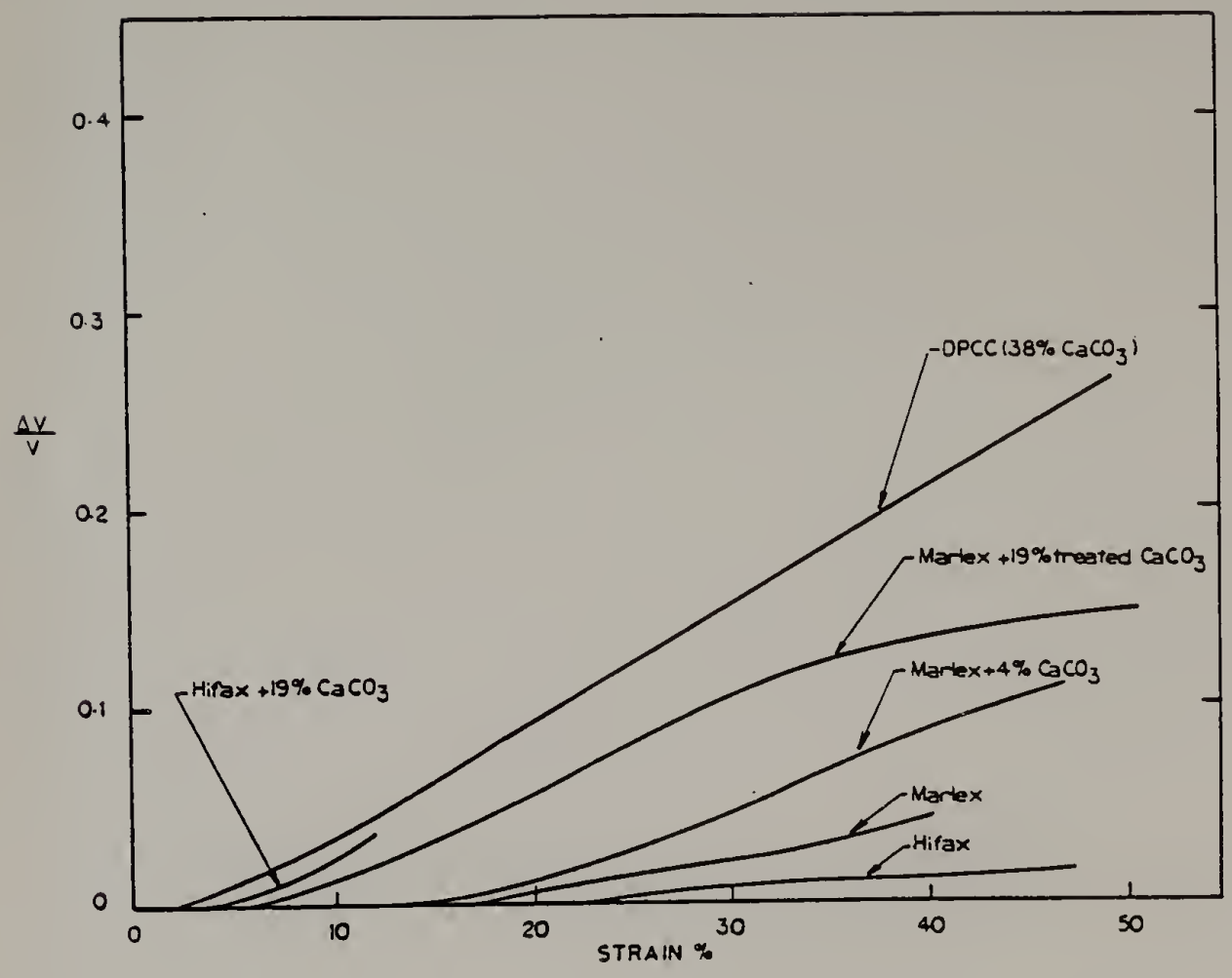

Figure 6.3 (b) Dilatation-strain curves for Marlex, Hifax, DPCC, Marlex + 4 vol % $CaCO_3$, Marlex + 19 vol % treated $CaCO_3$, Hifax + 19 vol % $CaCO_3$.

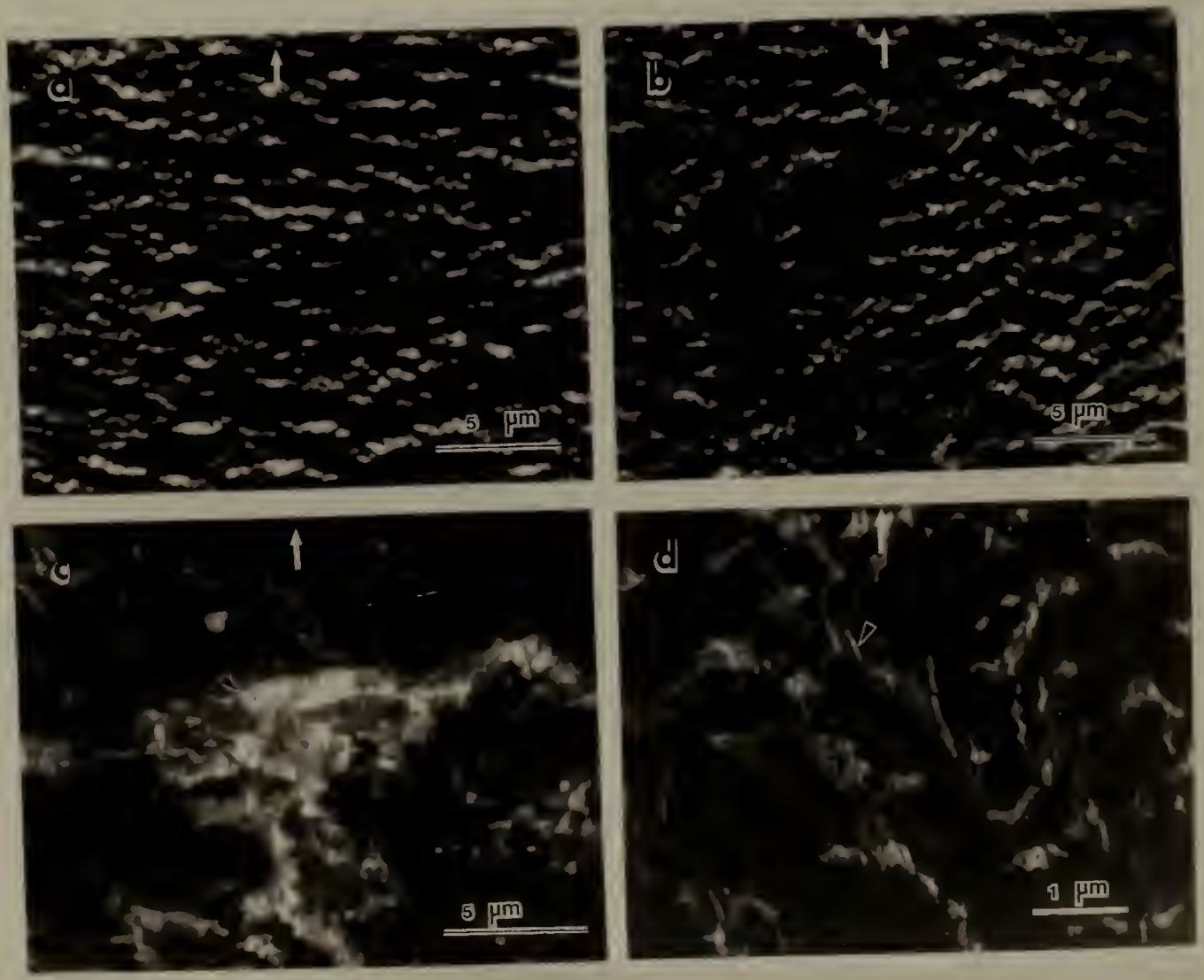

Figure 6.4 Morphology of strained specimens of Marlex (a and c) and Hifax (b and d) polyethylene. Fig. 4a and b at low strain and Fig. 4c and d at high strain (SEM-SEI).

undeformed polymer are about 0.75 μ thick. It is unlikely that they represent lamellae viewed edge-on due to this thickness. The bright regions represent plastically deformed polymer; though some fibrillation is evident, it is not predominant. At the higher elongation, differences in the two polyethylenes manifest themselves. Marlex® (Figure 6.4c) exhibits a neck and consequently fibrillation is dominant. The fibrillation involves the breakdown of dark lamellar regions into bright fibrils as the drawing progresses. Figure 6.4c reveals both undrawn and drawn regions in the neighborhood of the neck. Hifax® (Figure 6.4d), on the other hand, reveals even further extension similar to Figure 6.4b. Stretched fibrils are evident in between undeformed crystal blocks, but little fibrillation of the kind seen in Marlex® occurs at this elongation.

6.4.2 Filled Polyethylenes. Figure 6.5 reveals the deformation behavior of filled polyethylene. In this sequence of micrographs of a 4 vol % $CaCO_3$ filled Marlex® specimen, the nucleation of microfailure (see A) is seen to occur at the interface of a coarse particle. At a higher deformation more localized failure zones appear.

These micrographs do not reveal the nature of the failure zones because of information loss arising due to high secondary yield of electrons.

Figure 6.6 is a SEM-SEI of 19 vol% KR-TTS® treated $CaCO_3$ filled Marlex. Quite a few features in this micrograph are of interest. Two types of microfailure zones are in evidence. The more prominent

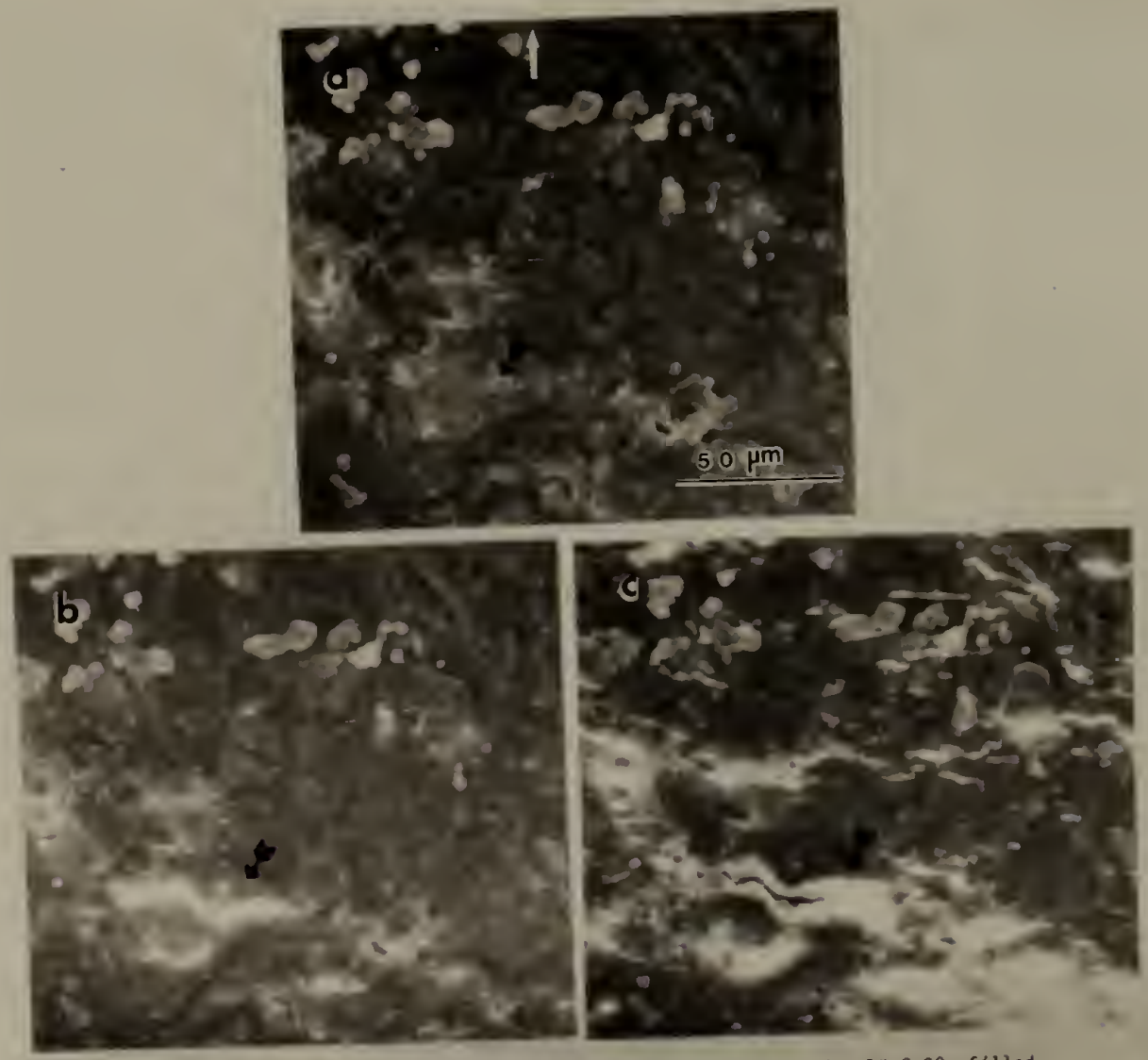

Figure 6.5 Stages in the formation of a region of microfailure in 4 vol% $CaCO_3$ filled Marlex (SEM-SEI).

Figure 6.6 Deformation morphology of 19 vol% $CaCO_3$ filled Marlex. Regions marked C are crazes while regions S are shear zones (SEM-SEI).

ones with length transverse to the tensile direction are tens of microns long and exhibit a craze-like structure with a fibril void formation. Interspersed between these crazes are micron sized zones which display a certain resemblance to shear bands in rubber modified thermoplastics [ref. 2, page 194]. These shear bands also resemble the type of deformation mechanism seen in unfilled polyethylenes (see Fig. 6.4).

Inspection of the crazes reveal quite consistently the presence of a coarse particle which was dewetted at their approximate center. Smaller particles are seen completely dewetted and entrapped in the fibrils of the craze.

The growth of these crazes is shown in Figure 6.7, in 19 vol% $CaCO_3$ filled Hifax®. It is seen that the dimensions of the crazes grow both laterally, and, to a significant extent, also in the tensile direction. This growth of crazes is at the expense of the regions initially composed of lamellar polyethylene. Local failure of the craze is also apparent in some of the crazes. This does not result in sample failure since the crazes do not propagate through the thickness of the sample. Similar crazing behavior is displayed in the DPCC composite (see Fig. 6.8a). However, higher magnification examination of crazes in DPCC (Figure 6.8b) reveals that fibrils extend from detached filler particles into the matrix indicating superior contact between polymer and filler in these composites.

A critical craze (a craze which results in sample failure) in 19 vol% $CaCO_3$ Marlex® is shown in Fig. 6.9a and b. The critical crazes

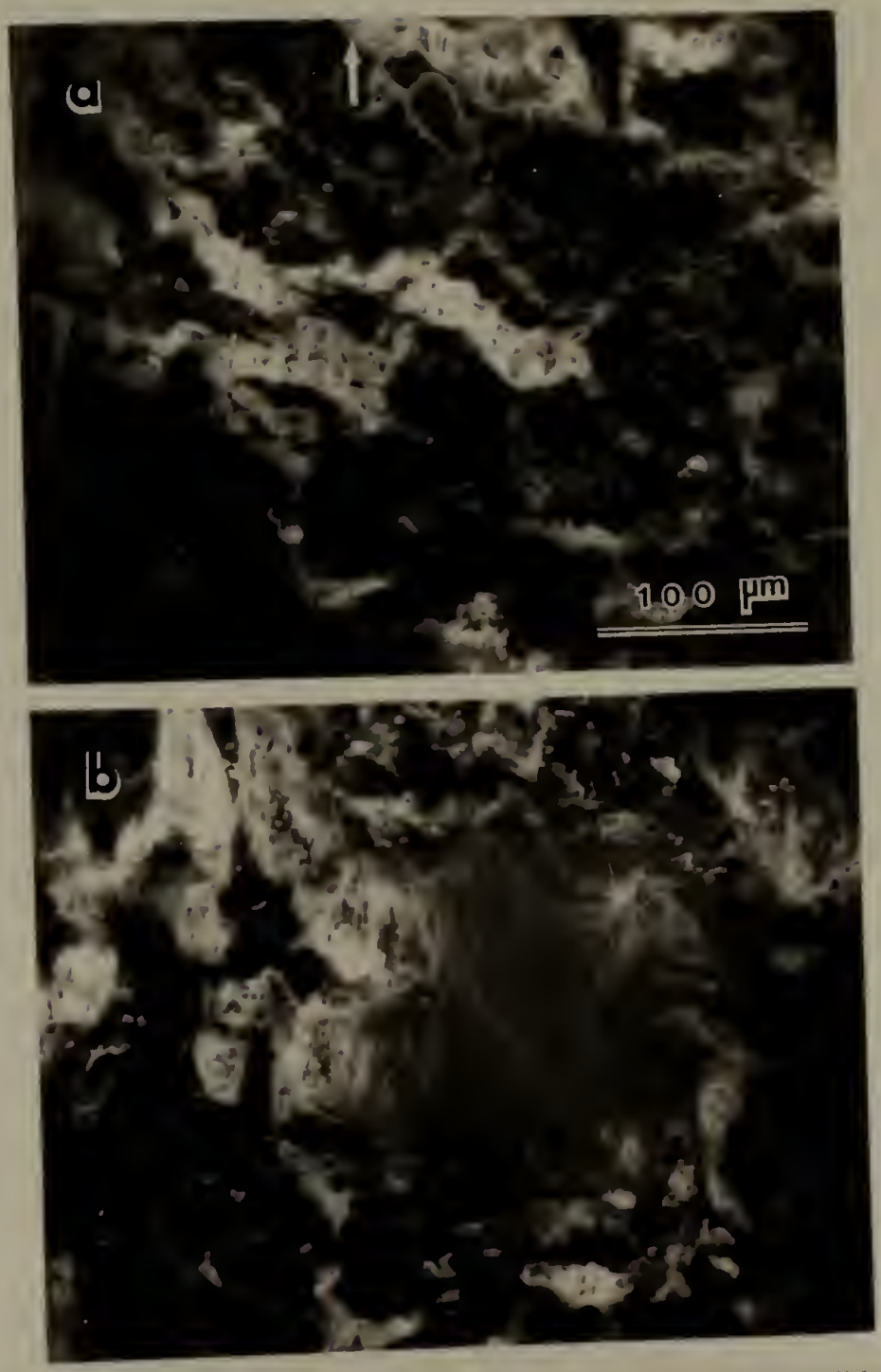

Figure 6.7 The growth of crazes in 19 vol% $CaCO_3$ filled Hifax (SEM-SEI).

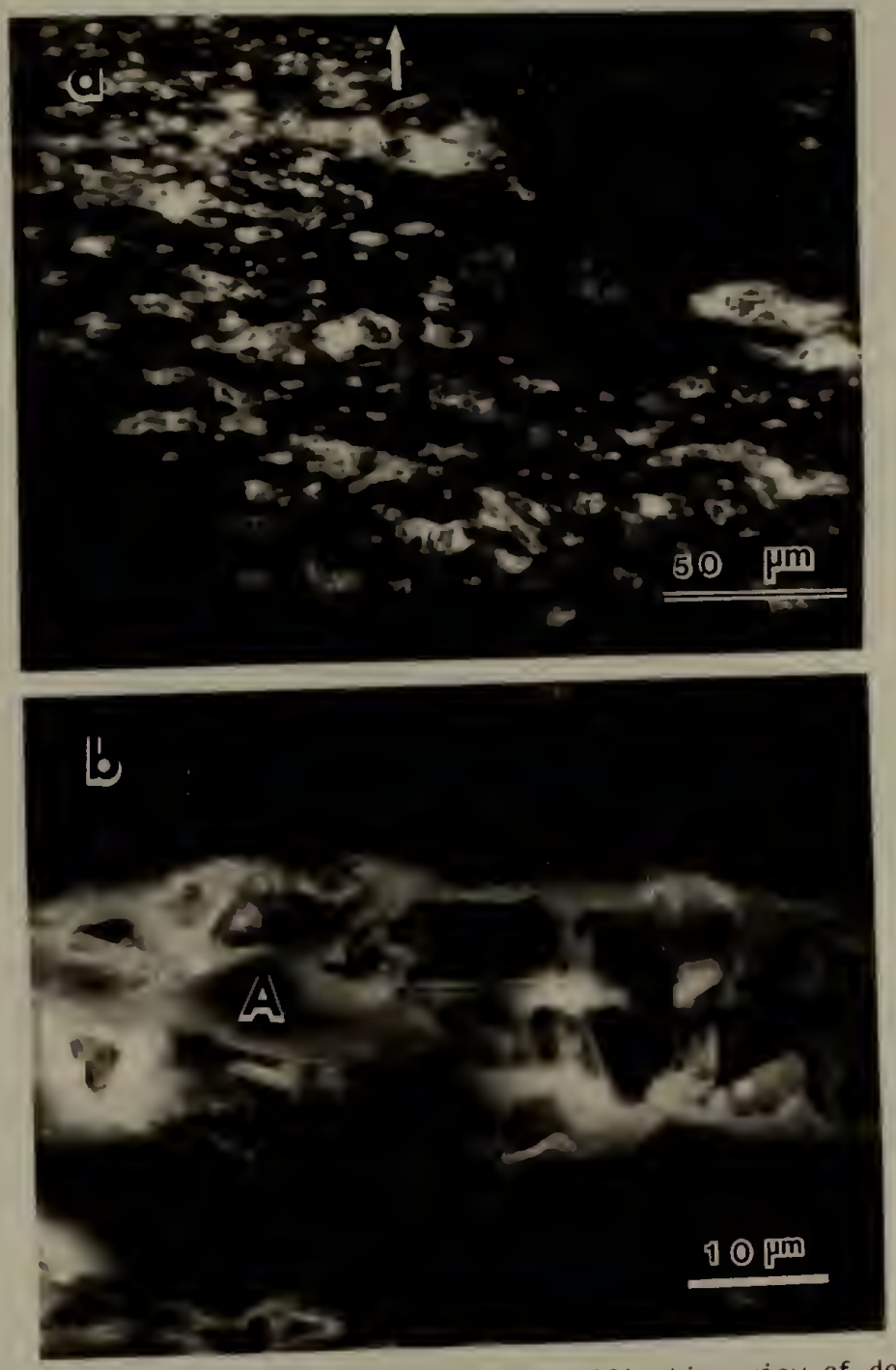

Figure 6.8 Crazes in DPCC (a) low magnification view of deformed morphology (b) craze morphology showing good adhesion of polymer to filler (see A) (SEM-SEI).

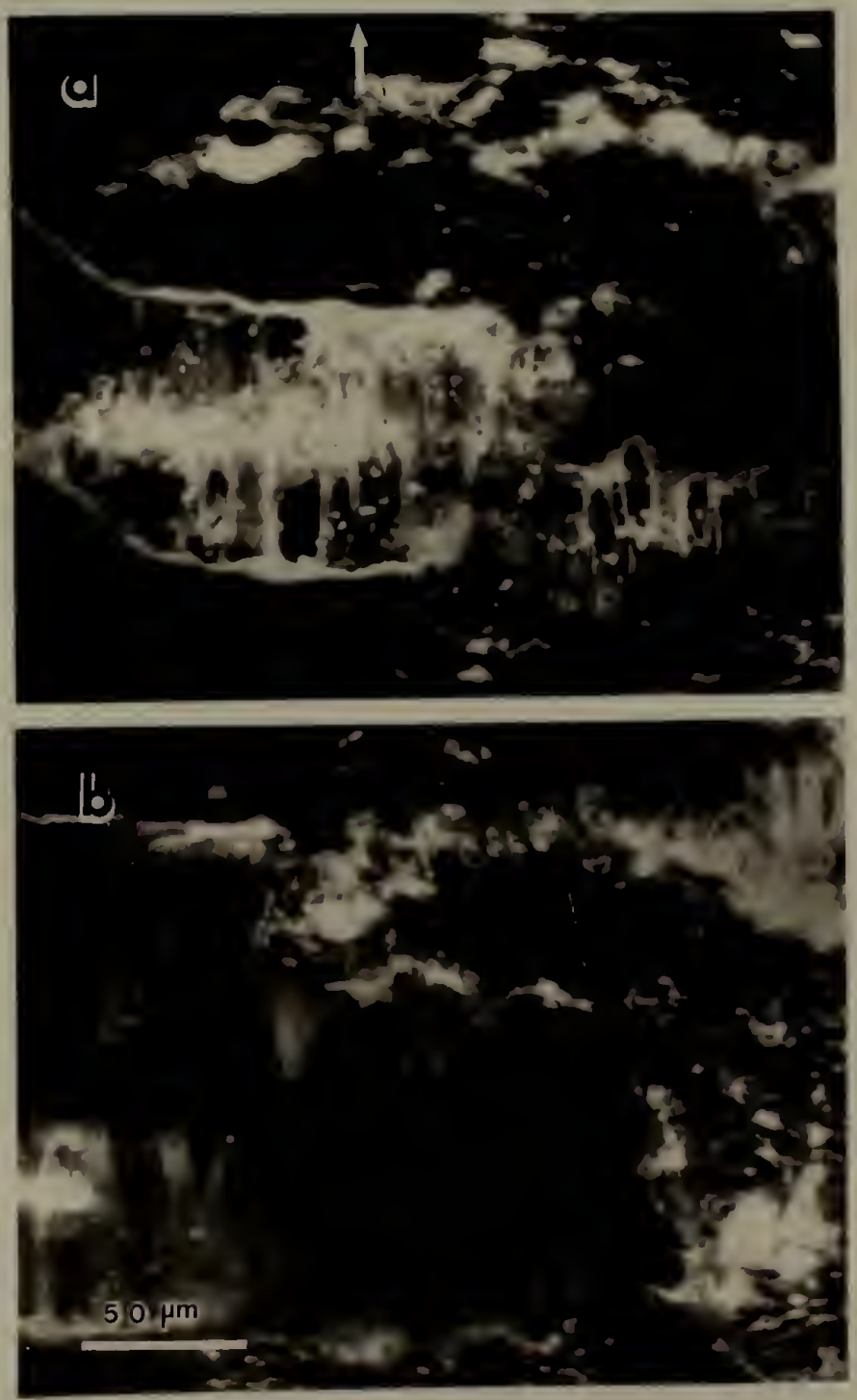

Figure 6.9 Critical craze in 19 vol% $CaCO_3$ filled Marlex (a) before and (b) after breakdown (SEM-SEI).

in filler Marlex exhibit a sharp edge which propagates easily through the sample. This is in contrast to crazes in $CaCO_3$ filled Hifax which exhibit blunt edges and fail in a manner more akin to tearing than cracking.

It is difficult to follow the growth of a craze to a crack by this method since most crazes terminate their growth prior to sample failure with consequent crazing occuring at a different location. However, non critical crazes in filled Marlex® were longer by a factor of 1.5 and thinner (in the stretching direction) by a factor of 3 as compared to the filled Hifax.

6.5 Discussion

The deformation behavior of unfilled and filled semicrystalline polymers has been a matter of continuing interest. Hay and Keller [6] noted fibrillation of thin spherulitic films of PE upon deformation. It was noticed that plastic deformation in spherulites was in certain cases confined to the equitorial regions of spherulites; thereby resulting in their inhomogeneous deformation.

Differences in the deformation of PE as a function of molecular weight have also been investigated before. Steidl and Pelzbauer [7] observed the presence of 300-500Å blocks oriented transverse to the stress direction in high molecular weight PE as opposed to fibrils oriented in the stress direction observed for the lower molecular weight sample. Their high and low molecular weight polyethylenes had similar stress-strain curves to those displayed by Hifax® and

Marlex®, respectively, in this study. These differences may be related to the differing amorphous content. Hifax® has an amorphous constant of about 45% while Marlex® has only about 25% amorphous material. The amorphous material in between lamellae will deform preferentially to the more rigid crystal blocks and at high elongations it may be expected that the crystalline blocks in Hifax® act essentially as macroscopic network junctions. At elongations beyond the yield Marlex® on the other hand will display plastic behavior involving the transformation of lamellar crystalline blocks into fibrils.

The rubbery character of Hifax® is also well displayed in cyclic stress strain tests: even after 400% elongation Hifax® retracts almost completely, a property not displayed by Marlex®.

As seen in the above section, the presence of $CaCO_3$ filler alters the deformation behavior quite considerably. Irrespective of molecular weight of polyethylene, crazes are formed in presence of filler. It is also noticed that almost all crazes had coarse particles in their centers. The smaller particles seem unable to affect in any way the growth of the crazes; they are present in a completely dewetted state among the fibrils at the surfaces of the craze.

This behavior can be compared to the observations of craze formation in high impact polystyrene by Donald & Kramer [8]. They observed that large occluded rubber particles initiated crazing while small rubber particles appeared incapable of blunting craze

growth. Donald and Kramer conceive of craze growth by the Taylor meniscus instability scheme, consequently the ability of coarse rubber particles to induce higher stresses in the neighboring glassy polymer up to 3 fibrils away is seen to be of importance in the nucleation of the craze.

The presence of crazes with a void-fibril structure (average diameter of fibril 500 Å) in filled polyethylene would indicate that a similar mechanism could be responsible for their formation. However, such a comparison must be approached with caution due to the obvious differences in the two heterogeneous materials compared.

Since in filled polyethylenes the polar stress concentration would imply that dewetting is a preferred process, it must indeed be the initial step in the microfailure process. The dewetting step would then result in the stress concentration shifting to the equatorial regions of the particle. Crazing can then initiate, possibly assisted by the irregular shape of the dewetting region resulting in further strain amplification in the neighboring matrix.

The observation of crazes in filled materials is possible only upon holding the sample at positive strain during microscopy. The release of stresses results in the closure of the crazes and instead of a fibrillated structure, the surface gives the appearance of crisscrossing lines with no apparent dilatational deformation. Hence microscopy must essentially be carried out on samples at constant overall strain. Electron microscopy is the preferred mode of observation because of magnification flexibility and high resolution

tion capability. However, charging and high secondary electron generation prove a problem, a situation which can be rectified by the use of ion generators available commercially.

The phenomenon of the existence of a large number of crazes which do not attain criticality can be looked upon in two different perspectives. It can be considered a localized strain hardening process akin to the necking process in unfilled Marlex (which is indeed a void fibril formation albeit a more dense one). It may also be that the craze tip is confronted with material which is resistant to further crazing either due to strain hardening processes which occurred earlier or due to a blunting of the craze tip due to some undetermined mechanism.

It is also pertinent to note that crazing is more commonly observed in glassy polymers though unfilled semicrystalline polymers have also been known to craze [9]. Deformation of semicrystalline polymers is currently understood to take place by lamellar slip, breakdown and drawing into fibrillated material at increasing strain. In this context one may also consider the crazing process to be due to the high strains induced by the presence of the void after the dewetting step.

The differences in the dimensions of the crazes in the two filled polyethylenes will obviously have a bearing on the ultimate properties of the two materials, the longer and thinner crazes in filled Marlex result in earlier failure of sample at lower elongations.

The technique described above, that of deforming specimens in the electron microscope, is perhaps a relatively novel approach to understanding the failure behavior of polymer composites. It is quite apparent that this study possesses quite a few limitations, some of which are now listed. The study was limited to tests at a low elongation rate (5×10^{-4} mm/sec) and hence neglected the important role of strain rate on failure behavior of materials. The specimens listed were fairly thick and suitable only for SEM. Electron charging problems associated with exposure of polymer without a conducting coating of gold limited high resolution studies. Reliable estimates of strain were not obtainable. Despite these limitations, some of which are definitely not insurmountable, it is believed that the advantages are of a nature which render the technique quite useful. It is thus possible to investigate the significant amount of noncritical microfailure occuring in a composite sample at different levels of resolution. This may be contrasted to fracture surface studies in which just the surface of the critical crack is observed after sufficient material retraction has taken place. The role of stress concentration in the deformation behavior of composites is rather well exposed. Finally, it points to the ubiquitous presence of crazes upon deforming polymer composites, irrespective of the relative modulus of inclusion and nature of polymer matrix.

6.6 Conclusions

The deformation morphologies of unfilled and $CaCO_3$ filled

polyethylenes of two molecular weights were investigated by scanning electron microscopy of film specimens deformed in the microscope. While both polyethylenes deformed similarly at low elongations, the high strain behavior differed with the medium molecular weight PE ($\overline{M}w$ = 200,000) deforming with draw, while the high molecular weight PE (1.5×10^6) deformed homogeneously with little fibrillation.

The presence of $CaCO_3$ filler resulted in the formation of crazes irrespective of molecular weight of PE. Non critical crazes were about 150% longer and 30% as thin in the filled medium molecular weight as compared to the high molecular weight PE.

The formation of crazes qualitatively explains the high dilatational deformation of filled polyethylenes which would not be possible by simple dewetting alone. The failure of filled semicrystalline mechanisms under tensile loading may be envisaged as consisting of the following steps occurring at higher strains:

1. Dewetting of coarse particles with formation of a void.
2. Localized craze formation nucleated by dewetting particles.
3. Growth and stabilization of a large number of crazes quite uniformly in the material.
4. Deterioration of a large craze into a critical craze which leads to specimen failure.

6.7 References

1. A.E. Oberth, Rubber Chem. Technol., 40(5), 1337, 1967.

2. "Toughened Plastics" by C.B. Bucknall, Applied Science, London, 1977.

3. L. Nicolais and M. Narkis, Polym. Engr. Sci., 11(3), 194, 1971.

4. R.J. Farris, Trans Soc. Rheol., 12(2), 315, 1968.

5. K. Freidrich and U.A. Karsch, J. Mat. Sci., 16, 2167, 1981.

6. I.L. Hay and A. Keller, Kolloid-Z., 204, 43, 1965.

7. J. Steidl and Z. Pelzbauer, J. Polym. Sci., Part C, 38, 345, 1972.

8. A.M. Donald and E.J. Kramer, submitted to J. Mat. Sci., September, 1981.

9. R.P. Kambour, J. Polym. Sci., Macromol. Rev., 7, 1, 1973.

CHAPTER VII

OVERALL SUMMARY AND CONCLUSIONS

In the preceding chapters the microstructure and mechanical behavior of one novel and a range of conventional $CaCO_3$-filled polyethylenes was investigated by a variety of techniques. In this concluding Chapter we shall attempt to highlight the salient points of this work, discuss the effect of variation of material parameters and thus attempt to discern a pattern by putting together the various pieces of evidence.

7.1 Diffraction Contrast in Electron Microscopy of PE Films

A major objective of Chapter II was to examine the reasons for image contrast in thin spherulitic films of PE undamaged by electron flux. While the perdetious effect of electron beams on polymer films has been known for quite some time, electron microgaphs of undamaged films are still quite rare.

BF and DF contrast features may be explained quite simply by considering the diffraction "efficiency" of various orientations of the PE crystal. Hence lamellae oriented perpendicular to the beam, possessing a multiplicity of high structure factor reflecting planes image dark in BF relative to crystals oriented otherwise. Thus banding observed in EM of undamaged thin films is a diffraction contrast feature rather than purely a mass thickness contrast feature. However, damage due to electron flux through PE crystals lengthens

crystals along the two axes perpendicular to the chain direction and reduces crystal thickness along the chain axis (see Chapter II, reference 2). This then can lead to a similar banding effect but with the contrast reversed.

The utility of electron microscopy in PE microstructure elucidation will be enhanced if the crystal orientation in lamellae can be clearly distinguished. We have demonstrated that using STEM techniques, discriminatory selection of which crystalline reflections contribute to image formation enables us to distinguish between differently oriented lamellae with ease. This was illustrated in particular in the case of oriented growth of PE crystals perpendicular to surfaces of $CaCO_3$ filler with the use of 110/200 annular DF STEM. This technique has another advantage, that of being able to image lamellae continuously, irrespective of local crystal deviation from the Bragg condition. Since flexibility in STEM imaging is attained by simply selecting appropriate apertures and beam stops, it is easily appreciated that even more discriminatory imaging is possible.

Finally, the electron microscopy of undamaged thin films of high molecular weight PE reveals doubly or triply intersecting bend contours in profusion pointing to curved lamellae lying in the plane of the film. If we may assume that the bend contour length is continuous along the lateral dimensions of the lamellae, it is then possible to estimate the width, length and thickness of undamaged, diffracting crystalline PE lamellae.

7.2 Effect of Filler Presence on the Structure and Properties of PE

7.2.1 Effect of Filler Presence on Morphology of PE. The morphological ordering of lamellae in PE into higher level structures is dependent upon melt viscosity, impurities, polymer molecular weight and molecular weight distribution and crystallization conditions; for a wide range of molecular weight in commercial PE's, spherulitic ordering is noticed. The presence of the crystalline $CaCO_3$ filler is seen to disrupt this. The extent of oriented crystalline growth normal to the filler surface points to the role of high nucleation density. Also important is the volume filling ability of the fillers, resulting in a fairly drastic reduction in center-to-center distances of simultaneously nucleating crystals. The lack of optical evidence for spherulites (resolvable Maltese crosses between crossed polars) and the inability to observe spherulites in filled PE films by electron microscopy both point to their absence in $CaCO_3$-filled systems.

Interfacial ordering of lamellae perpendicular to substrate crystal faces was observed. This ordering extends to 500 - 1000 nanometers. However, diffraction patterns obtained from 500 nm spots at the interface revealed only orthorhombic PE. No influence of substrate lattice spacings upon PE crystal form was observed.

7.2.2 Effect of Filler Presence on Dynamic Mechanical Behavior of Polyethylene. The determination of dynamic modulus and tan δ of unfilled and filled systems in the temperature range 100K to 400K revealed that the modulus of the composite is increased with filler content over the temperature range. The increase in modulus at temperatures in the vicinity of 150K was lower than predicted by theoretical composite models while the experimentally determined moduli at higher temperatures agreed quite well with theory.

A major result of this chapter is the use of the correspondence principle (following Hashin Chapter 4 ref.21) to predict the complex moduli (and therefore the tan δ) of model viscoelastic composites as a function of component properties. Thus it is seen that the complex moduli of model viscoelastic composites can be estimated as a function of temperature (or frequency) and deviation of experimentally determined values from model behavior estimated. Interfacial energy loss mechanisms in composites can thus be investigated more quantitatively than was previously attempted. It is appropriate to point out that this technique of estimation of dynamic moduli can be used also for predicting small strain behavior of phase separated polymer blends, glass fiber reinforced plastics, etc.

7.2.3 Effect of Filler on Tensile Properties of Polyethylene. It is observed that the presence of filler in general tends to cause the large strain properties of PE to deteriorate. Hence yield stress and elongation at break both decrease relative to unfilled polymer.

The dilatational behavior of filled polyethylene upon deformation has been unreported until now. Quite expectedly, the dilatation of filled polyethylene increases with increasing filler loading. The slope of the dilatation strain curve in all instances indicated that volume dilatation of a significantly greater magnitude than accountable by a simple dewetting process alone was taking place.

7.2.4 Effect of Filler Presence on Deformational Behavior of Polyethylene. Electron microscopy studies of specimens undergoing deformation revealed that the dominant effect of filler presence was the appearance of dilatational microfailure zones which resemble crazes observed in rubber modified glassy thermoplastics. In addition, in common with unfilled PE, shear zones were also identified.

It is postulated that the development of crazes arise due to initial dewetting of coarse particles followed by void fibril formation in the equitorial neighborhood of the surrounding polymer matrix. The reasons for the beakdown of previously continuous polymeric material in glassy thermoplastics into fibril-void structures is presently attributed to what is known as the meniscus instability mechanism.

7.3 Role of Intrinsic Variables in Filled Polymer Structure and Properties

7.3.1 Effect of Polymer Molecular Weight. Irrespective of polymer molecular weight it was found that filler presence disrupts superlamellar ordering in PE. In all cases studied interfacial ordering of

lamellae was noticed. However, the nature of the lamellar morphology in the composite is affected by molecular weight. Lamellae in low molecular weight PE are long, closely packed and quite linear. They become increasingly more curved and individual lamellae are distinctly resolved with increasing molecular weight.

Increasing molecular weight results in a loss of crystallinity which translates to a loss in elastic modulus and increase in the tan δ peak attributed to the amorphous faction of PE. Filler presence reduces the crystallinity (as measured by DSC) of the two lower molecular weight PEs; this effect decreases with increasing molecular weight.

Increasing the molecular weight brings about rather prominent changes in tensile behavior of PE. From a stiff, hard relatively brittle material it changes to a softer, stronger and considerably tougher material. This toughness may be attributed to the high amorphous content, greater length of polymer chains and increased entanglements. A serious drawback with the highest molecular weight PEs is the inability to melt process them by extrusion, injection molding, etc. This results in very poor mixing with $CaCO_3$ and consequently bulk samples of conventionally blended composites exhibit poor properties. On the other hand, the low molecular weight PE possessed such low melt strength that milling operations became quite difficult.

Hence, the best tensile properties in the conventionally filled polyethylenes were shown by the medium molecular weight polyethylene. Both the high molecular weight filled PE and the lower molecular

weight filled PE were inferior to the medium molecular weight filled PE for differing reasons.

The novel composite of ultrahigh molecular weight PE and 38 volume % $CaCO_3$ (DPCC) exhibited excellent elongation at break, and the impact strength reported is also remarkable, confirming that the poor behavior of conventionally prepared $CaCO_3$ filled high molecular weight PE is primarily due to the problem of filler dispersability (see Fig. 7.1 a and b).

Differences in deformation behavior were also noticed with shorter, more blunt crazes characterizing high molecular weight PE while longer, thinner crazes were observed in the medium molecular weight polyethylene.

7.3.2 Effect of Filler Volume Content. It is seen that even at as low a filler content as 2 vol %, the Maltese crosses which characterize the unfilled polymer disappear and a granular appearance results. This granularity increases with increased filler content. The trends in the dynamic mechanical properties and mechanical properties are as expected intutively. Examination of deformed morphology and the results of the dilatation study show that crazes are more numerous at higher filler content. The presence of completely dewetted small particles in the fibrils of the crazes indicates their lack of craze stopping ability. This may be because the thickness of the crazes is much larger than the diameter of the particles. The large particles, on the other hand, seem more prone to initiate crazes, as seen in the deformation morphology study.

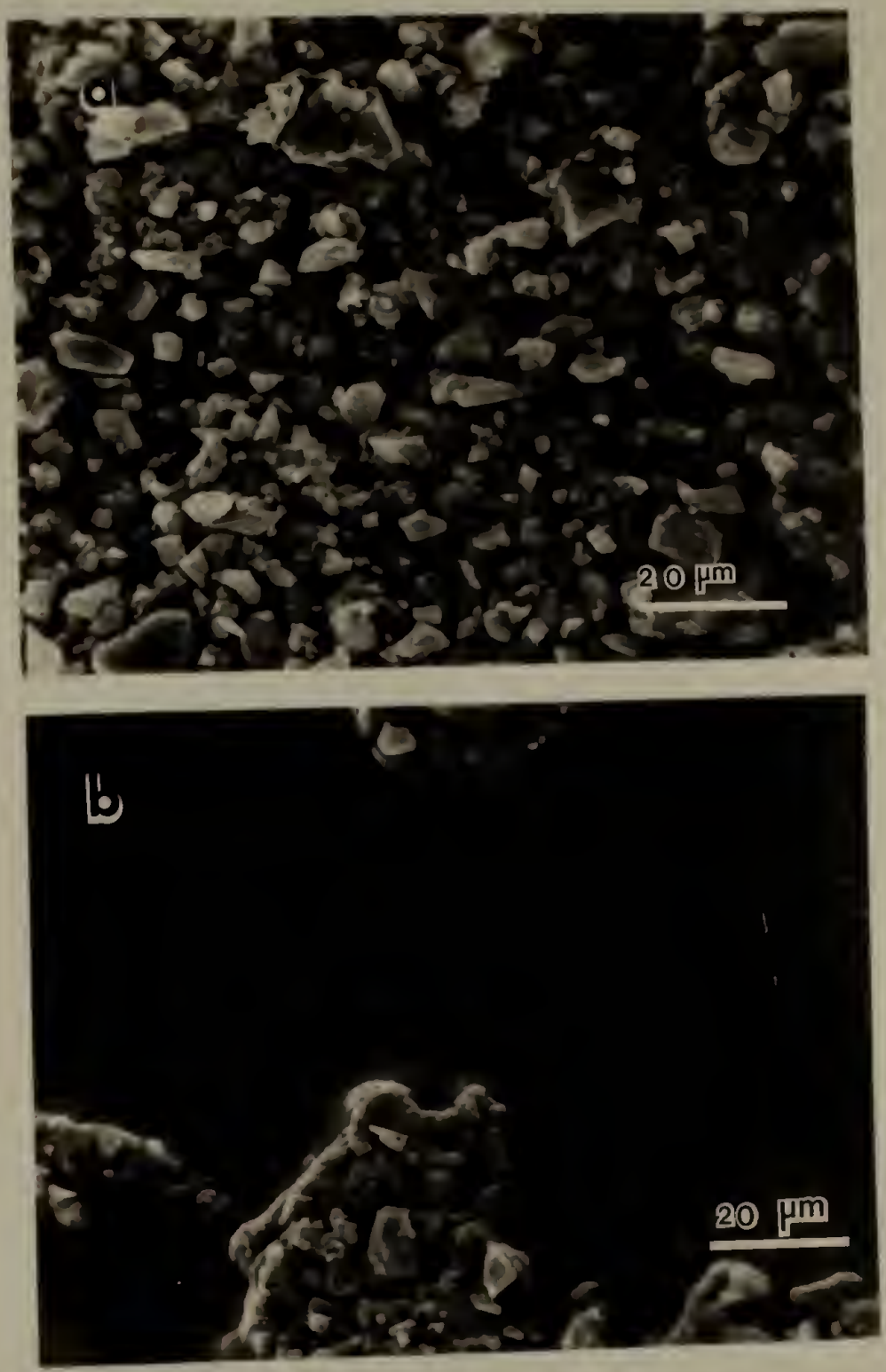

Figure 7.1 The problem of agglomeration (a) well dispersed $CaCO_3$ in DPCC (b) poorly dispersed $CaCO_3$ in Hifax.

7.3.3 Effect of Filler Treatment. Though the increased dispersion as a result of filler treatment was noted in the dynamic mechanical tests, crystallization studies and tensile tests, this effect was not observed by microscopy.

Storage moduli showed that treated samples exhibited broader transitions in the γ-transition region (150K) indicating improved dispersion. The amplitude of the tan δ peak at 150K decreased upon filler treatment. At higher temperatures the storage moduli for the two types of fillers were about the same, but the tan δ was slightly higher for the treated filler.

Elongation at break of samples filled with treated $CaCO_3$ increased significantly; however, the yield stress of filled samples dropped upon filler treatment. Both these observations may be explained in terms of improved dispersion of filler.

7.4 Effect of Polymerizing Matrix onto Filler Surface

All the characteristics of well dispersed filler presence were observed in the novel composite (DPCC). The deformation morphology study shows evidence of good adhesion between dispersed $CaCO_3$ particles and PE matrix. In addition crystallization studies (unpublished observations) show intimate contact between polymer and filler.

The remarkable properties of this composite are in great part due to the well dispersed nature of the filler and the high molecular weight of the polymer, both of which have been shown to be critical material parameters. Unanswered then is the question of the exact

role of surface polymerization of monomer. Does the fact that in the novel composite one end of each chain is essentially in the close neighborhood of the filler surface contribute to its superior properties? The transmission electron micrography studies show that in the DPCC composite and in conventional composites lamellar growth perpendicular to the filler interface is seen. Differences between the two kinds of composites in this regard are perhaps quantitative, though this was not investigated. The uniformity of transcrystalline crystallization is dependent, among other factors, upon degree of contact between polymer and filler surface and it is obvious that in DPCC such contact is indeed superior to conventionally prepared $CaCO_3$ filled high molecular weight PE.

Since a material is as strong as its weakest link, it is possible to argue in favor of surface polymerization with its more perfect interface as opposed to the other approaches to novel composite preparation discussed in Chapter I.

7.5 Suggestions for Future Work

During the course of this dissertation, there arose on many occassions the urge to explore an area of investigation in a more extensive fashion than what is reported. Such urges are perhaps typical of any investigation and are usually tempered by limitations of time, experimental difficulties and the need to complete the larger study so as to obtain somewhat more comprehensive picture of material behavior. In the following pages we shall list possible extensions to

this study.

In the study of the morphology of filled systems the role of substrate crystal facet orientation in influencing PE lamellar orientation needs to be investigated. This type of study is possible with the use of calcite crystals thin enough for diffraction studies. Such a study would answer some long standing questions on the nature of polymer epitaxy.

The interfacial energy loss at various temperatures and frequencies of oscillatory load would be an indication of the perfection of the polymer-filler interface. The effect of amplitude of oscillatory load on interfacial energy loss would be useful as an indicator of interfacial failure and the onset of nonlinear behavior of composites. Such studies would best be performed on a relatively perfect system (glass bead-epoxy) where the problem of morphological changes in matrix due to filler presence can be avoided.

The important role of strain rate on the tensile behavior and deformation morphology needs to be investigated as a function of filler content, polymer molecular weight and polymer-filler interface.

The important role thermal stresses play in determining the mechanical properties of composites has been largely ignored in this study. As pointed out earlier, the different thermal expansion coefficients of the two components results in a stressed interface which can influence the stress distribution at the interface in the event of externally imposed stress. This may alter the nature of interfacial failure. Since the matrix is viscoelastic, the stresses tend to relax

with time influencing material aging. Investigations in this area therefore will be of considerable import.

Preliminary calorimetric studies on the isothermal crystallization behavior of filled polyethylenes indicated that the crystallization half-time of filled polyethylenes was dependent upon surface treatment. Further work on the kinetics of crystallization would be quite useful.

As for the investigation of PE thin films by electron microscopy, the EM imaging of polymer crystal defects, and the role of such defects in the plastic deformation of polymer crystals is naturally of fundamental importance.

APPENDIX I

COMPLEX MODULI OF VISCOELASTIC COMPOSITES

The following result is abstracted from a paper by Z. Hashin, International J. Solids Structures, Volume 6, pages 539-552, 1970.

It is possible to show that effective relaxation moduli of statistically homogeneous viscoelastic composites may be defined by

$$\bar{\sigma}_{ij}(t) = \int_{-\infty}^{t} C_{ijk\ell}(t-\tau) \frac{\delta \bar{\varepsilon}_{k\ell}(\tau)}{\delta \tau} \delta\tau \qquad (1)$$

where σ_{ij} and ε_{ij} are stress and strain tensors, an overbar denotes local or global average of a statistically homogeneous field, $C^{*}_{ijk\ell}$ is the effective relaxation moduli tensor and τ is time. The assumption of statistical homogeneity implies that there exists a representative volume element of material small enough that local averaging may be performed over the element and those average quantities (stress and strain) are utilized.

Suppose that the composite is subjected to an average sinusoidal strain

$$\bar{\varepsilon}_{k\ell}(t) = \tilde{\varepsilon}_{k\ell} e^{i\omega t} \qquad (2)$$

where ω is the circular frequency and $\tilde{\varepsilon}_{k\ell}$ is a constant. Using equation 2 and a change of variable $u = t-\tau$ yields

$$\bar{\sigma}_{ij}(t) = \tilde{\varepsilon}_{k\ell} e^{i\omega t} \cdot i\omega \int_{0}^{\infty} C^{*}_{ijk\ell}(u) e^{-i\omega u} du \qquad (3)$$

Let

$$B^{*}_{ijk\ell}(i\omega) = i\omega \int_0^{\infty} C^{*}_{ijk\ell}(u)\, e^{-i\omega u}\, du \tag{4}$$

Then equation 3 can be rewritten as

$$\begin{aligned} \bar{\sigma}_{ij}(t) &= B^{*}_{ijk\ell}(i\omega)\, \bar{\varepsilon}_{k\ell}(t) \\ &= [B^{*R}_{ijk\ell}(\omega) + i\, B^{*I}_{ijk\ell}(\omega)]\, \bar{\varepsilon}_{k\ell}(t) \end{aligned} \tag{5}$$

The tensor components $B^{*}_{ijk\ell}$ are called effective complex moduli.

Now consider the Laplace Transform of the effective complex moduli.

$$\hat{C}^{*}_{ijk\ell}(p) = \int_0^{\infty} C^{*}_{ijk\ell}(t)\, e^{-pt}\, dt \tag{6}$$

Then the Laplace Transform of equation 1 is given by

$$\bar{\sigma}_{ij}(p) = G^{*}_{ijk\ell}(p)\, \bar{\varepsilon}_{k\ell}(p) \tag{7}$$

where

$$C^{*}_{ijk\ell}(p) = p\, \hat{C}^{*}_{ijk\ell}(p) \tag{8}$$

The tensor components $G^{*}_{ijk\ell}$ will be called transform domain (TD) effective moduli.

The Correspondence principle for elastic and viscoelastic heterogeneous media is stated thus: consider two statistically

homogeneous specimens of entirely identical phase geometries. In the first the phases are all elastic with elastic moduli ${}^{e}C^{(r)}_{ijk\ell}$ of the th phase. In the second the phases are all viscoelastic with relaxation moduli $C^{(r)}_{ijk\ell}(t)$ of the rth phase. Then, according to the Correspondence principle the effective transform domain moduli $G^{*}_{ijk\ell}$ are formed by replacement of ${}^{e}C^{(r)}_{ijk\ell}$ by equation 8 in the known expression for ${}^{e}C^{*}_{ijk\ell}$.

$$G^{*}_{ijk\ell}(p) = {}^{e}C^{x}_{ijk\ell}\left[G^{(r)}_{mnop}(p)\right]$$

Introduce equation 6 into equation 8:

$$G^{*}_{ijk\ell}(p) = p\int_{0}^{\infty} C^{*}_{ijk\ell}(t)\, e^{-pt}\, dt$$

It is seen that the functional dependence of $B^{*}_{ijk\ell}$ on $i\omega$ is the same as the functional dependence of $G^{*}_{ijk\ell}$ on p. Therefore

$$B^{*}_{ijk\ell}(i\omega) = G^{*}_{ijk\ell}(i\omega)$$

Define

$$B^{(r)}_{ijk\ell}(i\omega) = G^{(r)}_{ijk\ell}(i\omega) = i\omega\,\hat{C}^{(r)}_{ijk\ell}(i\omega) \qquad (9)$$

Then

$$B^{*}_{ijk\ell}(iw) = {}^{e}C^{*}_{ijk\ell}\left[B^{(r)}_{mnop}(iw)\right] \qquad (10)$$

This is the desired result. Stated in words: the effective complex

moduli of a viscoelastic heterogeneous specimen are found by replacement of phase elastic moduli by phase complex moduli in the expressions ${}^{e}C^{*}_{ijk\ell}$ for the effective elastic moduli of an associated heterogeneous elastic specimen with identical phase geometry.

APPENDIX II

COMPUTER PROGRAM FOR DETERMINATION OF COMPLEX MODULI OF MODEL VISCOELASTIC COMPOSITES

```
      PROGRAM MODLAS(INPUT,OUTPUT,TAPE1=INPUT,TAPE2=OUTPUT,TAPE3,
     1 TAPE4,TAPE5,TAPE6)
       IMPLICIT REAL(I,M,L,K,N)
      DIMENSION ESER(11),EPAR(11),EDIL(11),ECONC(11),KDIL(11)
     1 ,KCONC(11),MUDIL(11),MUCONC(11),CONC(11),TANPAR(11),TANSER(11)
     3 , GMODL(11),TANDL(11),TANGL(11),MODE(11),KMODL(11),TANKD(11)
     9 ,TANCN(11),COEFF(3),ROOT(2)
      COMPLEX CMP,MYM,MK,MMU,ESER,EIMAG,EPAR,KSUB,KDIL,
     8 MURAT,NUM,DENOM,MUDIL,EDIL,ETA1,ETA2,ETA3,A,B,CC,TERM1,TERM2
     7 ,ROOT,COEFF, FACT,MUCONC,ECONC,KCONC,RT1
C
C   IN THIS PROGRAM WE CALCULATE THE EFFECTIVE YOUNG'S MODULUS
C  FOR A PARTICULATE FILLED POLYMER CONTAINING VARYING CONCENTRATIONS
C  OF FILLER BY DIFFERENT MODULUS ESTIMATES.
C
C    READ THERELEVANT MODULI FOR EACH OF THE PHASES
C
      READ(1,*)MYM,MNU,IYM,INU,TANM
C
C  CALCULATE BULK MODULUS
C
      MK=MYM/(3*(1.-2*MNU))
      IK=IYM/(3*(1.-2*INU))
      MMU=MYM/(2*(1+MNU))
      IMU=IYM/(2.*(1.+INU))
C
C    CALCULATE SINM,COOOOOSM
C
      ANGL=ATAN(TANM)
      SINM=SIN(ANGL)  $  COSM=COS(ANGL)
C
C  IN THIS WE CALCULATE THE LOWER BOUND
C
      CMP=(0.,-1.)
      DO 15 J=1,11
      C=0.1*J-0.1
      ESER(J)=MYM*IYM/(C*MYM+(1.-C)*IYM)
      EREAL=ESER(J)
      EIMAG=ESER(J)-EREAL  $ EIMAG=EIMAG*CMP
      TANSER(J)=EIMAG/EREAL
      EPAR(J)=(1.-C)*MYM+C*IYM
      EREAL=EPAR(J)
      EIMAG=EPAR(J)-EREAL  $EIMAG=EIMAG*CMP
      TANPAR(J)=EIMAG/EREAL
   15 CONTINUE
      GO TO 21
   21 CONTINUE
C  IN THIS SECTION WE  CALCULATE THE MODULUS FOR THE DILUTE CASE
C  AFTER ESTIMATING BOTH THE EFFECTIVE BULK MODULI AND SHEAR MOD
C  ULUS
C
```

```
C
C
      KSUB=IK-MK
      DO 30 J=1,11
      C=0.1*J-0.1
      KDIL(J)=MK+KSUB*C/(1. +KSUB/(MK+1.33*MMU))
C
C TO ESTIMATE THE SHEAR MODULUS
C
      MURAT=IMU/MMU
      NUM=15.*(1.-MNU)*(1.-MURAT)*C
      DENOM=7.-5*MNU+2.*(4.-5.*MNU)*MURAT
      MUDIL(J)=(1.-NUM/DENOM)*MMU
      EDIL(J)=9.*KDIL(J)*MUDIL(J)/(3*KDIL(J)+MUDIL(J))
      EREAL=EDIL(J)
      EIMAG=EDIL(J)-EREAL  *EIMAG=EIMAG*CMF
      TANDL(J)=EIMAG/EREAL
      CONC(J)=C
   30 CONTINUE
C
C  AT LAST FOR THE CONCENTRATED SUSPENSION CASE
C
      MURAT=IMU/MMU
      FACT=MURAT-1.
C
C CALCULATION OF TERMS IN THE EXPRESSION
C
      ETA1=(49.-50.*INU*MNU)*FACT+35.*MURAT*(INU-2*MNU)
     2 +35.*(2.*INU-MNU)
      ETA2=5. *INU*(MURAT-8.)+7.*(IMU/MMU+4)
      ETA3=MURAT*(8.-10.*MNU)+(7.-5.*MNU)
C
      DO 40 J=1,11
       C=0.1*J-0.1
      TERM1=2.*(63.*FACT*ETA2+2.*ETA1*ETA3)*C**(7./3.)
      TERM2=252. *FACT*ETA2*C**(5./3.)
C
      A=8.*FACT*(4.-5.*MNU)*ETA1*C**(10./3.)-TERM1+TERM2
     3 -50.*FACT*(7.-12*MNU+8.*MNU**2)*ETA2*C+4.*(7.-10.*MNU)*
     4 ETA2*ETA3
C
      B=-2*FACT*(1.-5.*MNU)*ETA1*C**(10./3.)+TERM1-TERM2+75.*FACT*(3.
     5 -MNU)*ETA2*MNU*C+1.5*(15.*MNU-7.)*ETA2*ETA3
C
      CC=4.*FACT*(5.*MNU-7)*ETA1*C**(10./3.)-TERM1+TERM2+25.*FACT
     6 *(MNU**2-7)*ETA2*C-1.*(7+5.*MNU)*ETA2*ETA3
C
C     REDEFINE A,B,CC
C
```

```
C
C
      KSUB=1K-MK
      DO 30 J=1,11
      C=0.1*J-0.1
      KDIL(J)=MK+KSUB*C/(1. +KSUB/(MK+1.33*MMU))
C
C TO ESTIMATE THE SHEAR MODULUS
C
      MURAT=IMU/MMU
      NUM=15.*(1.-MNU)*(1.-MURAT)*C
      DENOM=7.-5*MNU+2.*(4.-5.*MNU)*MURAT
      MUDIL(J)=(1.-NUM/DENOM)*MMU
      EDIL(J)=9.*KDIL(J)*MUDIL(J)/(3*KDIL(J)+MUDIL(J))
      EREAL=EDIL(J)
      EIMAG=EDIL(J)-EREAL  *EIMAG=EIMAG*CMF
      TANDL(J)=EIMAG/EREAL
      CONC(J)=C
   30 CONTINUE
C
C  AT LAST FOR THE CONCENTRATED SUSPENSION CASE
C
      MURAT=IMU/MMU
      FACT=MURAT-1.
C
C CALCULATION OF TERMS IN THE EXPRESSION
C
      ETA1=(49.-50.*INU*MNU)*FACT+35.*MURAT*(1NU-2*MNU)
     2 +35.*(2.*INU-MNU)
      ETA2=5. *INU*(MURAT-8.)+7.*(IMU/MMU+4)
      ETA3=MURAT*(8.-10.*MNU)+(7.-5.*MNU)

C
      DO 40 J=1,11
       C=0.1*J-0.1
      TERM1=2.*(63.*FACT*ETA2+2.*ETA1*ETA3)*C**(7./3.)
      TERM2=252. *FACT*ETA2*C**(5./3.)
C
      A=8.*FACT*(4.-5.*MNU)*ETA1*C**(10./3.)-TERM1+TERM2
     3 -50.*FACT*(7.-12*MNU+8.*MNU**2)*ETA2*C+4.*(7.-10.*MNU)*
     4 ETA2*ETA3
C
      B=-2*FACT*(1.-5.*MNU)*ETA1*C**(10./3.)+TERM1-TERM2+75.*FACT*(3.
     5 -MNU)*ETA2*MNU*C+1.5*(15.*MNU-7.)*ETA2*ETA3
C
      CC=4.*FACT*(5.*MNU-7)*ETA1*C**(10./3.)-TERM1+TERM2+25.*FACT
     6 *(MNU**2-7)*ETA2*C-1.*(7+5.*MNU)*ETA2*ETA3

C
C     REDEFINE A,B,CC
C
```

An International Mathematical & Statistical Library subroutine ROOTCP is used to calculate the roots of the quadratic equation in the CLK expression (see Table 4.1)